AD-A076 421 BOEING WICHITA CO KS F/G 1/3
EVALUATION OF THE CRACK GAGE CONCEPT FOR MONITORING AIRCRAFT FL--ETC(U)
JUN 79 G G CASSATT F33615-77-C-5073
UNCLASSIFIED AFWL-TR-79-4037-VOL-1 NL

1 OF 2
AD
A076421

(18) (19) AFML-TR-79-4037-Vol-I

(2) LEVEL II

A076320

(6)

Evaluation of the Crack Gage Concept for Monitoring Aircraft Flaw Growth Potential.

Volume I. - Technical Discussion.

Boeing Wichita Company
A Division of The Boeing Company
3801 South Oliver
Wichita, Kansas 67210

(10) Gary G. Cassatt

(11) June 1979 (12) 113

Technical Report AFML-TR-79-4037, Vol I.

(15) F33615-77-C-5073 (16) ILIR (17) 00

(9) Final Report, for period July 1977 - Dec 1978

A076320
L110IF

Distribution Statement

Approved for public release: distribution unlimited

Prepared for

United States Air Force
Air Force Systems Command
Aeronautical Systems Division/PPMRR
Wright-Patterson AFB, Ohio 45433

059650

NOTICE

When Government drawings, specifications, or other data are used for any purpose other than in connection with a definitely related Government procurement operation, the United States Government thereby incurs no responsibility nor any obligation whatsoever; and the fact that the government may have formulated, furnished, or in any way supplied the said drawings, specifications, or other data, is not to be regarded by implication or otherwise as in any manner licensing the holder or any other person or corporation, or conveying any rights or permission to manufacture, use, or sell any patented invention that may in any way be related thereto.

This report has been reviewed by the Information Office (OI) and is releasable to the National Technical Information Service (NTIS). At NTIS, it will be available to the general public, including foreign nations.

This technical report has been reviewed and is approved for publication.

Alten F. Grandt Jr.

ALTEN F. GRANDT, Jr.
Project Engineer
Metals Behavior Branch
Metals and Ceramics Division

NG Tupper

NATHAN G. TUPPER, Chief
Metals Behavior Branch
Metals and Ceramics Division

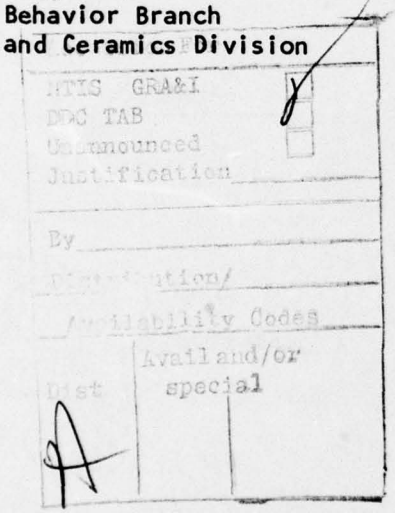

"If your address has changed, if you wish to be removed from our mailing list, or if the addressee is no longer employed by your organization please notify AFML/LLN, W-PAFB, OH 45433 to help us maintain a current mailing list".

Copies of this report should not be returned unless return is required by security considerations, contractual obligations, or notice on a specific document.

AIR FORCE/56780/1 October 1979 — 270

SECURITY CLASSIFICATION OF THIS PAGE *(When Data Entered)*

REPORT DOCUMENTATION PAGE		READ INSTRUCTIONS BEFORE COMPLETING FORM
1. REPORT NUMBER AFML-TR-79-4037, Vol. I	2. GOVT ACCESSION NO.	3. RECIPIENT'S CATALOG NUMBER
4. TITLE *(and Subtitle)* EVALUATION OF THE CRACK GAGE CONCEPT FOR MONITORING AIRCRAFT FLAW GROWTH POTENTIAL		5. TYPE OF REPORT & PERIOD COVERED Final Report July 1977 - December 1978 6. PERFORMING ORG. REPORT NUMBER
7. AUTHOR(s) Gary G. Cassatt		8. CONTRACT OR GRANT NUMBER(s) F33615-77-C-5073
9. PERFORMING ORGANIZATION NAME AND ADDRESS Test Engineering Unit Boeing Wichita Company Wichita, Kansas 67210		10. PROGRAM ELEMENT, PROJECT, TASK AREA & WORK UNIT NUMBERS ILIR - 0092
11. CONTROLLING OFFICE NAME AND ADDRESS United States Air Force Wright-Patterson AFB, Air Force Systems Command Ohio 45433 Aeronautical Systems Division/PPMRR		12. REPORT DATE June 1979 13. NUMBER OF PAGES
14. MONITORING AGENCY NAME & ADDRESS *(if different from Controlling Office)* Air Force Materials Laboratory (AFML/LLN) Air Force Wright Aeronautical Laboratories Wright-Patterson Air Force Base, Ohio 45433		15. SECURITY CLASS. *(of this report)* Unclassified 15a. DECLASSIFICATION/DOWNGRADING SCHEDULE
16. DISTRIBUTION STATEMENT *(of this Report)* Approved for public release; distribution unlimited.		
17. DISTRIBUTION STATEMENT *(of the abstract entered in Block 20, if different from Report)*		
18. SUPPLEMENTARY NOTES		
19. KEY WORDS *(Continue on reverse side if necessary and identify by block number)* Crack Gage Stepped Design Flaw Growth Fleet Tracking		
20. ABSTRACT *(Continue on reverse side if necessary and identify by block number)* The results of a test program to evaluate the ability of a bonded on precracked coupon to monitor the growth of flaws in the basic structure are included. All testing utilized 7075-T651 aluminum from a single plate. Both constant thickness and stepped crack gages were evaluated. Evaluation of a wide range of sensitivity in crack gage crack growth response was made. Structure flaws of, 1) corner flaw at a hole, 2) through flaws at a hole and 3) center notch		

DD FORM 1 JAN 73 1473 EDITION OF 1 NOV 65 IS OBSOLETE

SECURITY CLASSIFICATION OF THIS PAGE *(When Data Entered)*

flaw were evaluated. The cyclic test loading included constant amplitude of two R ratios and three representative aircraft usage flight profiles. Strain gage instrumentation was used to measure structure stresses and load transferred into the crack gages.

FOREWORD

The experimental research program reported herein was the responsibility of the Test Engineering Unit of the Boeing Wichita Company. The work was conducted in the time period from 1 July 1977 to 1 December 1978. The work was performed to fulfill the requirements of the Air Force Materials Laboratory Contract F33615-77-C-5073.

A. F. Grandt was the AFML technical monitor. Dr. Grandt's guidance and interest were of great benefit to the program. Gary G. Cassatt of the Test Engineering Unit was the principal investigator for Boeing Wichita and all aspects of this program were conducted under his direction.

Specimen fabrication and preparation were performed by personnel of the Structures Laboratory of the Boeing Wichita Company.

Analytical contributions were the product of Ramesh Shah of BMAD, Boeing Aerospace Company of Seattle, Washington. Dr. Shah's contributions added much to the success of the program.

Program Management was the responsibility of Jack L. Bickhard of the Boeing Wichita Company.

Significant effort was supplied by Bill Evans and Betty Dunegan for data processing and report preparation. The publication of the final report was accomplished by the Industrial Graphics Department.

TABLE OF CONTENTS

TABLE OF CONTENTS (Continued)

TABLE OF CONTENTS (Continued)

LIST OF ILLUSTRATIONS

LIST OF ILLUSTRATIONS (Continued)

LIST OF ILLUSTRATIONS (Continued)

LIST OF TABLES

NOMENCLATURE

Symbol	Description	Units
a	Crack Length	mm (Inches)
A	Cross Section Area	
ASIP	Aircraft Structural Integrity Program	
b	One Half of Width W	mm (Inches)
B	Back (Side 2) Location or Thickness	mm (Inches)
BAC, BMS	Boeing Company Specifications	---
BMAD	Boeing Military Airplane Development	---
BWC	Boeing Wichita Company	---
c	Crack Length on Surface Out of Hole	mm (Inches)
CA	Constant Amplitude	
CNS	Center Notch Stepped	---
CPM	Cycles Per Minute	Hz
da/dn	Crack Growth Rate	mm/cy(in/cy)
DFHS	Double Flawed Hole Stepped	---
E	Elastic Modulus in Tension	M Pa (PSI)
EDM	Electrical Discharge Machining	---
F	Front (Side 1) Location	---
FPL	Forest Products Laboratories	---
H	Unbond Length or Height	mm (Inches)
IN	Inches	---
k	Structure Spring Constant	kn/mm (Pounds/Inch)
K_I, SIF	Stress Intensity Factor	M Pa$\sqrt{m}$(PSI$\sqrt{IN}$)
K_{TH}	Threshold Stress Intensity Value	---
L	Length	mm (Inches)
mm	Millimeters	---
MTS	MTS System Corporation, Minneapolis, Minn.	---
P	Load	kN (Lbs.)

NOMENCLATURE (Continued)

Symbol	Description	Units
PABST	Primary Adhesive Bonded Structure	---
PSI	Stress	M Pa (Lbs/In^2)
R	Ratio of Minimum Load to Maximum Load	---
R.H.	Relative Humidity	---
SENCT	Single Edge Notch Constant Thickness	---
SENS	Single Edge Notch Stepped	---
t	Thickness	mm (Inches)
URS	Unflawed Reference Stepped	---
v	Displacement	mm (Inches)
W	Width	mm (Inches)
σ	Stress	M Pa (PSI)
Δ	Deflection	mm (Inches)

Subscripts

S	Structure
G	Gross Area
g	Crack Gage
O	Average
T	Total
N	Net Section

SECTION I

INTRODUCTION

The current Air Force philosophy on structural integrity relies heavily on the use of damage-tolerance design requirements defined in USAF Document MIL-A-83444 (Reference 2) to protect safety-of-flight structure from catastrophic failure. Damage tolerance is defined as the ability of the airframe to resist failure due to the presence of flaws, cracks or other damage for a specified period of unrepaired usage. The damage-tolerance design requirements are based on the hypothesis that initial flaws exist in the structure, and that these flaws grow during operational use under the influence of repeated stress cycles, thermal, chemical and other environmental factors that vary with usage.

The overall airplane structural integrity program requirements for Air Force aircraft are defined in USAF Document MIL-STD-1530A (Reference 3). These requirements include an individual airplane tracking program to predict the potential flaw growth in critical areas of each airframe. The potential flaw growth is monitored and compared with the growth limits specified in MIL-A-83444. Results from the individual airplane tracking program will be used by the Air Force to aid in making Force Management decisions throughout the operational life of the airplane.

The test program was initiated to evaluate the applicability of using a bonded-on-crack-gage to relate flaw growth in the crack gage to flaw growth in the airframe critical areas.

1. BACKGROUND

The influence of crack growth and brittle fracture has been recognized for three decades. The Comet failures of the 1950's and the experience with high-performance military and civilian aircraft in the fifties and sixties brought the problem of crack propagation and brittle fracture into focus. Since that

time, extensive effort has been expended by industry and government agencies to understand fracture and crack propagation. These efforts have been primarily directed at understanding material properties, more specific definition of aircraft usage, and attempts to analytically predict crack growth rates, safe inspection levels and critical flaw sizes.

A new philosophy and approach to structural safety, durability, and Force Management have been developed and adopted by the United States Air Force. The overall requirements for an aircraft structural integrity program based on this new philosophy are delineated in MIL-STD-1530A.

Damage tolerance design requirements for safety of flight structure are defined in MIL-A-83444. For compliance with this specification, the assumption must be made that initial flaws exist in the most critical location at each major structural component. Further requirements are that the flaws will not grow beyond limits specified in MIL-A-83444, which are dependent on the degree of inspectability, inspection interval, and design concept applicable to the structure.

An individual airplane tracking program is essential to effective management of a fleet of aircraft during operational usage. The objective of the individual airplane tracking program is to predict the cumulative "potential" crack growth in critical areas of each airframe in order to provide a basis for the establishment of inspection and economic repair times. The tracking program also provides data that can be used to predict the effects of changes in usage.

2. PROGRAM OBJECTIVES

The objective of the program described in this report was to obtain experimental data which is adequate to evaluate the applicability of the crack growth gage for tracking structural flaw growth potential.

Included in the program were the following elements:

1. An adhesive system was selected and evaluated for crack gage installations.
2. Five gage designs were evaluated.
3. Stress in each crack gage type was measured by strain gage instrumentation.
4. Experimental testing and measurement of crack growth versus cycles was obtained for a wide range of constant amplitude and spectrum (flight-by-flight) loading.

In addition to presenting a concise assemblage of data for future researchers' analysis and evaluation, it is the purpose of this report to provide a cursory first analysis of the results obtained in light of the program objectives.

3. SUMMARY OF THE FINAL REPORT

This report consists of two volumes. Volume I is the technical report. Volume II contains specimen instrumentation details and tabulations of raw test data.

Volume I includes presentations on test specimen design, test conditions and procedures, instrumentation, test equipment, analytical determination of stress intensity factors and discussion of results.

Volume II segregates the test data into the stress-survey test, strain gage measurements, crack propagation data of the major tests, computer calculations and plots of K_{MAX} versus da/dn, and crack propagation data from the thin section crack gage material.

The SI system of units is used in Volume I. The raw test data in Volume II is presented in English units as it was recorded.

SECTION II

TEST PROGRAM

1. INTRODUCTION

This program utilized large aluminum plates 9.5 x 305.0 x 914.0 mm (.375 x 12.0 x 36.0 inches) simulating aircraft structure containing holes and flaws. Attached to the simulated structural element were crack gages of five different configurations. These assemblies of flawed plate and crack gages complete with strain-gage instrumentation were tested under constant-amplitude and spectrum-load conditions.

1.1 Purpose

The purpose of the experimental testing was to obtain data which can answer the following questions:

A. Is the gage-crack-versus-structural-crack relationship independent of load history?

B. Is the gage-attachment method capable of reproducibly introducing a known load into the gage during the cyclic life of the crack gage?

C. Does the analytical model of Reference 6 provide a resonable estimate of the relationship between gage and structural crack lengths? Is such a relationship repeatable and predictable?

D. Does the crack gage provide a means for estimating the structural-crack size? To what accuracy and sensitivity can the structural crack size be estimated by the crack gage?

1.2 Scope

This program included six of the structural element/crack-gage specimen tests. Three of the tests were conducted under constant amplitude loading and three were tested under spectrum (flight by flight) loading. The constant amplitude loading was conducted at R ratios of .05 and .33. Two specimens were tested at the R ratio of 0.05.

The spectrum load conditions consisted of a KC-135 tanker full-scale-wing cyclic test spectrum, a fighter flight profile and a KC-135 fin spectrum. Crack gages were evaluated in both the constant-thickness and equal-neck-down (stepped) design. The constant-thickness-gage design utilized a single-edge-notch flaw. The neck-down type crack gages were tested 1) without any flaws for reference and adhesive evaluation, 2) with a single-edge notch, 3) with a center-notch flaw and 4) with a double-flawed hole. A matrix describing each test and its associated conditions is presented in Table 1.

In addition to the six tests described, six small-coupon tests in the crack-gage thickness with a center notch were tested to evaluate da/dn characteristics of the crack-gage material. Before any of the matrix testing was started, a stress survey was conducted to evaluate basic panel stress field values at each flaw location.

Table 1.

Test Matrix, Crack Gage Evaluation Program

Specimen and Test Number	Alloy	Fatigue Testing									Crack Gage Testing				
		Constant Amplitude [3]		Spectrum Loading			Flaw Sizes (mm) and Numbers				Constant Thickness		Stepped Design		
		R=.05	R=.33	KC-135 Wing [1]	Fighter [2]	KC-135 Fin [4]	.13	.50	1.0	5.1	H/W=.375	H/W=1.0	Center Notch	Edge Notch	Notched Hole
1	7075-T651	X					2		2	1	2		2	2	2
2			X				2		2	1	2		2	2	2
3				X				2	2	1		2	4	2	
4					X			2	2	1		2	2	4	
5		X						2	2	1		2	4	2	
6	7075-T651					X		2	2	1		2	4	2	

[1] KC-135 5.1-Hour Tanker Mission Profile

[2] Fighter Flight Profile

[3] σ_{max} = 68.95 MPa (10 KSI)

[4] KC-135 Fin Spectrum, Climb Segment, 297 Kips Gross Weight

2. TEST SPECIMEN DESIGN

All test structural elements; the large plate, crack gages and thin section da/dn coupons were taken from a single sheet of 9.5-mm (0.375-In.)-thick 7075-T651 aluminum.

2.1 Alloy Selection

The 9.5-mm-thick 7075-T651 aluminum plate was obtained from Boeing material stock. It was a stretcher-leveled, skin-quality, bare plate manufactured by the Reynolds Aluminum Company. This material and thickness were selected to be representative of large transport aircraft primary wing structure.

2.2 Simulated Structural Component

The simulated structural component utilized was a rectangular plate 254-mm (10.0-In.)-wide in the test area flaring to 305-mm (12.0-In.)-wide in the end grip area. Specimen length was 914-mm (36.0-In.). The plate was used in the full 9.5-mm "as rolled" thickness.

Specimen dimensions were chosen to provide a large width and length to minimize free edge and end effects during peak loads. This specimen size allowed room sufficient for multiple flaws and multiple crack gage installations on a single component without undue influence from flaw to flaw or crack-gage to crack-gage.

The simulated structural element contained flaws of three discrete geometries. They consisted of two 6.4-mm (0.25-In.) holes with corner flaws in the range of 0.1 to 0.5-mm (0.005 to 0.02-In.); two 6.4-mm holes each with a single 1.0-mm (0.04-In.) through-the-thickness flaw and a single 0.1 x 5.0-mm (0.005 x 0.2-In.) through-the-thickness center-notch EDM slot. See Figure 1 for details on specimen fabrication.

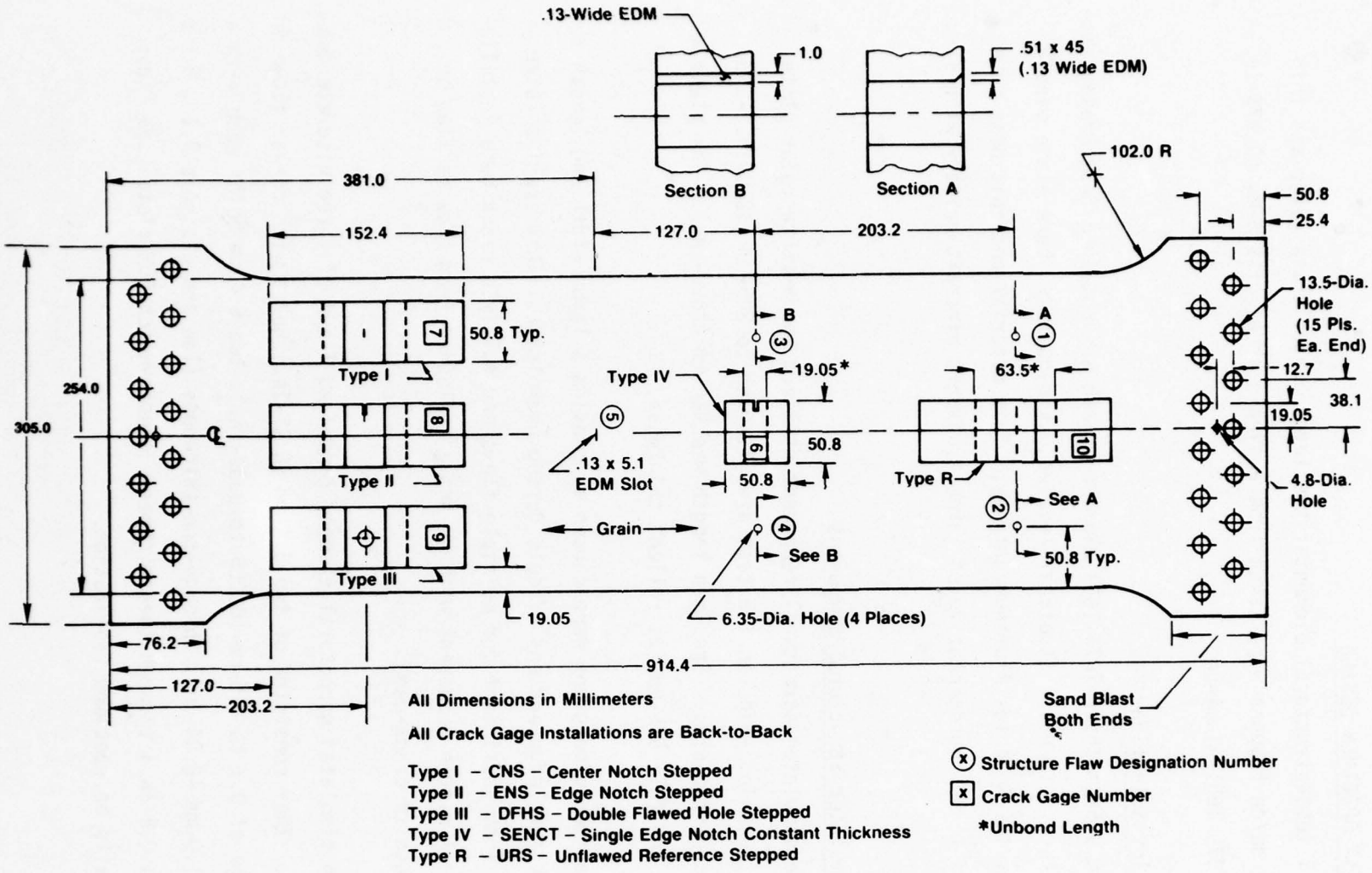

Figure 1. Crack Gage Evaluation Specimen

2.3 Stress Survey Specimen

A specimen identical (except for holes and flaws) to that used for the crack-gage-evaluation testing was utilized. Unflawed crack gages were bonded onto the plate at the proper locations. Strain gages were applied to measure basic panel gross area stress, stress at each proposed flaw location, and on the crack gages. See Section II of Volume II for complete details on the stress survey specimen fabrication and installation.

2.4 Thin-Section da/dn Coupon

These test coupons were fabricated by the same techniques used for making the crack gages. They consisted of 2.54-mm (0.10-In.)-thick end sections and a 0.50-mm (0.02-In.) thick, neck-down section. The neck-down test section was 37.6-mm (1.48-In.)-wide by 56.4-mm (2.2-In.)-long for an H/W ratio equal to 1.50. A 0.13-mm (0.005-In.)-wide by 2.54-mm (0.10-In.) EDM center notch was installed as a starter flaw. See Figure 2 for specimen details.

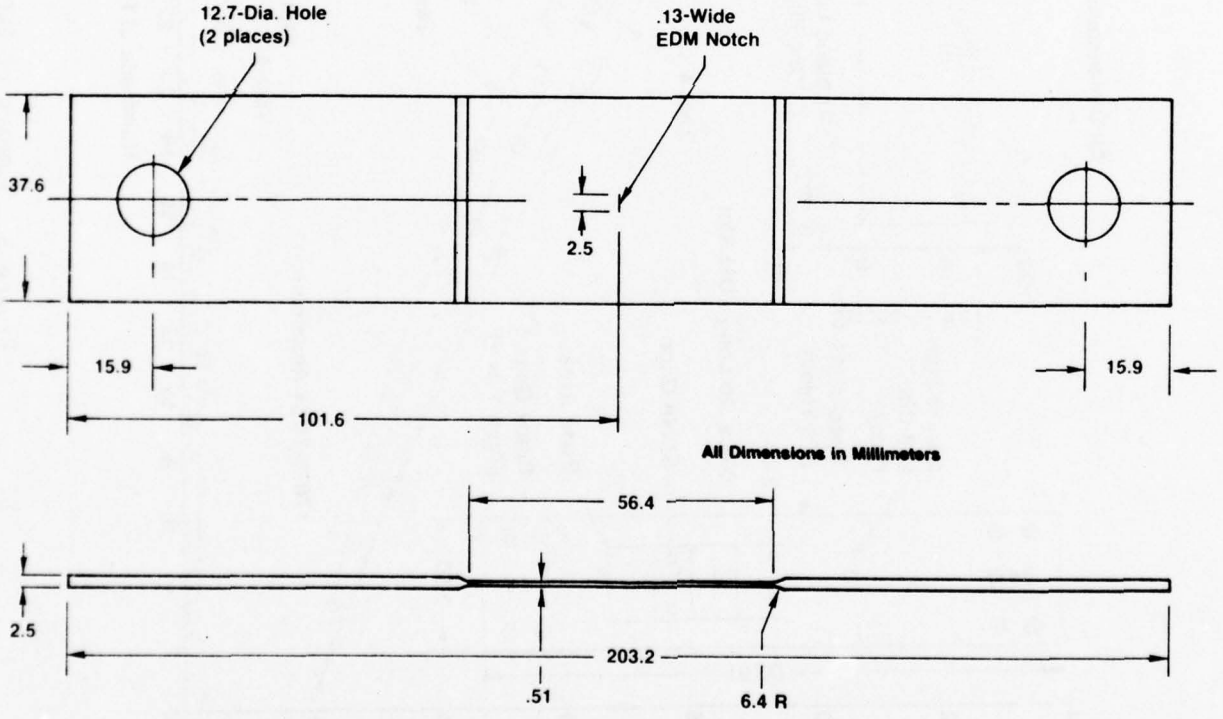

Figure 2. Thin Section da/dn Coupon

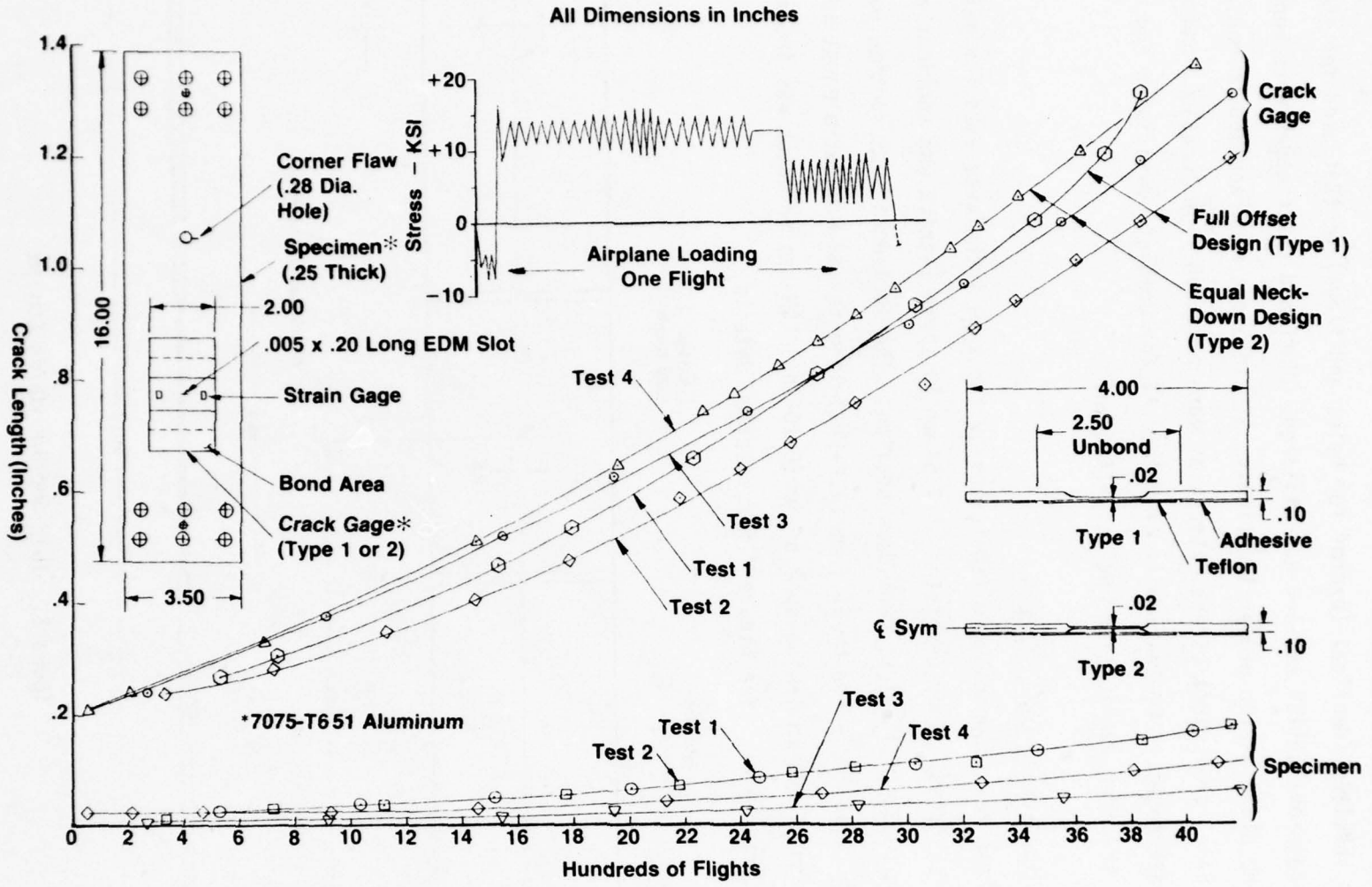

Figure 3. Summary of BWC 1977 Crack Gage IR&D

2.5 Crack Gage Design

Three types of through-the-thickness flaw geometries were utilized in this program. They are: (1) center-notch type, (2) single-edge-notch, and (3) cracks emanating from a central hole. The edge-notch was used in both a constant-thickness and an equal-neck-down (stepped) design. The constant-thickness designs are derivatives of the "fatigue damage indicator" described in U.S. Patent No. 3,979,949 described in Reference 4.

The neck-down (stepped) design is a concept developed at the Boeing Wichita Company. The neck-down design provides the increased sensitivity to track flaw growth from the center notch and through flaws at holes. A patent is pending on the neck-down-designed crack gage.

The stepped crack-gage design used in the performance of this program was an iteration of design improvement over the full-offset design presented at the start of the program. That iteration in design was the result of Boeing Wichita Company IR&D efforts in progress at the time. A summary of those studies is presented in Figure 3. It was found that both the full-offset design and the symmetrical-neck-down design gave similar results. It was also found that the symmetric design had sufficient compression stability and less bending under tension loading that did the full-offset design. The taper on the end (Figure 5) of the crack-gage design was added to provide a less severe transition for the adhesive bond shear stress buildup.

All crack gages were machined out from the center one-fourth of the 9.5-mm plate. They were fabricated with the ends extra long and containing (two) 12.7-mm (0.50-In.) holes at each end. The 12.7-mm holes were used to attach the crack gage into a test machine for precracking. Once precracked, the ends were cut off and tapered to complete the fabrication.

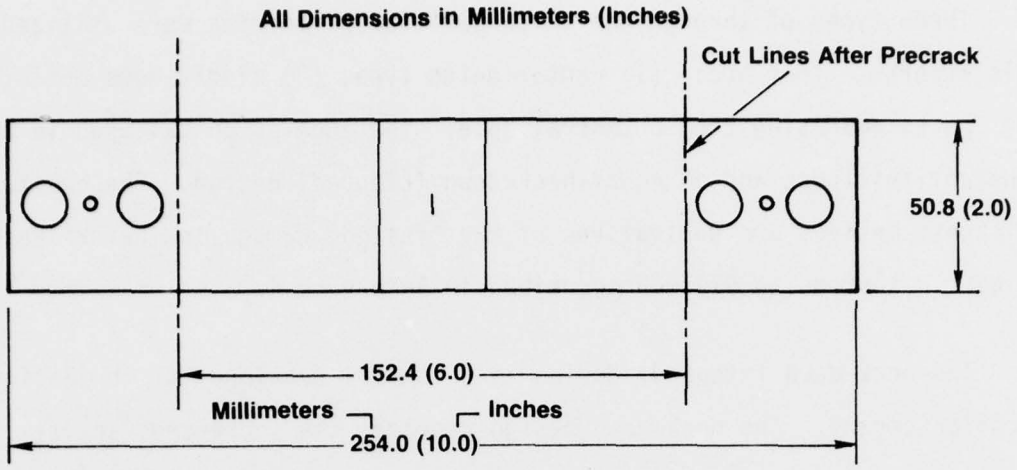

Figure 4. Crack Gage Configuration for Precracking

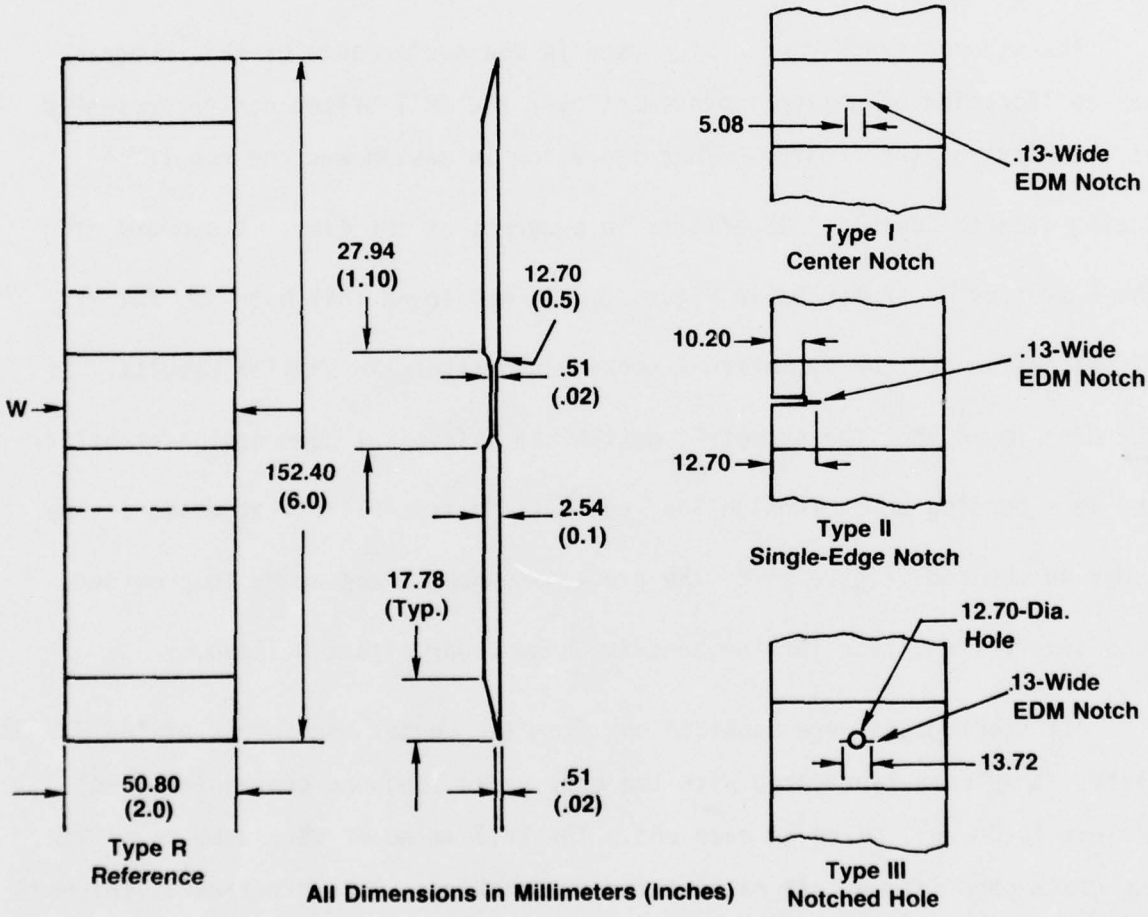

Figure 5. Stepped Design Crack Gage Details

Figure 4 describes the dimensions of a stepped design before precracking. Fabrication details of all crack-gage types in the final machined state are presented in Figures 5 and 6. A matrix summarizing crack-gage usage is presented in Table 2.

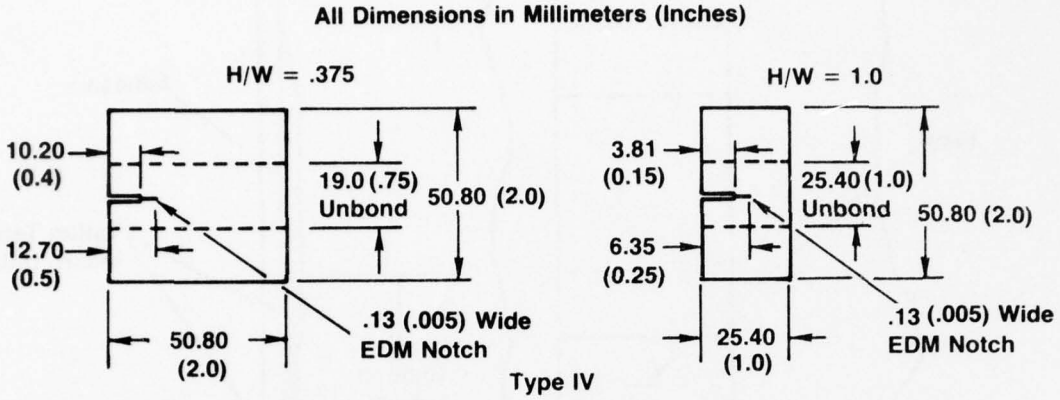

Figure 6. Constant Thickness Crack Gage Details

Table 2. Crack Gage Usage Summary

Test	Specimen	Crack Gage Type at Locations				
		6	7	8	9	10
1	AFCG-1	Constant Thickness H/W = .375	Center Notch (Stepped)	Edge Notch (Stepped)	Double Notched Hole (Stepped)	Reference (Stepped)
2	AFCG-2	Constant Thickness H/W = .375	Double Notched Hole (Stepped)	Edge Notch (Stepped)	Center Notch (Stepped)	Reference (Stepped)
3	AFCG-3	Constant Thickness H/W = 1.0	Reference (Stepped)	Edge Notch (Stepped)	Center Notch (Stepped)	Center Notch (Stepped)
4	AFCG-4	Constant Thickness H/W = 1.0	Edge Notch (Stepped)	Reference (Stepped)	Center Notch (Stepped)	Edge Notch (Stepped)
5	AFCG-5	Constant Thickness H/W = 1.0	Center Notch (Stepped)	Edge Notch (Stepped)	Center Notch (Stepped)	Reference (Stepped)
6	AFCG-6	Constant Thickness H/W = 1.0	Center Notch (Stepped)	Edge Notch (Stepped)	Center Notch (Stepped)	Center Notch (Stepped)

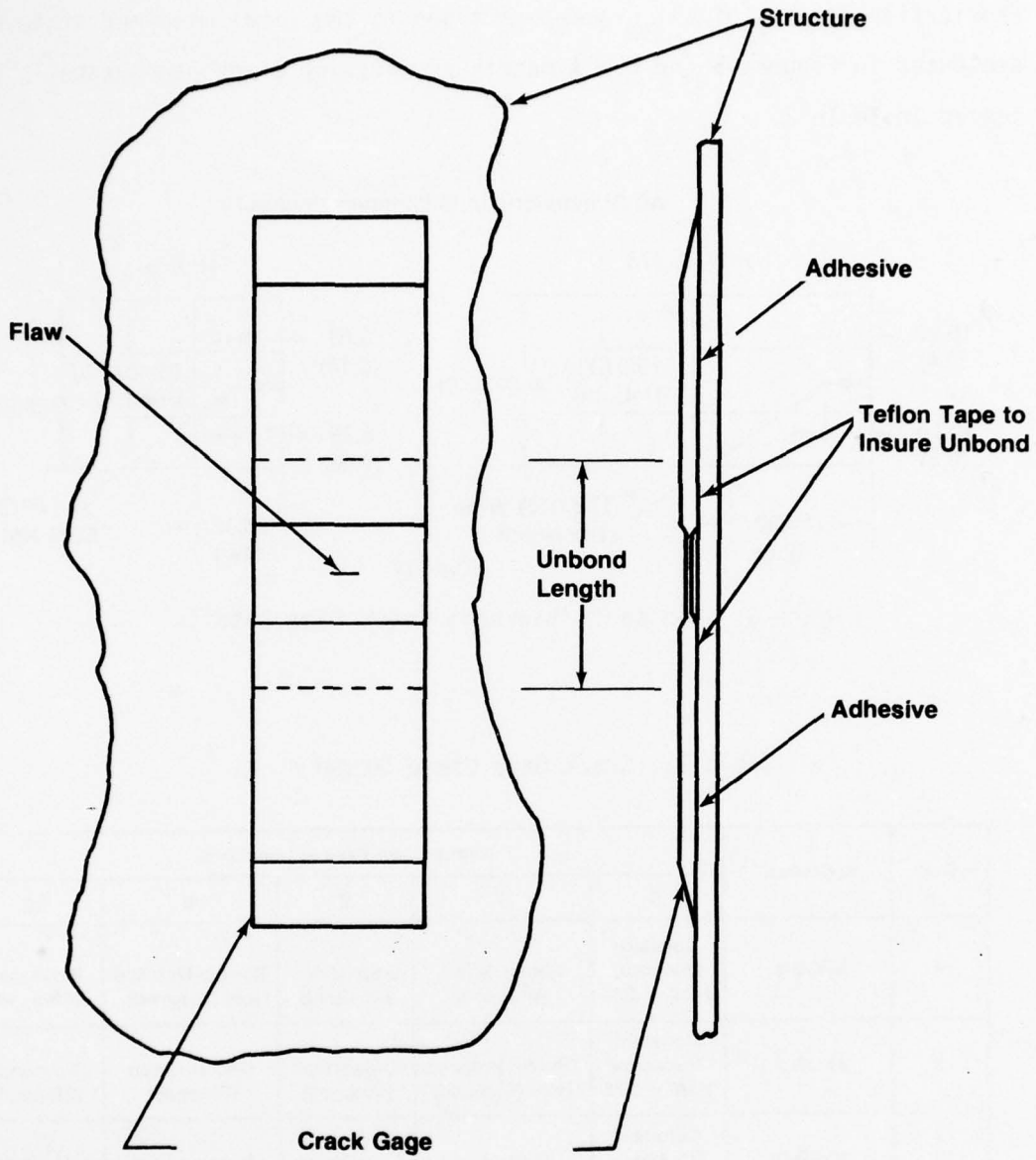

Figure 7. Crack Gage Concept

2.6 Adhesive System

The adhesive system used in this program is that technology known by the trade name "PABST". This technology, "PABST", is the product of an Air Force development program for "Primary Adhesive Bonded Structure", (Reference 8). Basically, this adhesive system consists of doing an FPL sodium hydroxide etch, a phosphoric acid anodize, application of a corrosion-inhibiting primer, followed by bonding with FM-73M heat cure structural adhesive.

In this program, the phosphoric acid anodizing followed BAC 5555 Specifications. Priming of the anodized surfaces was by spray application of BR-127 procured to Boeing Specification BMS 5-89. The adhesive FM-73M is a product of the Cyanamid Company. It is a modified epoxy adhesive with a random Dacron mat carrier. Grade 5 (0.1-mm-thick) was used in this program. The film adhesive was qualified to BMS 5-101 and cured per BAC 5514. Acceptance testing on standard single-shear coupons gave shear-stress strengths above 39.9 MPa (5.8 KSI).

A typical crack-gage installation is described in Figure 7.

The following list and Figures 8, 9, and 10 describe the essential ingredients and steps used to bond the crack gages onto the structural plates.

PABST ADHESIVE SYSTEM

BASIC INGREDIENTS

1. CHEMICAL CLEAN & FPL ETCH
   a. Vapor Degrease (Tri-Clorethylene)
   b. Nitric Acid Clean (15 minutes). Removes all organic materials
   c. Water Rinse
   d. Caustic Etch - Sodium Hydroxide Solution
   e. Water Rinse and Air Dry

2. PHOSPHORIC ACID ANODIZE
   a. 20 to 25 Minutes Immersion (See Figure 8)
   b. Conduct Tests
      1. Visual, Purple Haze (See Figure 9)
      2. Adhesive Tape, Adhesive Stays on Part
   c. Water Rinse and Dry at 200-250°F for 20 to 30 minutes, Return to Room Temperature
   d. Spray on BR-127 Primer, 1/2 to 1 Mil Thick (2 Hours Maximum Between Anodize and Prime)

3. BOND
   a. Cut Cold FM-73 Sheet to Size, Insert Between Parts
   b. Bag and Install in Autoclave (See Figure 10)
      1. Pull Vacuum
      2. Pressurize Chamber to 40 to 50 psi
      3. Open Vacuum Line
   c. Bond at 225-250°F for 90 Minutes
   d. Return to Room Temperature. Ready for Use.

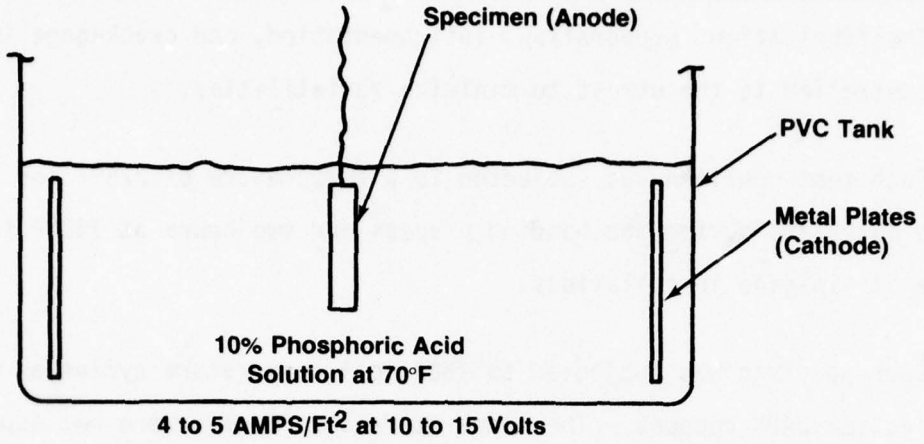

Figure 8. Phosphoric Acid Anodize Setup

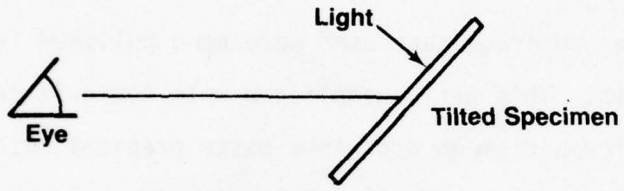

Figure 9. Visual Test for Anodize Quality

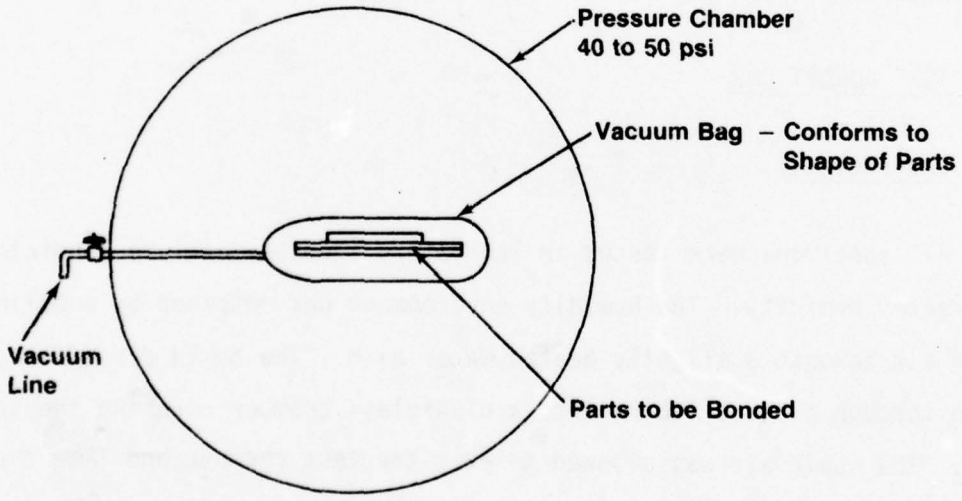

Figure 10. Bonding Autoclave Schematic

2.7 Specimen Preparation and Crack Gage Installation

The fabrication, preparation, instrumentation, and crack-gage installation were controlled to the utmost to minimize variabilities.

Each test specimen was subjected to a temperature of 225°F for 90 minutes in the autoclave during the bonding process and two hours at 140°F for curing of the strain-gage installations.

Each specimen was subjected to identical temperature cycles as was the thin-section DADN coupons. The temperature cure cycles were not expected to affect the material behavior but keeping the temperature time history identical on all test articles should eliminate any possible concern.

Each specimen and crack gage used were hand polished in the areas of expected crack growth. This was accomplished with 400-grit sand paper and water followed by a 1 micron diamond dust in a paste preparation. The diamond paste is a product of the Buehler Ltd. Co. Polishing is necessary to adequately define crack lengths. Areas where the specimen fit into the test machine were sandblasted to enhance the friction gripping action of the end fittings. All specimens were vapor degreased before testing.

3. TEST CONDITIONS

3.1 Environment

All specimens were tested in laboratory room temperature conditions at 90% or greater humidity. The humidity environment was obtained by bubbling bottled clean air through a slightly heated water bath. The humid air effluent was then piped through plastic tubing into a plexiglass chamber covering the specimen test area. The humid air was allowed to exit the test chamber and flow through a small auxiliary chamber containing a humidity sensor. By maintaining a slight

air flow and a 1 to 2°C water temperature increase above room temperature, the required humidity of greater than 90% was maintained. The 90% humidity was selected because it was desirable to eliminate the humidity variable in this program and it is more representative of actual aircraft crack growth environment than dry or laboratory room air conditions.

3.2 Cyclic Rates and Crack Monitoring

The constant-amplitude testing on the thin-section DADN specimens was conducted at 8 Hz (480 cpm). The cyclic rate used on all other tests was 5 Hz (300 cpm). All cracks were measured with Gaertner 50X measuring microscopes.

3.3 Spectrum Load Definition

This section contains descriptions of the spectrum (flight-by-flight) loadings used in this program on Specimens AFCG-3, AFCG-4 and AFCG-6.

The KC-135-wing-spectrum test on AFCG-3 utilized actual stress values measured by a strain gage at Lower Wing Skin Station 340 near Stiffener S-8 during the 1972 full-scale cyclic test conducted at BWC. See Figure 11 and Table 3 for definition of that spectrum.

The fighter spectrum (See Table 4 and Figure 11a) utilized on Specimen AFCG-4 came from Reference 9. The limit load stress was lowered from 213 to 122 MPa (30.9 to 17.65 KSI) for Test 4 to keep the maximum stress in agreement with the maximum experienced for the KC-135 cyclic test spectrum.

The fin spectrum for AFCG-6 came from a mission segment defined during the performance of "The Influence of Fleet Variability on Crack Growth Tracking Procedures for Transport/Bomber Aircraft" program (Reference 5). It is defined in Figure 12 and Table 5.

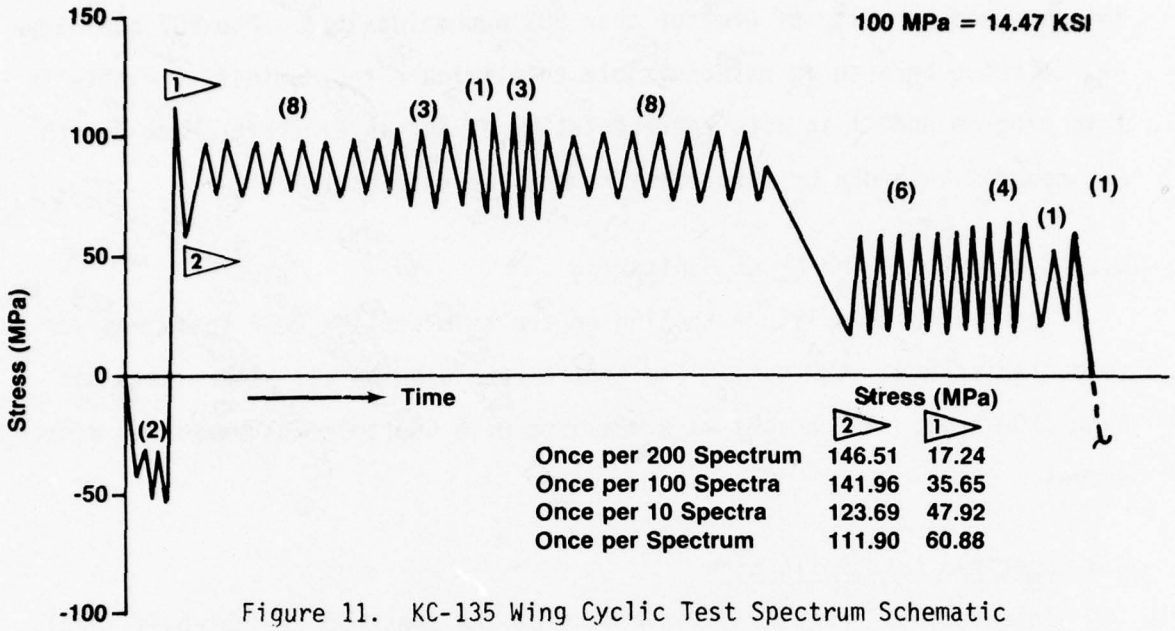

Figure 11. KC-135 Wing Cyclic Test Spectrum Schematic

Table 3. KC-135 Wing Cyclic Test Definition

Stress Number	Maximum Stress (MPa)	Minimum Stress (MPa)	R	Number of Cycles
1	-29.72	-53.64	1.81	2
2	111.90 [1]	60.88 [2]	.54	1
3	97.01	75.08	.77	8
4	103.42	69.43	.67	3
5	106.94	67.29	.63	1
6	109.07	63.78	.58	3
7	101.28	72.26	.71	8
8	58.05	16.00	.28	6
9	63.78	16.00	.25	4
10	53.09	20.89	.39	1

100 MPa = 14.47 KSI

	Stress (MPa) [1]	Stress (MPa) [2]
Once per 200 Spectra	146.51	17.24
Once per 100 Spectra	141.96	35.65
Once per 10 Spectra	123.69	47.92
Once per Spectrum	111.90	60.88

Table 4. Fighter Spectrum Definition

Load Layer	Load* (% Limit) Max.	Load* (% Limit) Min.	Cycles Per Mission	Step	Load* (% Limit) Max.	Load* (% Limit) Min.	Cycles per Mission
1	63.2	17.5	10	34	103.1	5.8	1
2	55.3	17.5	9	35	70.8	3.4	5
3	70.8	3.4	1	36	47.0	16.4	4
4	28.9	13.2	13	37	46.5	-18.9	1
5	70.8	3.4	1	38	37.5	17.5	5
6	37.5	17.5	39	39	63.2	17.5	1
7	70.8	3.4	1	40	28.9	13.2	1
8	84.8	7.0	1	41	47.0	16.4	16
9	47.0	16.4	18	42	70.8	3.4	3
10	37.5	17.5	39	43	55.3	17.5	13
11	28.9	13.2	26	44	37.5	17.5	39
12	76.4	4.6	1	45	28.9	13.2	13
13	47.0	16.4	18	46	47.0	16.4	18
14	28.9	13.2	13	47	63.2	17.5	5
15	47.0	16.4	19	48	28.9	13.2	13
16	76.4	4.6	1	49	70.8	3.4	1
17	55.3	17.5	28	50	47.0	16.4	19
18	37.5	17.5	39	51	37.5	17.5	39
19	63.2	17.5	5	52	55.3	17.5	9
20	47.0	16.4	19	53	28.9	13.2	13
21	37.5	17.5	39	54	37.5	17.5	39
22	70.8	3.4	1	55	28.9	13.2	13
23	63.2	17.5	4	56	63.2	17.5	5
24	76.4	4.6	1	57	76.4	4.6	1
25	94.4	14.7	5	58	37.5	17.5	39
26	37.5	17.5	12	59	55.3	17.5	9
27	63.2	17.5	2	60	47.0	16.4	36
28	76.4	4.6	2	61	55.3	17.5	9
29	66.4	22.2	7	62	70.8	3.5	3
30	63.2	17.5	10	63	84.8	7.0	1
31	66.4	22.2	4	64	63.2	17.5	10
32	55.3	17.5	30	65	118.1	4.1	1 Every 6 Starting With 1st Mission
33	47.0	16.4	7	66	120.4	-14.2	1 Every 18 Starting With 18th Mission

*Limit Stress = 122 MPa (17.65 KSI)

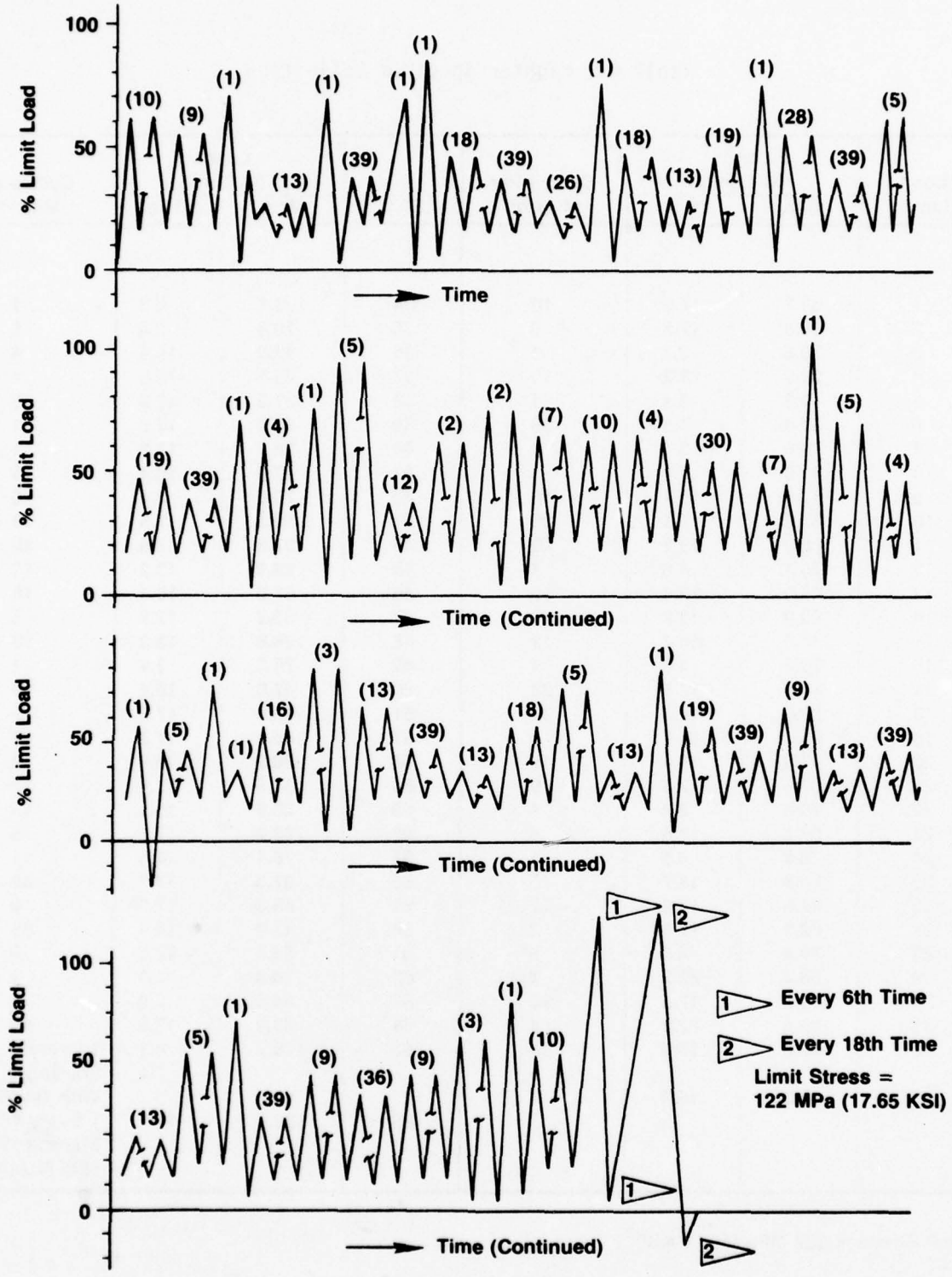

Figure 11a. Fighter Spectrum Schematic

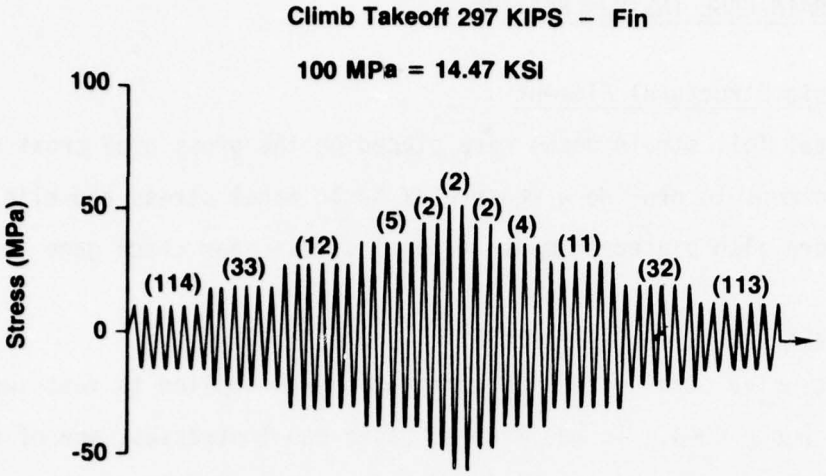

Figure 12. Fin Climb Spectrum Schematic, Takeoff 297 KIPS Gross Weight

Table 5. KC-135 Fin Climb Segment Definition

Stress Number	Maximum Stress MPa	Minimum Stress MPa	R	Number of Cycles
Climb, T.O. 297 KIPS, Fin				
1	13.17	– 13.17	–1.00	114
2	21.99	– 21.99	–1.00	33
3	30.75	– 30.75	–1.00	12
4	39.58	– 39.58	–1.00	5
5	48.33	– 48.33	–1.00	2
6	57.16	– 57.16	–1.00	2
7	48.33	– 48.33	–1.00	2
8	39.58	– 39.58	–1.00	4
9	30.75	– 30.75	–1.00	11
10	21.99	– 21.99	–1.00	32
11	13.17	– 13.17	–1.00	113

100 MPa = 14.47 KSI

4. STRAIN GAGE INSTRUMENTATION

4.1 Basic Structural Element

Metal foil strain gages were placed on the gross area cross section of all specimens to provide a measure of basic panel stress and alignment. Strain gages were also placed to measure panel stress near crack gage locations.

4.2 Crack Gage Load Measurement

Extensive strain gage instrumentation was applied to test specimens AFCG-2, AFCG-3, and AFCG-4. In addition to basic panel stresses, one of each crack gage type was instrumented. The purpose being was to measure crack gage stress distributions and thereby obtain load transferred through each crack gage type. Strain gage installations and the data obtained are described in detail in Section III of Volume II of this report.

5. TEST SETUP AND EQUIPMENT

5.1 Test Machine Description

All crack propagation testing was conducted in a 100 metric ton (220 KIP) capacity MTS Model 810.07 test machine equipped with a Digital Equipment Corporation PDP 11/05 Central Processor. A photograph of this machine is presented in Figure 13.

This system incorporates a BASIC computer language capability, dual drive tape cassette mass storage device and 16K of core memory. Load accuracy was maintained within .25% of operating load range.

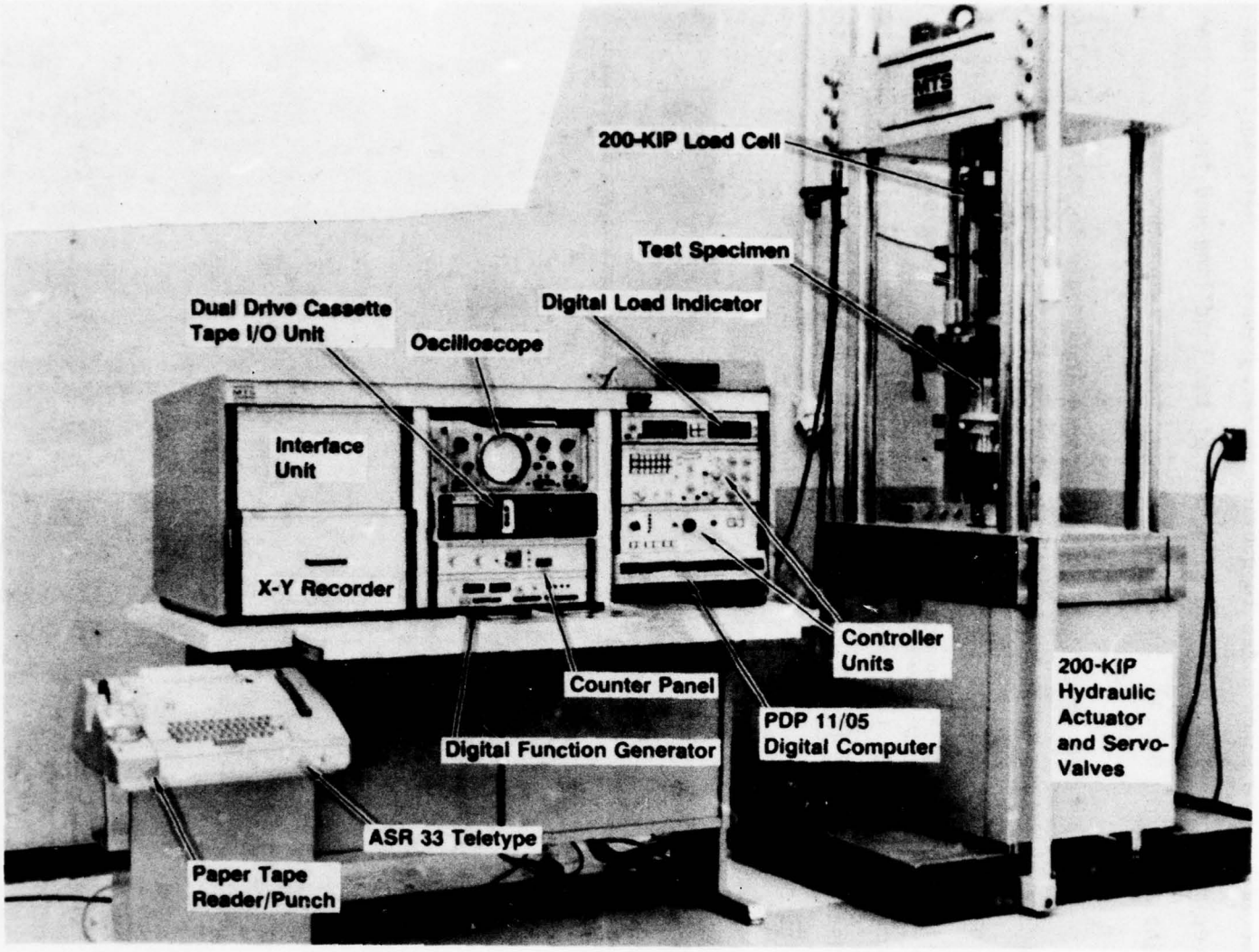

Figure 13. 220-KIP MTS Test System

5.2 Specimen Installation

Grips were utilized which held the specimens by friction. The ends of the specimens were sandblasted to provide better gripping. Alignment holes in the specimen and grips permitted alignment of the load line and the specimen centerline to within 0.5-mm (.020-In.).

The specimen length and thickness were inadequate to resist buckling under high compressive loads experienced on the spectrum load tests. Therefore, edge type buckling restraints were used. These consisted of phenolic bars slotted to slide over the specimen edges and stiffened by steel angles. Sheets of Teflon were used between the phenolic bars and the specimen. A view of Specimen AFCG-3 installed in the test machine, complete with buckling restrainers, is shown in Figure 14.

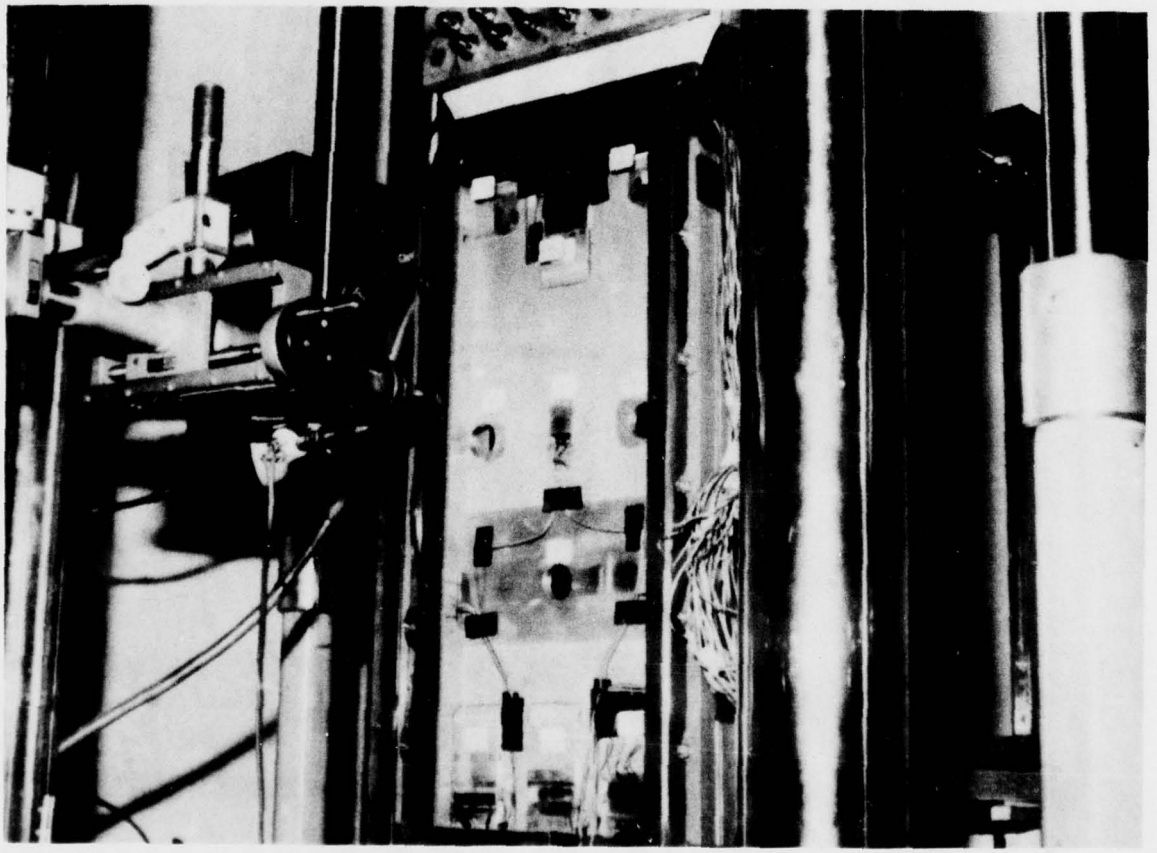

Figure 14. Test Setup - Specimen AFCG-3

5.3 Test Procedures

This section describes the detailed test procedures used to test the specimens of this program.

5.3.1 Stress Survey Specimen

Testing of this panel consisted of 1) applying loads up to 333.75kN (75 KIPS) axial load and recording strain-gage readings at each load increment then 2) removing the crack gages and again recording strain readings at the same load increments.

5.3.2 Precracking of Crack Gages

The crack gages were precracked 0.5-mm (.02-In.) past the EDM notch under constant-amplitude loading. The crack gages were precracked in a Sontag SF10-U Fatigue Machine. Loading was kept low to apply no greater than 11.0 MPa-$m^{\frac{1}{2}}$ (10 KSI $IN.^{\frac{1}{2}}$) stress intensity at the end of the precrack operation. An R ratio of 0.05 was used.

5.3.3 Primary Specimen Testing

A detail description of test procedures is presented in the following list:

1. The appropriate holes, 1 and 2, (Figure 1) were EDM corner flawed 0.5-mm (0.02-In.) maximum.

2. The corner flawed holes were then precracked to 0.5-mm (0.02-In.) maximum crack length. Precracking loads used were constant amplitude providing a basic panel gross area maximum stress of 68.9 MPa (10 KSI) at an R ratio of 0.05.

3. The through flaws at holes 3 and 4 and the center notch flaw at location 5 were then produced by EDM. Precracked flaws at holes 1 and 2 were protected by Chemical milling mastic during the second EDM operation.

4. A second installation into the test machine and precrack effort produced the sharp cracks required at the other flaw locations.

5. Holes 1 and 2 were then reamed oversize to leave 0.1-mm (0.005-In.) on tests 1 and 2 and 0.5-mm (0.02-In.) on tests 3 through 6.

6. Strain gages were then bonded onto the test panel and crack gages.

7. The precracked crack gages were then bonded on according to procedures described in Section 2.6.

8. Instrumentation was completed and the test proper was conducted.

9. The order of testing was as presented in the Text Matrix, Table 1.

The test proper consisted of applying the constant-amplitude or spectrum loading and periodically stopping the test and recording crack lengths. All crack-length measurements were taken while holding at zero load. This was a caution taken to ensure that adhesive creep did not occur while holding at a high positive load condition for long periods of time.

Strain readings were taken at the start of all tests and periodically throughout tests 2, 3 and 4. Test AFCG-4 was stopped short as a result of operator error which caused compression buckling.

5.3.4 Thin Section da/dn Coupons

Testing consisted of applying constant-amplitude loading and periodically recording crack length and cycles. This testing was also conducted in the 220-KIP MTS Machine. A 20-KIP-capacity load cell was utilized with a 4-KIP-load range to provide the necessary load accuracy for these small coupons.

SECTION III

ANALYTICAL CONSIDERATIONS

1. FINITE ELEMENT ANALYSIS OF BASIC PANEL

A finite element analysis was conducted for the basic large 305-mm (12.0-In.) x 915-mm (36.0-In.) plate. Symmetry permitted modeling of one-fourth of the panel. One hundred seventy three (173) nodes and 145 rectangular membrane elements were used in the analysis. Figure 15 describes the analysis model used and presents stress distribution plots for various cross sections through the panel. The analysis was made for an applied load of 333.75 kN (75 KIPS) which corresponded to a panel gross area stress of 137.9 MPa (20 KSI). This analysis shows that the ends of the crack gages are getting into the influence of the eliptical flareout (Section 6). However, by the end of the unbond (Section 5) the stress in the panel varies from 133.1 to 144.8 MPa (19.3 to 21.0 KSI) which is on the order of 5% or less deviation. It was therefore concluded to retain the crack gage placement originally planned and to apply an uncracked gage alternately at each location to measure actual load transfer at each location.

2. STRUCTURAL SPRING ANALOGY OF CRACK GAGES

The concept of using classical analysis equations to relate end deflections to load and stress in crack gages is presented in this section. The following presentation is included to describe aspects of crack gage designs, sensitivity increase of the neck-down (stepped) design and expected load versus crack length response.

The relationship between load P_G in a constant thickness crack gage and the stress σ_S in the structure to which it is bonded is presented as equation 1 (Reference 6)

$$P_G = \sigma_S \, BWf \qquad (1)$$

where f is a complex expression containing material properties and geometry parameters. A somewhat more simplified approach to understanding gage load and stress is presented below.

Consider an uncracked constant thickness gage of unbond length H attached to a structure at a control point experiencing stress σ_S (Figure 16).

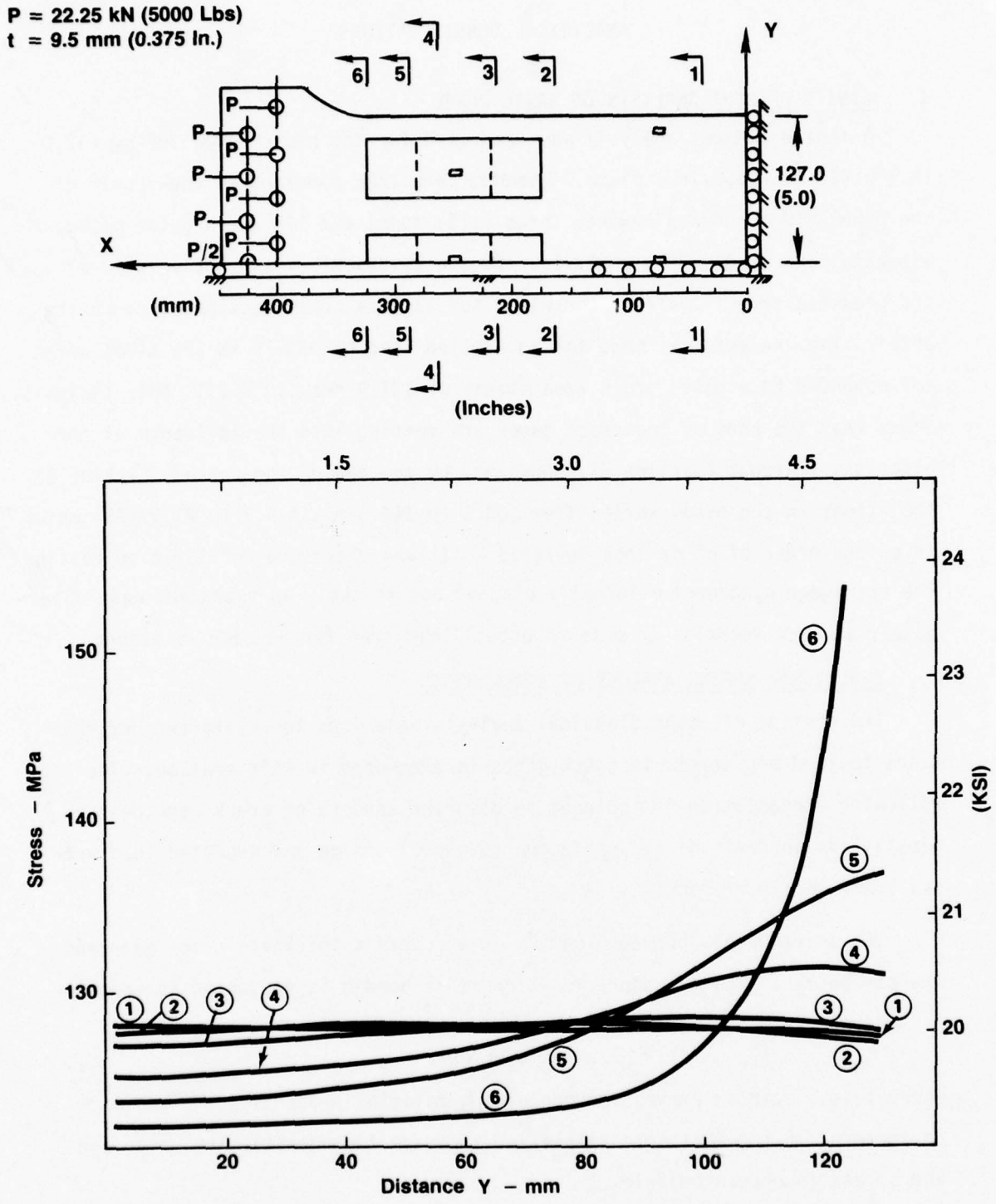

Figure 15. Stress Survey Specimen Model and Results

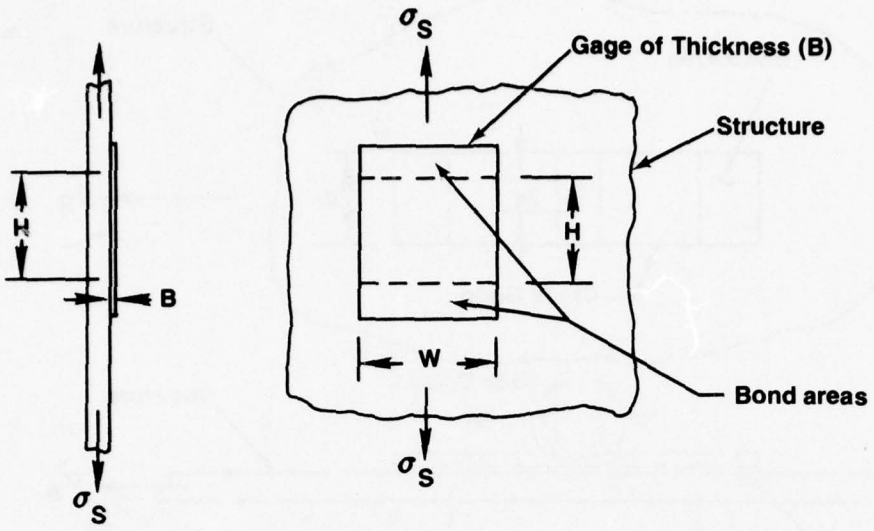

Figure 16. Constant Thickness Crack Gage Concept

For a given stress σ_S, a deflection is associated with the unbond length H. It is

$$\Delta L = \frac{\sigma_S}{E_S} H \tag{2}$$

This deflection becomes the deflection input for the crack gage. The deflection equation for the gage also is of the form $\Delta L = \frac{P_G H}{BW E_G}$. Combining these two equations, the gage load is obtained.

$$\frac{P_G H}{BW E_G} = \frac{\sigma_S H}{E_S}, \quad P_G = \frac{E_G}{E_S} \sigma_S BW \tag{3}$$

Stress in the gage then becomes

$$\sigma_G = \frac{E_G}{E_S} \sigma_S \tag{4}$$

The stress in the gage becomes equal to the structure stress limited only by flexibility of the adhesive bond when the elastic modulus of crack gage and structure are the same.

A stretched spring analogy (Figure 17) is used to demonstrate the ability of the stepped gage concept to increase sensitivity.

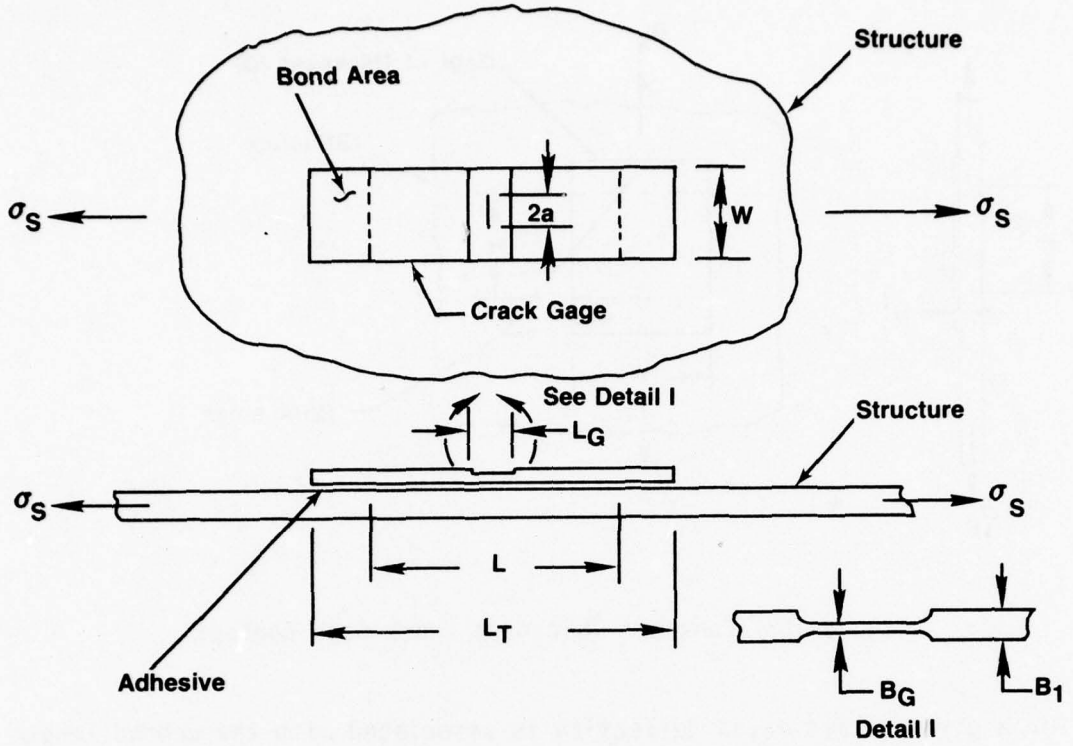

Figure 17. Stepped Crack Gage Concept

Each segment of the stepped gage design can be considered to be a structural spring which follows the relationship $k = P/\Delta$ where k is the spring constant (See Figure 18). For structural elements, $\Delta = \frac{PL}{AE}$ so $k = \frac{AE}{L}$.

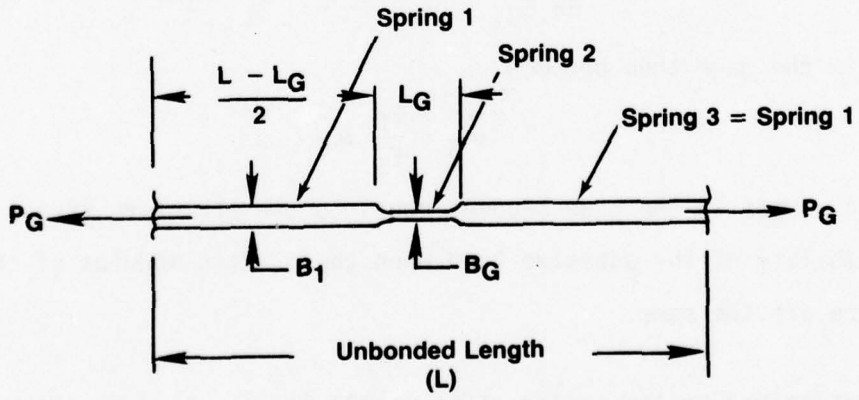

Figure 18. Structural Spring Analogy

The deflection of each spring can be calculated in terms of gage load as follows:

Spring 1 $$\Delta_1 = P_G \left(\frac{L-L_G}{2}\right)/B_1 W E_G \quad (5)$$

Spring 2 $$\Delta_2 = P_G (L_G)/B_G W E_G \quad (6)$$

Also the deflections are related by:

$$2\Delta_1 + \Delta_2 = \Delta_T \quad (7)$$

Combining the above equations results in:

$$\frac{P_G(L-L_G)}{B_1 W E_G} + \frac{P_G(L_G)}{B_G W E_G} = \frac{\sigma_S}{E_S} L \quad (8)$$

Solving for gage load results in the following:

$$P_G = \frac{E_G}{E_S} W\sigma_S L/\left[\frac{L-L_G}{B_1} + \frac{L_G}{B_G}\right] \quad (9)$$

Looking at the specific case of this program where $E_G = E_S$, $B_1 = 5B_G$ $L_G = 27.93$ mm (1.10 In.) and L = 63.5 mm (2.50 In.) the expression reduces to:

$$\sigma_G = \frac{P_G}{B_G W} = 1.81\sigma_S \quad (10)$$

which is a 1.81 factor sensitivity increase over a constant thickness design of the same unbond length.

Calculations were made using the above-described analogy for the reference (unflawed) crack gage used in this program. The results of that exercise are presented as a plot of stress amplification ration versus unbond length in Figure 19. Stress amplification ratio is defined as the ratio of stress in the uncracked reference crack gage to the average stress in the basic panel at the crack gage location.

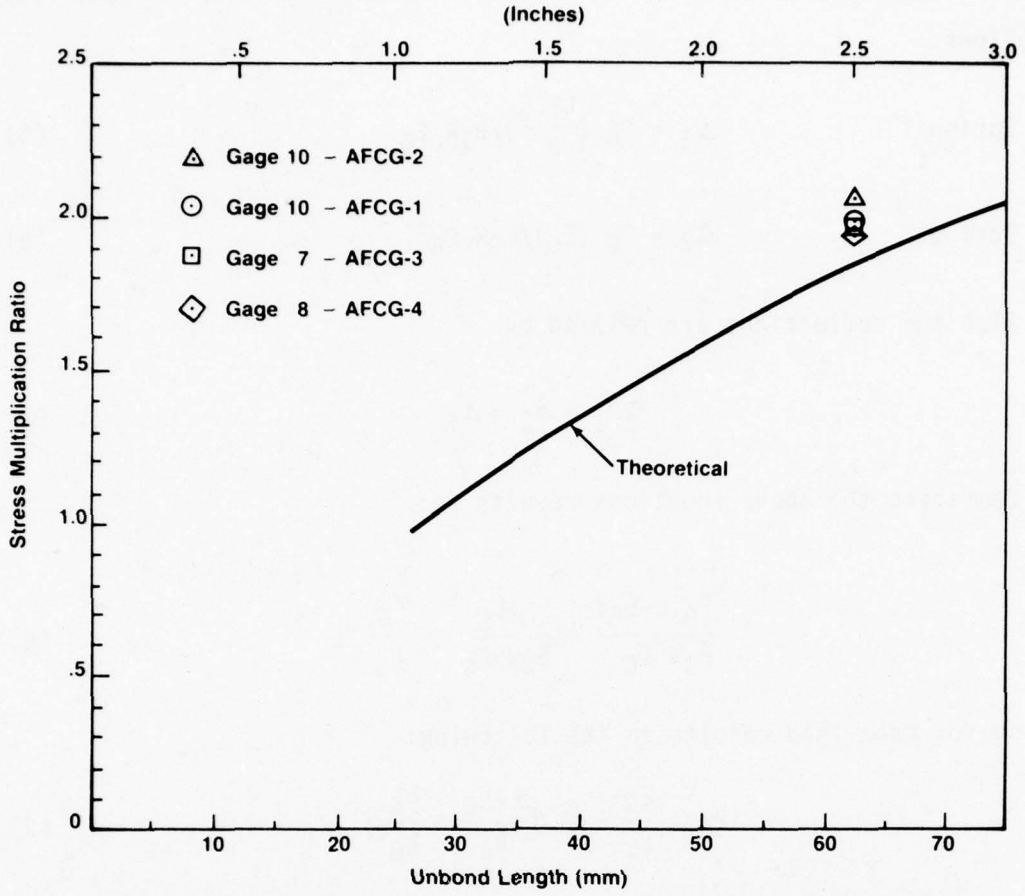

Figure 19. Stress Amplification Plot for Unflawed Stepped Crack Gage

Also plotted on this figure are actual stress amplification ratios obtained from strain gages on the test specimens of this program.

The theoretical calculations ignore any reduction in basic panel stress from load shedding to the crack gage. Including the load-shedding correction would bring the experimental results more in agreement with the theoretical values.

The following discussion expands this concept to a crack gage containing a flaw.

The simplified analogy again would relate load in the crack gage by the spring constant of the uncracked ligament. Considering a center-flawed crack

gage with a flaw extending to 2a/W = .5, the theoretical load would be one-half of that for an uncracked gage. For the stress amplification ration of 1.81 a basic panel stress of 68.95 MPa (10 KSI) and the stepped gages of net section .5-mm (.02-In.) x 50.8-mm (2.0-In.) the gage load would be 3.22 kn (724 pounds) for the uncracked gage and 1.61 kn (362 pounds) for a crack gage with a 2a/W flaw of .5.

The actual load would be expected to be larger than calculated from the uncracked ligament method as that simplified approach ignores stiffness contribution of material above and below the flaw. This expectation is verified later in this report from actual stress measurements taken on crack gages (Figure 52).

3.0 STRESS INTENSITY FACTOR ANALYSES

This section contains the analyses, both classical and numerical, that provide estimates of stress intensities versus flaw length for crack gage designs used in this program. Also presented are the calculations defining stress intensity ranges experienced by the structure flaws.

3.1 Structure Flaws

The stress intensity ranges experienced by each structure flaw throughout its growth during the test have been calculated and are presented below in Table 6.

Table 6. Structure Flaws Stress Intensity Ranges

Flaw Type	Flaw Size mm (Inches)	K Factor Range MPa -m1/2 (KSI - in 1/2)	
		Max = 68.95 MPa (10.0KSI)	Max = 146.5 MPa (21.25 KSI*)
Center Notch	5.1 (.20) 25.4 (1.00)	6.15 (5.6) 13.74 (12.5)	13.08 (11.9) 29.19 (26.56)
Thru Flaw at Hole	1.0 (.04) 20.4 (.80)	8.10 (7.37) 13.96 (12.70)	17.21 (15.66) 29.66 (26.99)
Corner Flaw	0.1 (.005) 5.10 (.20)	3.02 (2.75) 7.36 (6.70)	6.42 (5.84) 13.45 (12.24)

*Once per 200 Flight Stress on KC-135 cycle test spectrum

The equations used in the analysis were taken from pages 6, 7 and 8 of NASA TN D-8244 (Reference 11) and are presented below.

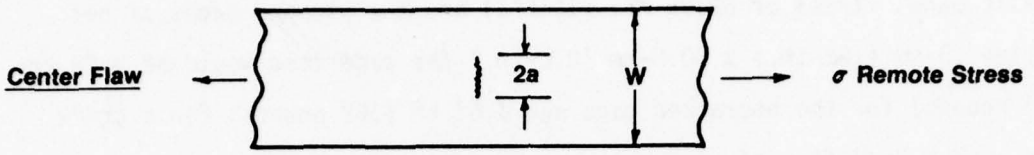

$$K_I = \sigma\sqrt{\pi a}\ \sqrt{\frac{w}{\pi a}\tan\frac{\pi a}{w}} \quad \text{(IRWIN)} \qquad (11)$$

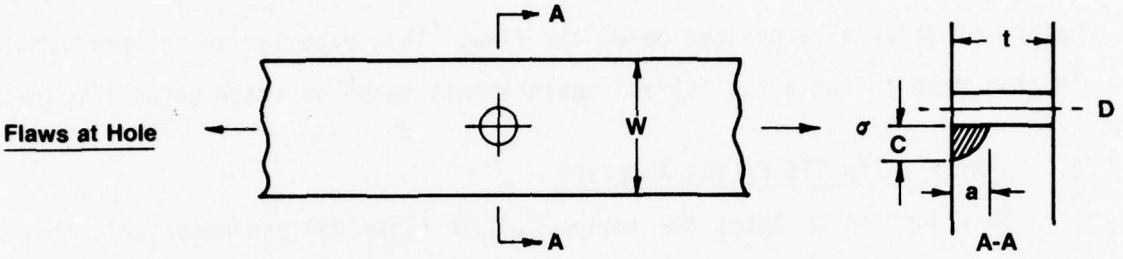

$$K_I = \sqrt{\pi \frac{a}{cQ}}\ \text{me}\ f_b\ \sqrt{\sec\frac{\pi D}{2w}} \qquad \text{Where} \qquad (11a)$$

$$M_e = \left[M_1 + \left(\sqrt{\frac{Qc}{a}} - M_1\right)\left(\frac{a}{t}\right)^p\right] \text{ fw,}$$

$$P = 2 + 8\left(\frac{a}{c}\right)^3 \text{ , fw} = \sqrt{\sec\left(\frac{\pi}{2} - \frac{D + bc}{w - 2c + bc}\sqrt{\frac{a}{t}}\right)}$$

$$M_1 = 1.2 - 0.1\frac{a}{c} \qquad a/c \leq 1.0 \text{ Corner Flaw}$$

$$M_1 = \sqrt{\frac{c}{a}}\left(1 + 0.1\frac{c}{a}\right) \qquad a/c > 1.0 \text{ Thru Flaw}$$

$$Q = 1 + 1.47\left(\frac{a}{c}\right)^{1.64} \qquad a/c \leq 1.0 \text{ Corner Flaw}$$

$$Q = 1 + 1.47\left(\frac{c}{a}\right)^{1.64} \qquad a/c > 1.0 \text{ Thru Flaw}$$

$$f_b = 0.707 - 0.18\lambda + 6.55\lambda^2 - 10.54\lambda^3 + 6.85\lambda^4 \quad \text{Where} \quad \lambda = \frac{1}{1 + \frac{2c}{D}}$$

These equations do not account for the eccentricity for the hole flaws not being on panel centerline. The deviation is expected to be negligible for the flaw lengths used in this program. A width (W) of 101.6-mm (4.0-In.) was used in the hole flaw calculations.

3.2 Constant-Thickness Crack Gage

Finite element analyses were conducted under Boeing Company BMAD/IR&D to determine the stress intensity factors of the constant-thickness crack gages used in this program. This analysis approach presented here is also explained in more detail in Reference 12.

Stress intensity factor (SIF) solutions for a rectangular single-edge cracked specimen subjected to uniform normal displacements (fixed-grip conditions) were not available previous to this program. These solutions were needed to determine the crack-gage response and were derived by finite element techniques.

Finite element analyses were conducted for the crack gage in Figure 20 for H/W ratios of 2.0, 1.0 and 0.5 and a/W ratios of 0.1 to 0.8. Since the specimen is symmetric with respect to the x-axis, one-half of the specimen was idealized with rectangular plate elements for the membrane analysis only. Finite element idealizations consisted of 275 to 425 nodes and 234 to 384 rectangular elements depending upon a/W and H/W ratios. The smallest elements were located near the crack tip and were square. The element length was five percent of the crack length a or lower. The ends of the specimen, $y = \pm H/2$, were subjected to uniform displacement $v_o = \pm 0.001$ inch and E was assumed as 10×10^6 psi (E for aluminum). Strain energy release rates were computed for the crack extension of $\Delta a = 0.01$ inch and SIFs K_I were then computed. Computed SIFs K_I were nondimensionalized with K_o as given by Equations (12) and (13).

$$\text{Nondimensional SIF} = K_I/K_o \tag{12}$$

$$K_o = \frac{2Ev_o}{H} \cdot \sqrt{\pi a} \tag{13}$$

where E is the elastic modulus of the material and $\pm v_o$ is the applied uniform displacement at the ends.

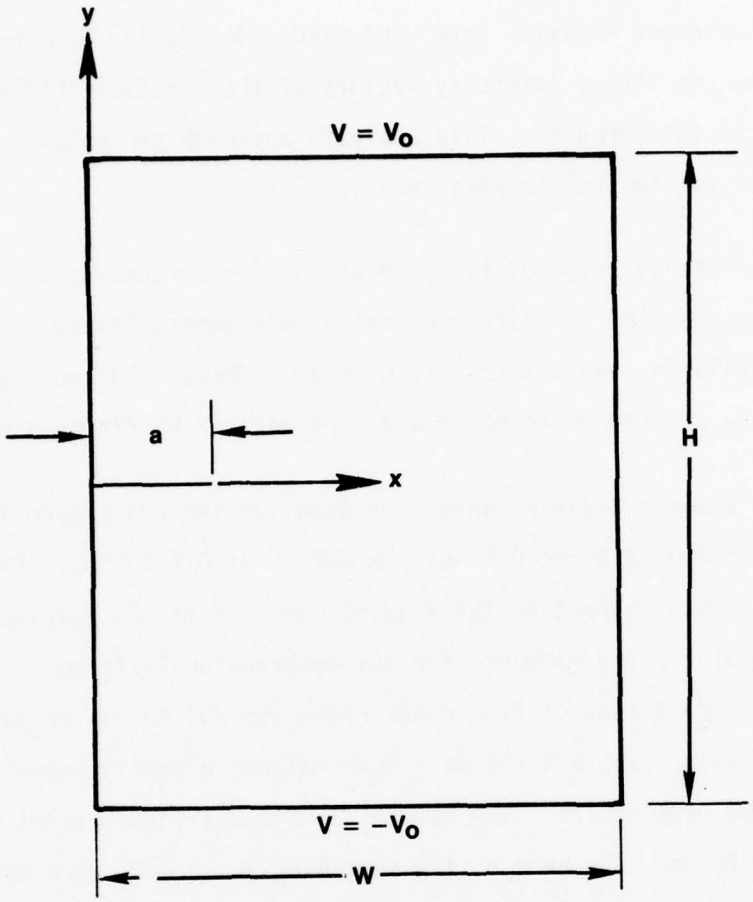

Figure 20. Crack Gage Analysis Model - Uniform Normal Displacement

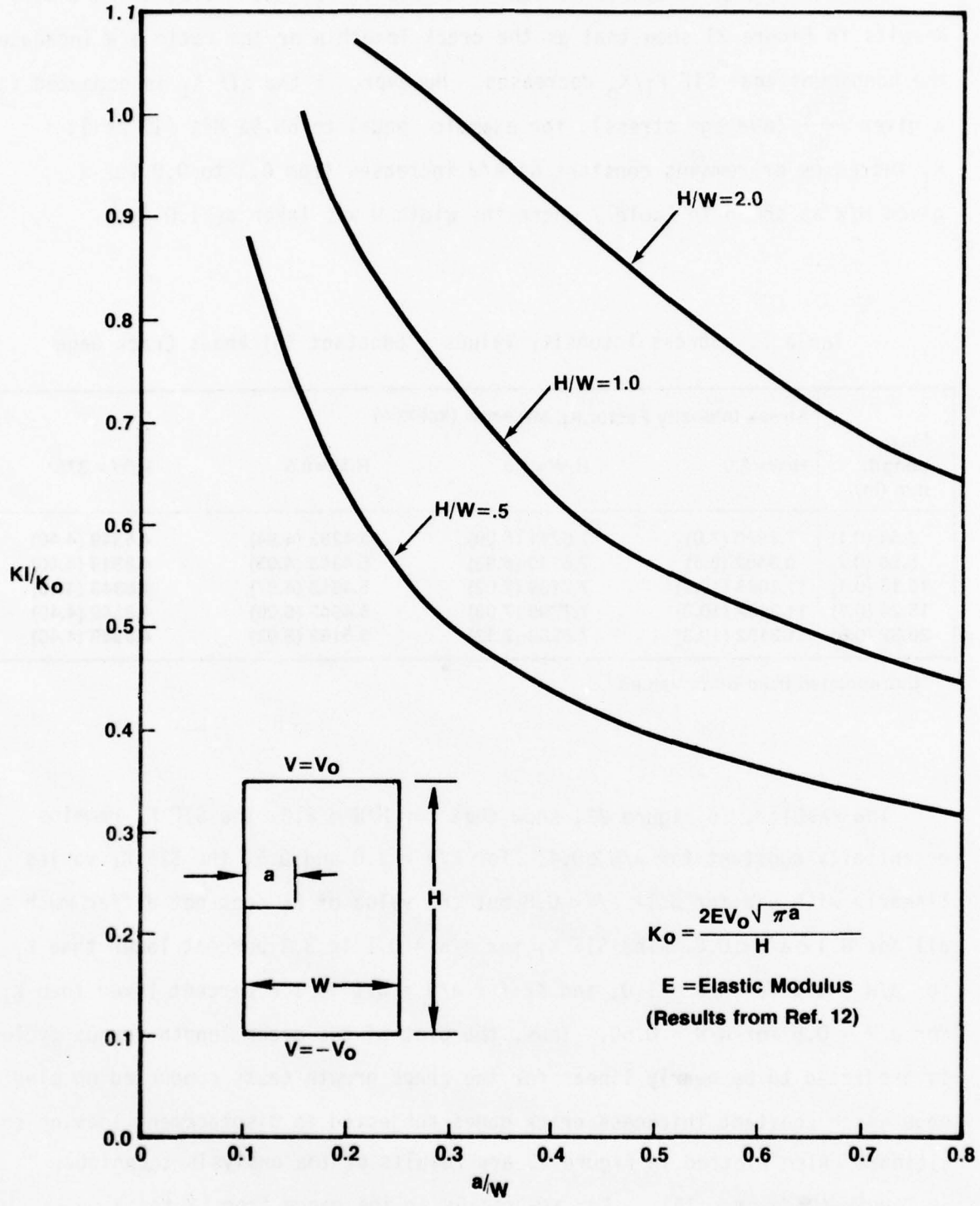

Figure 21. Normalized K_I Vs a/w for an Edge Crack in a Rectangular Crack Gage Subjected to Uniform Normal Displacement

Plots of K_I/K_o vs a/W are shown in Figure 21 for H/W = 2.0, 1.0 and 0.5. Results in Figure 21 show that as the crack length a or the ratio a/W increases, the nondimensional SIF K_I/K_o decreases. However, if the SIF K_I is computed for a given $\frac{2Ev_o}{H}$ (average stress), for example, equal to 68.95 MPa (10 ksi), K_I increases or remains constant as a/W increases from 0.1 to 0.8 for a given H/W as shown in Table 7 where the width W was taken as 1.0 inch.

Table 7. Stress Intensity Values - Constant Thickness Crack Gage

Flaw Length mm (in)	Stress Intensity Factor, K_I, MPa-m½ (ksi-in½) H/W=2.0	H/W=1.0	H/W=0.5	H/W=.375*
2.54 (0.1)	7.6920 (7.0)	7.5711 (6.89)	5.4283 (4.94)	4.8349 (4.40)
5.08 (0.2)	9.3402 (8.5)	7.6150 (6.93)	5.4393 (4.95)	4.8349 (4.40)
10.16 (0.4)	11.2083 (10.2)	7.7139 (7.02)	5.4613 (4.97)	4.8349 (4.40)
15.24 (0.6)	11.3182 (10.3)	7.7799 (7.08)	5.4943 (5.00)	4.8349 (4.40)
20.32 (0.8)	11.3182 (10.3)	7.8238 (7.12)	5.5162 (5.02)	4.8349 (4.40)

*Extrapolated from other values

The results, in Figure 22, show that for H/W = 2.0, the SIF K_I remains essentially constant for $a/W \geq 0.4$. For H/W = 1.0 and 0.5, the SIF K_I varies linearly with a/W for $0.1 < a/W < 0.8$ but the value of K_I does not differ much at all for $0.1 < a/W < 0.8$. The SIF K_I for a/W = 0.1 is 3.3 percent lower than K_I for a/W = 0.8 for H/W = 1.0, and K_I for a/W = 0.1 is 1.6 percent lower than K_I for a/W = 0.8 for H/W = 0.50. Thus, the plot of the crack length versus cycles is predicted to be nearly linear for the crack growth tests conducted on single edge notch constant thickness crack gages subjected to displacement loading conditions. Also plotted in Figure 22 are results of the analysis technique of Torvik (Reference 15). For a/W ratios in the range from .2 to .8. Both analyses give excellent agreement.

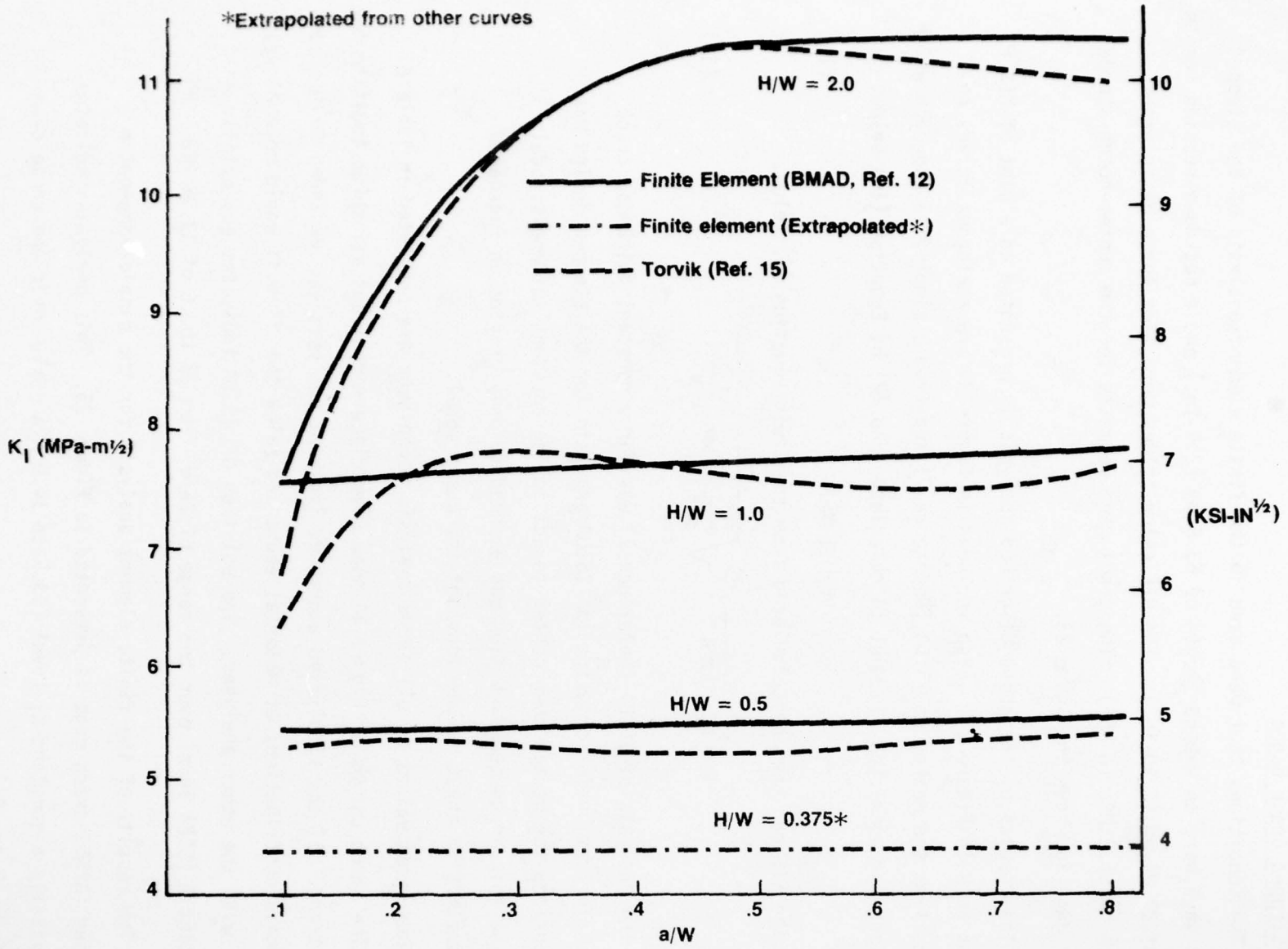

Figure 22. K_I for an Edge Crack in a Rectangular Crack Gage Subjected to Uniform Normal Displacements Vs a/W

3.3 Stepped Crack Gages

The conditions that were used in the finite element analysis of the stepped crack gage were an unbond length of 63.5-mm (2.5-In.) and a neckdown section length (4) of 27.94-mm (1.10-In.). The SIF calculations were made for a basic panel stress of 55.2 MPa (8 KSI). The crack gage geometry for the center-notch-stepped crack gage is shown in Figure 23.

The results of the above described analysis is presented as a plot of K(SIF) versus 2a/W in Figure 24. Also included in Figure 24 are analogous curves obtained from the method of ISIDA (Reference 7) and from a simplified approach which utilized the uncracked ligament to calculate load (P) by Equation (14) below.

$$\Delta = PL/AnE \tag{14}$$

The SIF can then be calculated from the Irwin Equation 15, below.

$$K = \sigma_G \sqrt{\pi a} \cdot \sqrt{\frac{W}{\pi a} \tan \frac{\pi a}{W}} \tag{15}$$

The analysis of ISIDA (Reference 7) was for a constant thickness crack gage. The rationale for using the ISIDA analysis for the stepped design was to consider the necked down center to act as the constant thickness model and the thicker unbonded portion was assumed to only provide an increased end deflection input to the constant thickness model.

Tabulated values of all three analysis techniques are presented in Table 8.

The three curves of Figure 24 show some disagreement but all three indicate the same trend. If the simplified uncracked ligament analysis was expanded to include stiffness contributions of material above and below the flaw it would more closely agree with the other analyses. The solution of ISIDA indicates essentially a constant K (SIF) level over the range of 2a/W from .3 to .6 of 12.32 MPa - $m^{\frac{1}{2}}$.

The results of the finite element analysis for the single-edge-notch stepped (SENS) crack gage is presented in Figure 25. This analysis indicates essentially a constant K_I level (13.5 to 14.0 MPa - $m^{\frac{1}{2}}$) over the range of a/W from .2 to .8.

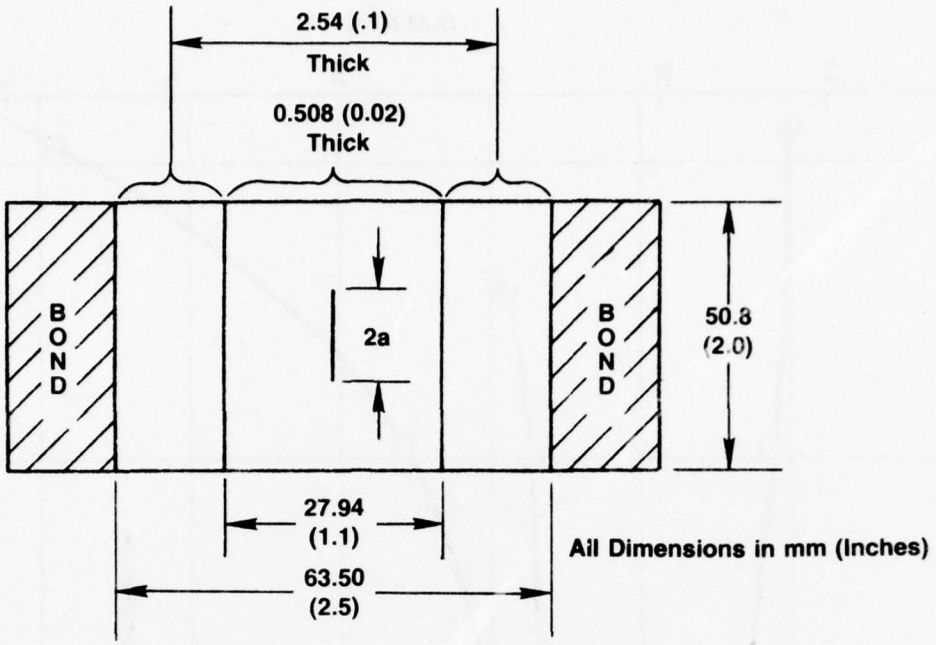

Figure 23. Finite Element Crack Gage Model

Table 8. K_I Calibration Data of Figure 24

Relative Flaw Length, 2a/W	Stress Intensity Factor, K (MPa-m½)		
	Finite Element (BMAD)	Net Area Spring (BWC)	Theoretical ISIDA (Ref. 7)
.1	9.03	8.11	9.28
.2	11.96	10.39	11.64
.3	13.19	11.50	12.34
.4	13.59	11.94	12.32
.6	13.89	11.44	12.31
.8	13.97	9.11	–

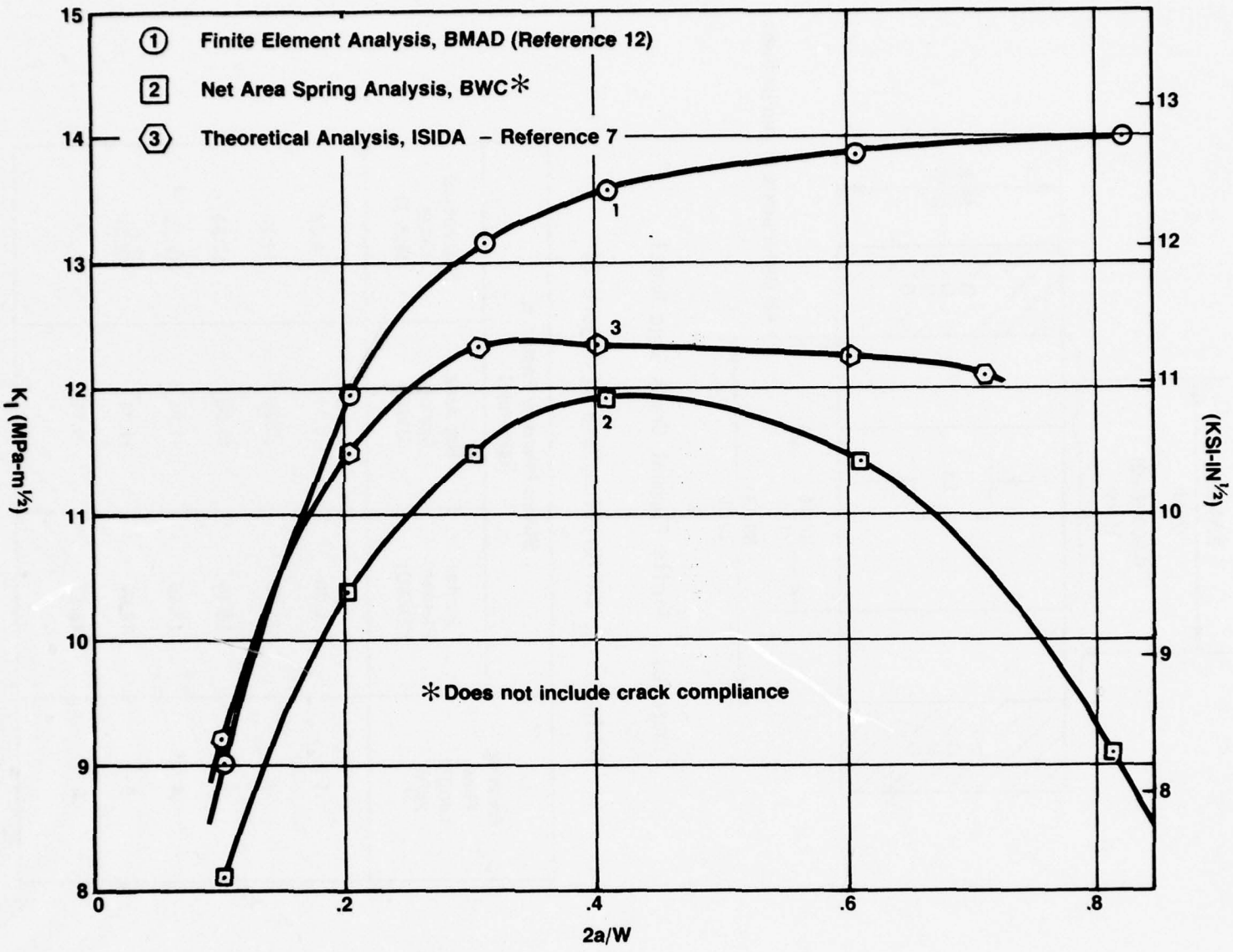

Figure 24. Stress Intensity, K_I Vs 2a/w for Symetrically Stepped Crack Gage With Center Flaw

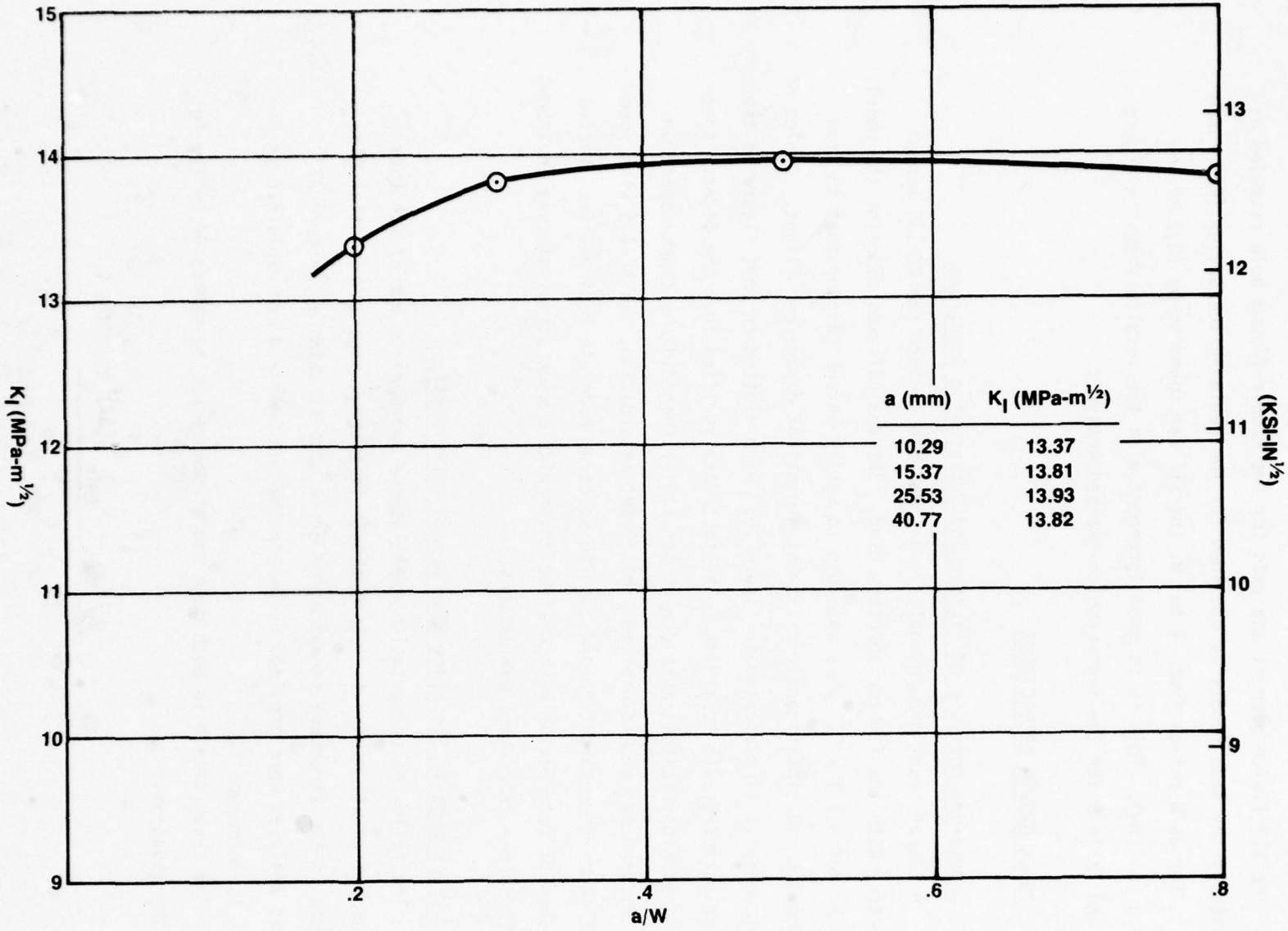

Figure 25. Stress Intensity, K_I VS a/W for Symetrically Stepped Crack Gage with Edge Flaw

The SIF finite element analysis for the double-flawed hole revealed essentially the same result as obtained for the center-crack design (Reference 12). For 2a/W ratios from .4 to .8, the SIF was found to be 13.2 MPa-$m^{1/2}$ (12.0 ksi-$In^{1/2}$). This is in good agreement with the results shown in Figure 24 and Table 8 for the center-notch-stepped analysis.

4. CRACK GROWTH PREDICTIONS

4.1 Unretarded Analysis of Fighter and Tanker Wing Spectrums

A linear crack growth analysis was made to compare the KC-135 tanker spectrum with the fighter spectrum used. The analysis was made for the panel center notch, Flaw 5. This was done to verify before testing that the two spectrums had significantly different amounts of damage per flight. A plot of that analysis is presented in Figure 26. Also plotted in that figure is the actual crack-growth test data. The test data verified that the fighter spectrum had significatnly more damage per flight than did the tanker spectrum. The fighter spectrum exhibited significant retardation, the KC-135 wing spectrum moderate retardation and the fin spectrum moderate retardation. Varied amounts of retardation were desired to provide a wide stress history environment for the crack-gage evaluations.

4.2 Crack Gage Vs Structure Flaw Growth Relationships

The following presentation explains the appropriate use of fracture mechanics relationships to relate growth in a crack gage to potential flaw growth in the structure to which the crack gage is attached (Figure 27). These analyses were provided by Ramesh Shah of BMAD and are explained in detail in Reference 12.

The crack growth in both gage and structure can be expressed by the following equations:

$$\left(\frac{da}{dN}\right)_g = \frac{C_g\,(K_{max} - K_{TH})_g^{m_g}(\Delta K)_g^{n_g}}{(K_{cr} - K_{max})_g^{P_g}} \qquad (16)$$

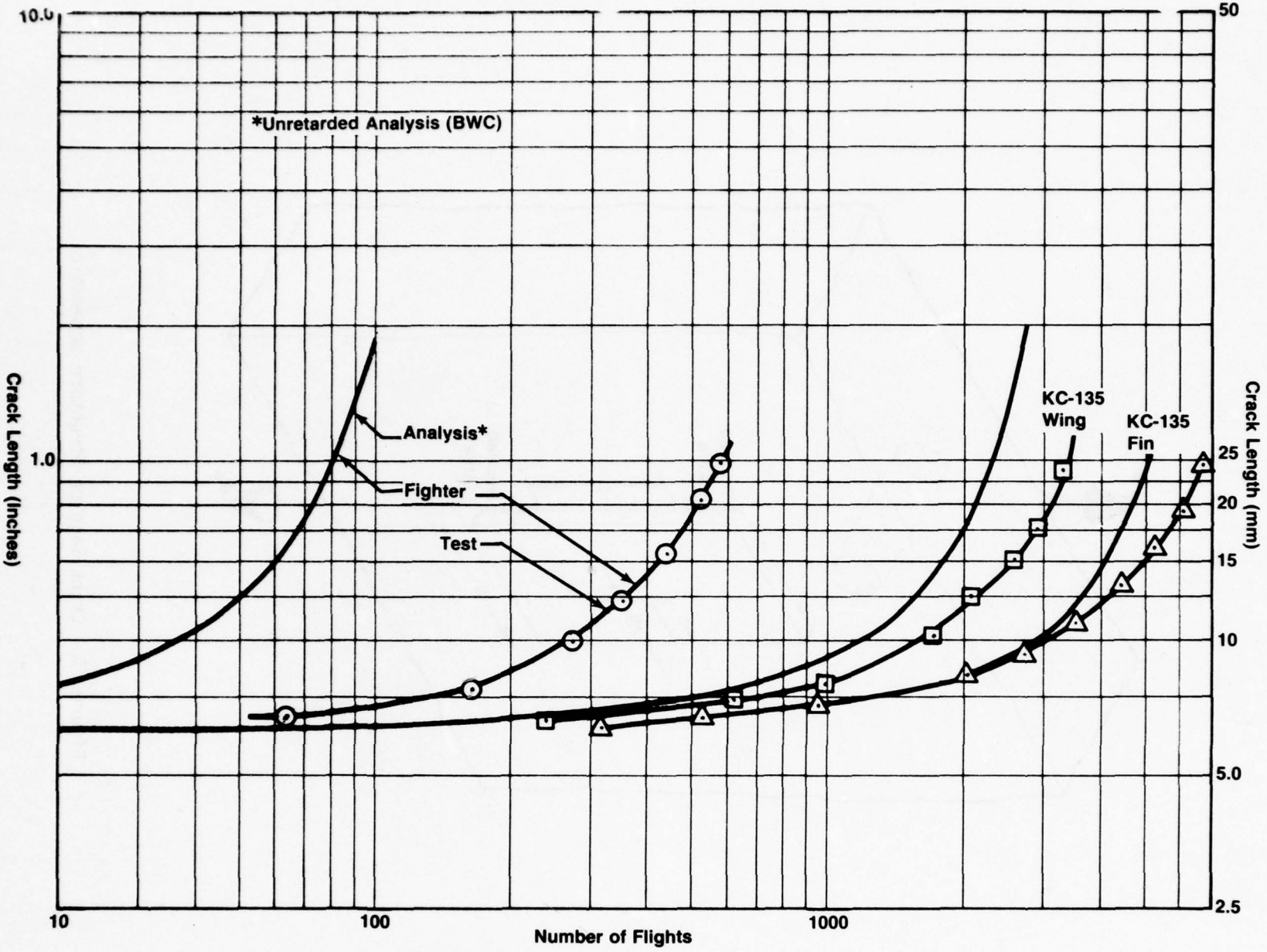

Figure 26. Flaw 5 Crack Propagation Prediction and Test Comparisons

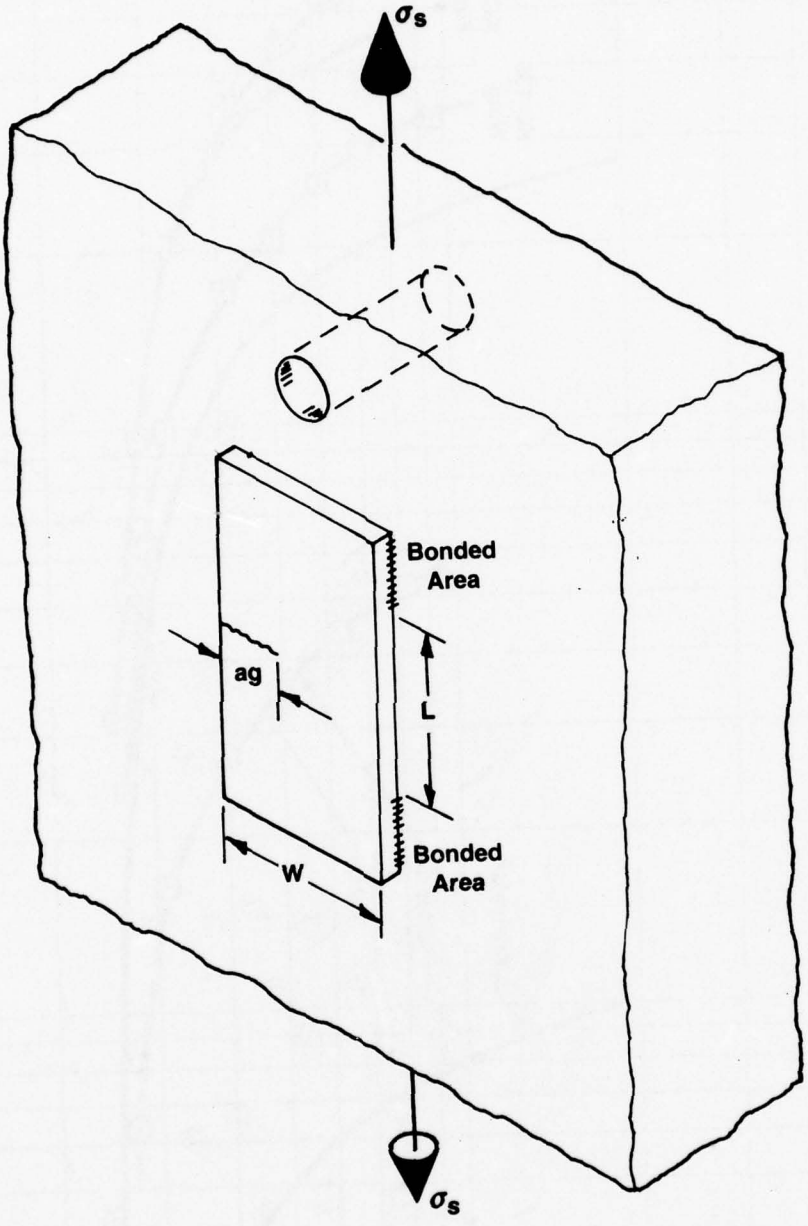

Figure 27. Crack Gage on Structure Schematic

$$\left(\frac{da}{dN}\right)_s = \frac{C_s\,(K_{max} - K_{TH})_s^{m_s}\,(\Delta K)_s^{n_s}}{(K_{c_r} - K_{max})_s^{P_s}} \qquad (17)$$

In the above equations, K_{max} refers to the maximum stress intensity factor (SIF) during a loading cycle, ΔK denotes the difference between the maximum and minimum SIF during a loading cycle, K_{TH} stands for the threshold SIF for the fatigue crack growth, C is the constant and m, n and p are exponents in the crack growth rate equation. Subscripts g and s pertain to quantities associated with the gage and the structure. The simplest way to relate the growth of cracks in the gage and structure is to obtain relationships between the number of cycles applied, N, to the crack growth (or the total crack size) in the gage and the structure for the applied loads to the structure, as given by Equations 18 and 19. These relationships can then be used to derive relationships between the gage crack size and the structural crack size for various assumed initial crack sizes in the gage and/or structure.

$$N_g = \sum_{j=0}^{q} (N_g)_j = \sum_{j=0}^{q} \left[\int_{a_{gi} + j\Delta a_g}^{a_{gi} + (j+1)\Delta a_g} \frac{(K_{cr} - K_{max})_g^{P_g}\, da}{C_g (K_{max} - K_{TH})^{m_g} (K)_g^{n_g}} \right] \qquad (18)$$

$$N_s = \sum_{j=0}^{q} (N_s)_j = \sum_{j=0}^{q} \left[\int_{a_{si} + j\Delta a_s}^{a_s + (j+1)\Delta a_s} \frac{(K_{cr} - K_{max})_s^{P_s}\, da}{C_s (K_{max} - K_{TH})^{m_s} (K)_s^{n_s}} \right] \qquad (19)$$

where

$$a_{g_f} = a_{g_i} + q\,\Delta a_g$$

$$a_{s_f} = a_{s_i} + q\,\Delta a_s \qquad (20)$$

In Equations 18 and 19, subscripts i and f relate to initial and final conditions. Equations 18 and 19 can be readily evaluated with numerical quadratures, if solutions for computations of K are known. The above integrations in Equations 18 and 19 are carried out for incremental crack growth of Δa_g and Δa_s for cracks in the gage and the structure. Thus, a continuous curve of crack length a versus number of applied cycles n can be obtained from q + 1 discrete points for cracks in the gage and the structure.

4.3 Structure Flaw Growth Predictions

In this analysis the following assumptions and conditions were used: $K_{TH} = 0$, $P_g = P_s = 0$ and $m_g + n_g = m_s + n_s = 4$. The analysis was made for a structure flaw of 6.4-mm (.25-In.) diameter hole containing a single 1.3-mm (.05-In.) through flaw. Constant-amplitude loading of 68.95 MPa (10 KSI) and an R ratio of zero was used. The Stress Intensity Factor (SIF) for such a flaw is expressed by Equation 21 taken from Reference 13.

$$K = \sqrt{\pi a}\ F(a/R) \tag{21}$$

F(a/R) is given in a tabular form for various values of a/R. For numerical integration a functional form is needed. F(a/R) was least square fitted with a polynomial given by Equation 22 which represents within 1.4 percent accuracy the F(a/R) given by Reference 13 for $0.1 \leq a/R < 5.0$.

$$F(a/R) = 0.666008 + 0.886701\ (R/a) - 0.229838\ (R/a)^2 + 0.0309499\ (R/a)^3 - 0.0014769\ (R/a)^4 \tag{22}$$

Growth of the crack in the structure versus the number of cycles was computed with Equation 19 by numerical integration for constant amplitude cycles of stress and is shown in Figure 28.

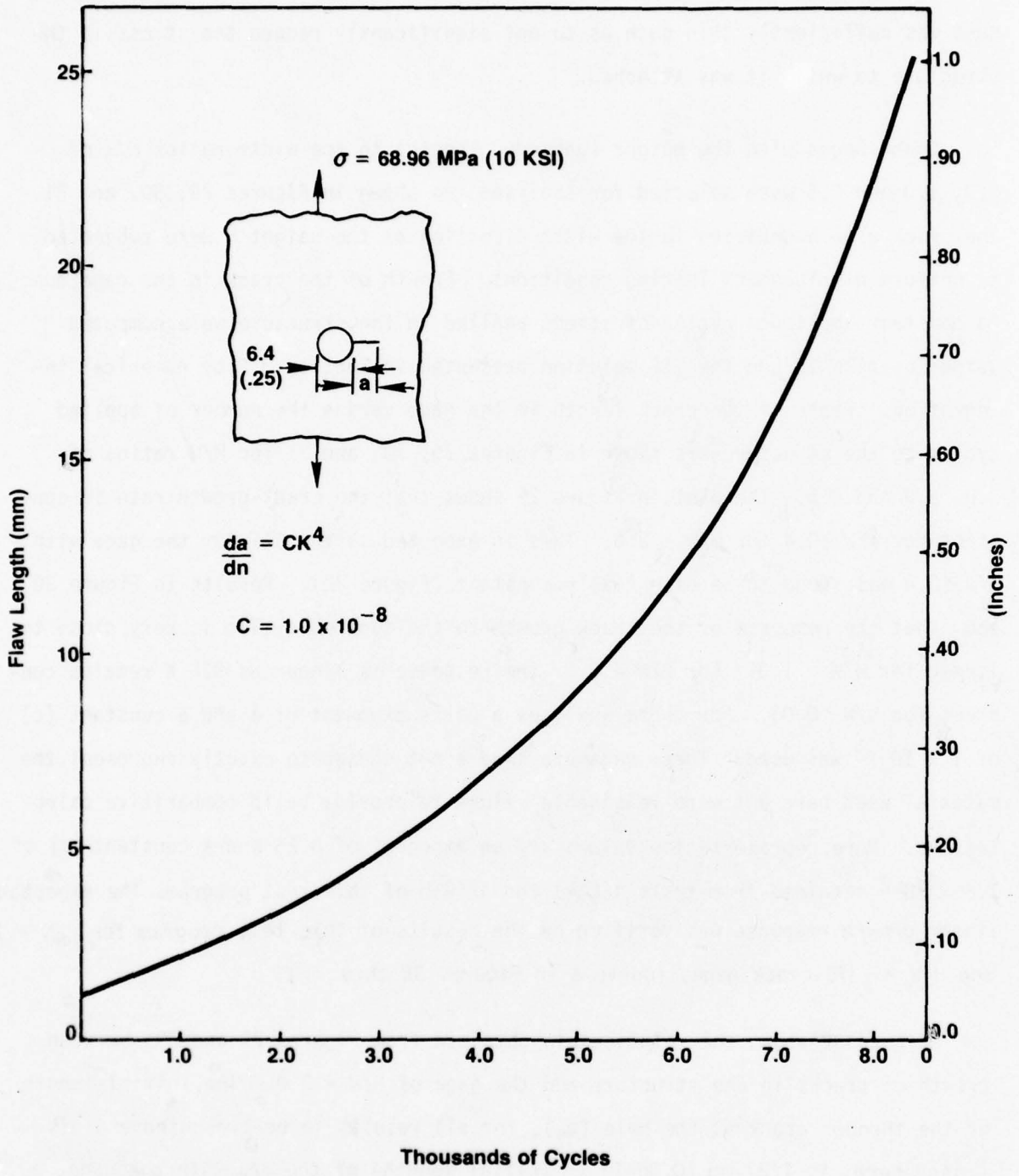

Figure 28. Theoretical Crack-Growth Response for Flaws 3 and 4

4.4 Constant-Thickness Crack Gage Growth Prediction

For the crack-gage-flaw-growth analysis it was assumed that the gage thickness was sufficiently thin such as to not significantly reduce the stress in the structure to which it was attached.

Crack Gages with the height (unbonded length) to the width ratios H/W of 2.0, 1.0 and 0.5 were selected for analyses, as shown in Figures 29, 30, and 31. The crack gage boundaries in the width direction at the height H were subjected to uniform displacement loading conditions. Growth of the crack in the gage due to constant amplitude cycles of stress applied to the structure were computed using Equation 18 and the SIF solution presented in Section 3.2 by numerical integration. Plots of the crack length in the gage versus the number of applied cycles to the structure are shown in Figures 29, 30, and 31 for H/W ratios of 2.0, 1.0 and 0.5. The plot in Figure 29 shows that the crack-growth rate is constant for $a/W \geq 0.4$ for H/W = 2.0. This is expected as the SIF for the gage with $a/W \geq 0.4$ was found to be essentially constant (Figure 22). Results in Figure 30 show that the response of the crack growth to the applied cycles is very close to linear for H/W = 1.0. For H/W = 0.5, the response is linear as SIF K remains constant for $a/W \geq 0.05$. For these analyses a paris exponent of 4 and a constant (c) of 1×10^{-8} was used. These parameters were not chosen to exactly represent the material used here but were reasonable values to provide valid comparitive calculations. More representative values are an exponent of 3.25 and a constant (c) of 1.8×10^{-2} obtained from tests AFCG-1 and AFCG-5 of this test program. The expected linear growth response was verified by the results of this test program for H/W = 1.0 and H/W = .375 crack gages (curve 6 in Figures 35 thru 40).

Figure 32 shows the relationship obtained from Figures 28 and 29, between growth of cracks in the structure and the gage of H/W = 2.0. The initial length of the through crack at the hole (a_s), for all results to be presented and discussed here, is 1.27-mm (0.05-In.) Initial lengths of the crack in the gage, a_g, are taken as 1.27-mm (0.05), 2.54-mm (0.10), and 3.81-mm (0.15) for the gage of H/W = 2.0. Results in Figure 32 show that, if the initial crack in the gage a_{gi}

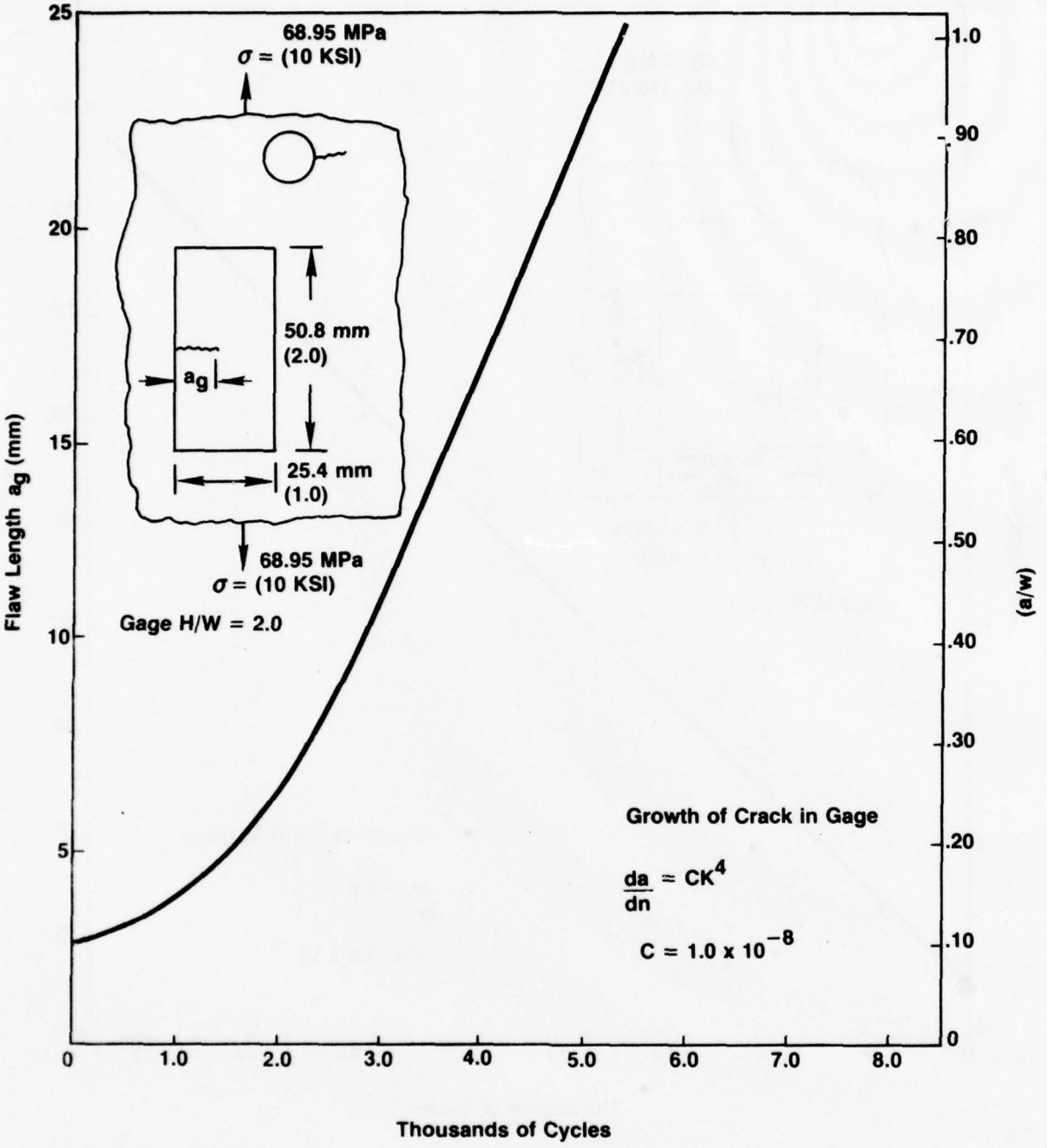

Figure 29. Flaw Length Vs Cycles Prediction for Constant Thickness Crack Gage of H/W = 2.0

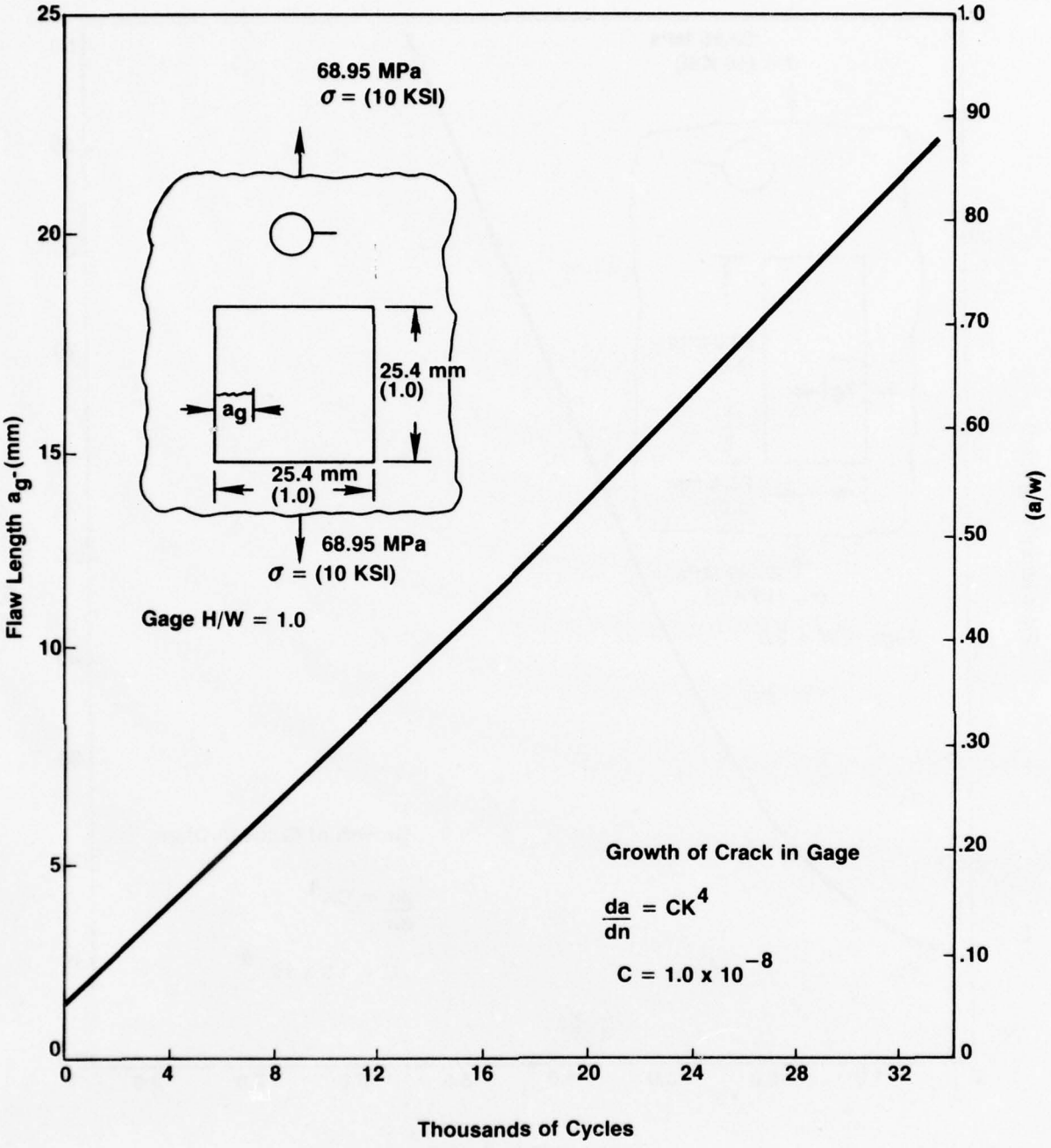

Figure 30. Flaw Length Vs Cycles Prediction for Constant Thickness Crack Gage of H/W = 1.0

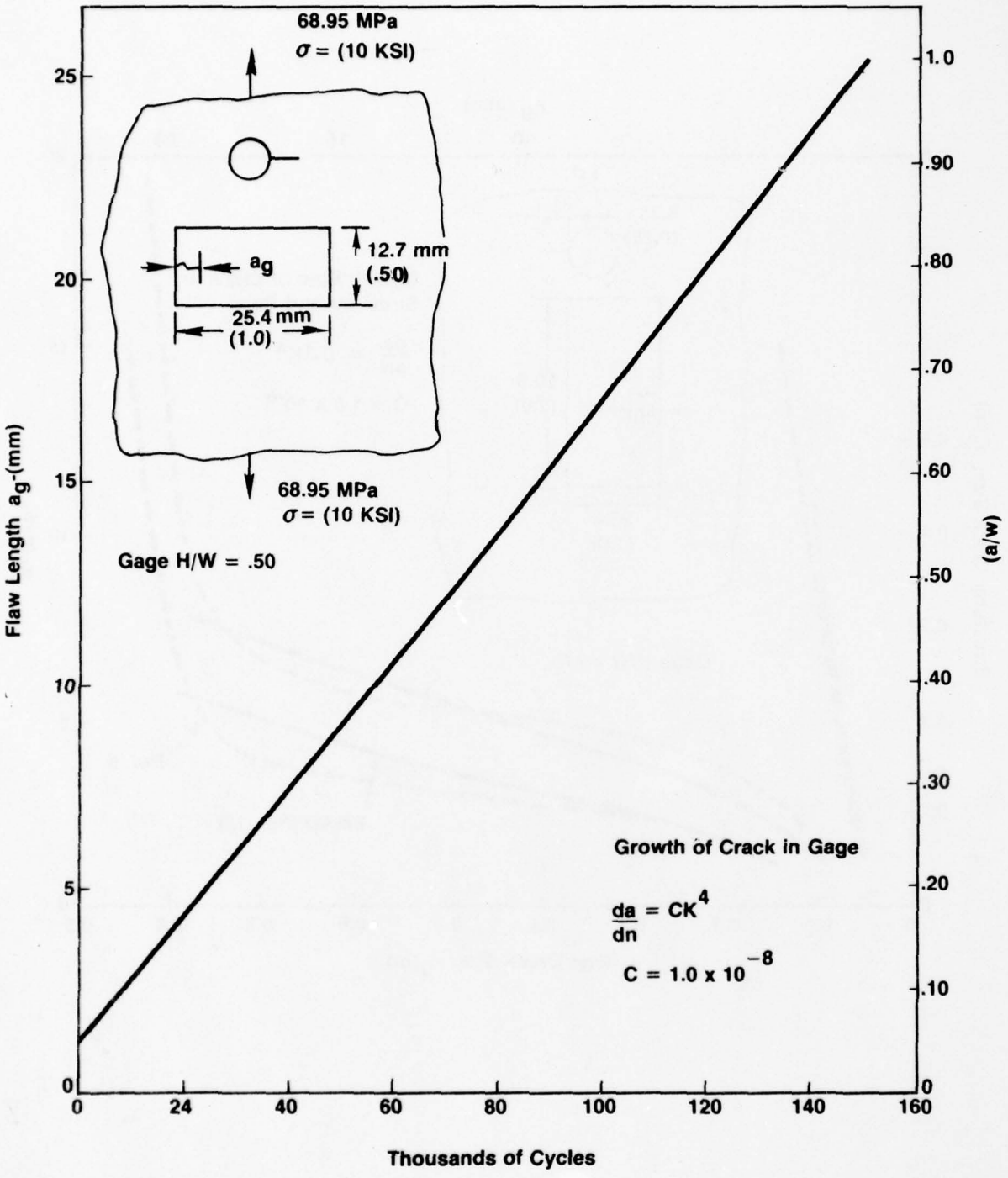

Figure 31. Flaw Length Vs Cycles Prediction for Constant Thickness Crack Gage of H/W = 0.5

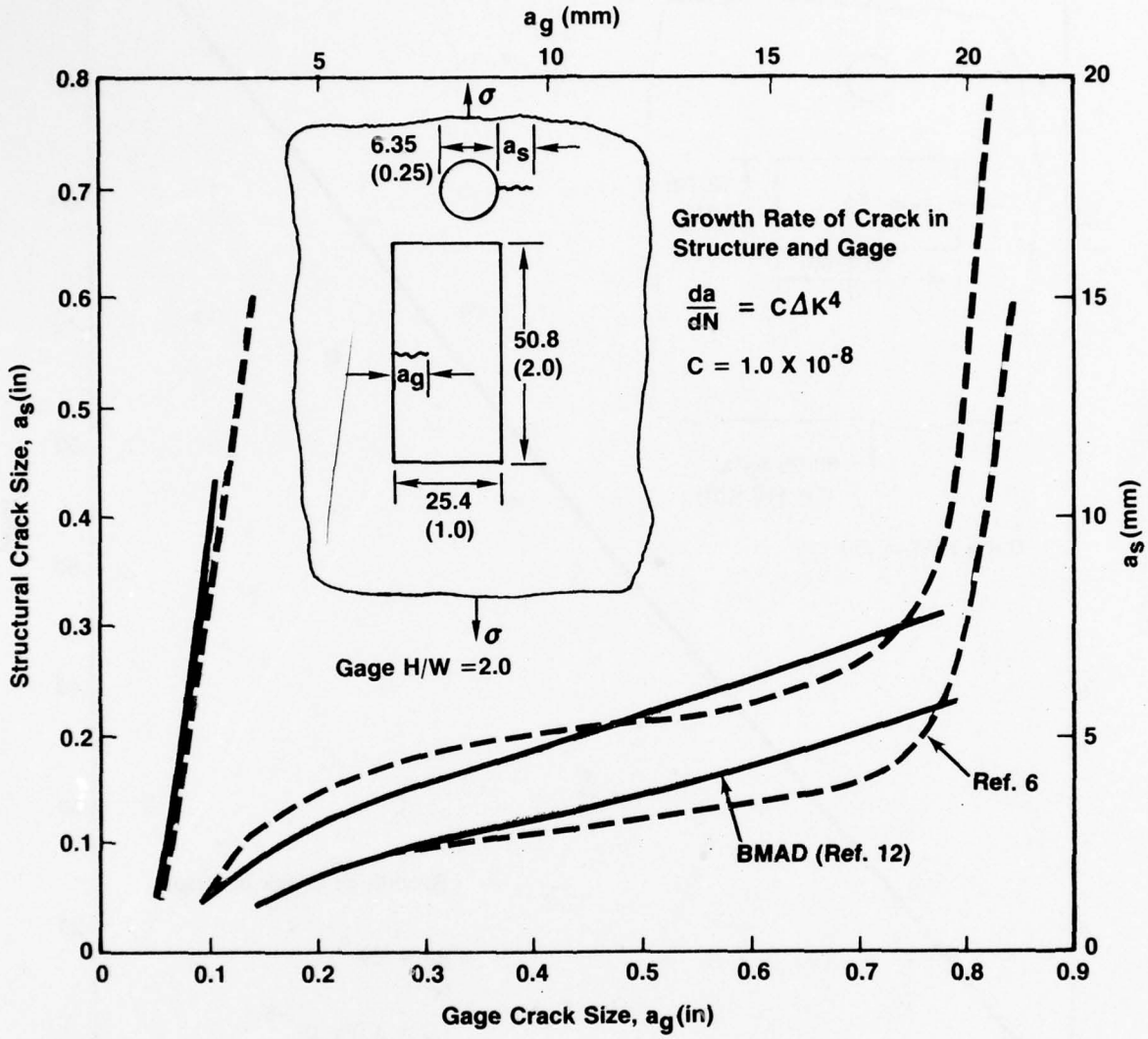

Figure 32. Relationship Between Crack Growths in Structure and Gage of H/W = 2.0

is the same as the initial crack length in the structure ($a_{gi} = a_{si}$ = 1.27-mm (0.05 inch), the crack in the structure would grow considerably faster. However, if a_{gi} is 2.54 or 3.81 mm, the crack in the gage would grow faster.

This type of behavior was also predicted by Crane, Grandt, and Gallagher in Reference 6. The results of Reference 6 are also plotted in Figure 32 for comparison. The correlation is quite good except at very long crack gage flaw lengths.

Results in Figure 33 show the similar relationships as those in Figure 32 for the gage of H/W = 1.0. They show that it is not possible for any size of the initial crack length to grow faster than the crack in the structure. Results in Figure 34 show the correlation between the structural crack size to the gage size for the gage of H/W = 0.5. Here, analysis shows that the crack in the specimen is growing at an order of magnitude faster than any size of the initial crack length in the gage.

Included in Figure 33 are test results taken from Test Panel AFCG-5 which was tested by constant-amplitude fatigue with σ_{max} = 68.95 MPa (10 KSI) and an *R ratio of* .05.

The agreement between tests results and the analytical predictions is excellent. It should be noted that the predictions were made for a material having material constants of C = 1.0 x 10^{-8} and m = 4 and the material used in this program had constants of C = 1.8 x 10-2 and m = 3.25. The agreement obtained between test and predictions indicates that the cross correlation between crack gage and structure is independent of material constants C and m.

4.5 Stepped Crack Gages

With the K factor relationships provided in this report (Figures 24 and 25) and using the same techniques described in Reference 12, similar predictions could be made for the stepped-design crack gage and are expected to give similar agreement with test results as was obtained for the constant-thickness crack gage. The K_{max} vs da/dn data for use in that analysis is found in Volume II, Section V and VI for the structure flaw and crack gage thin section respectively.

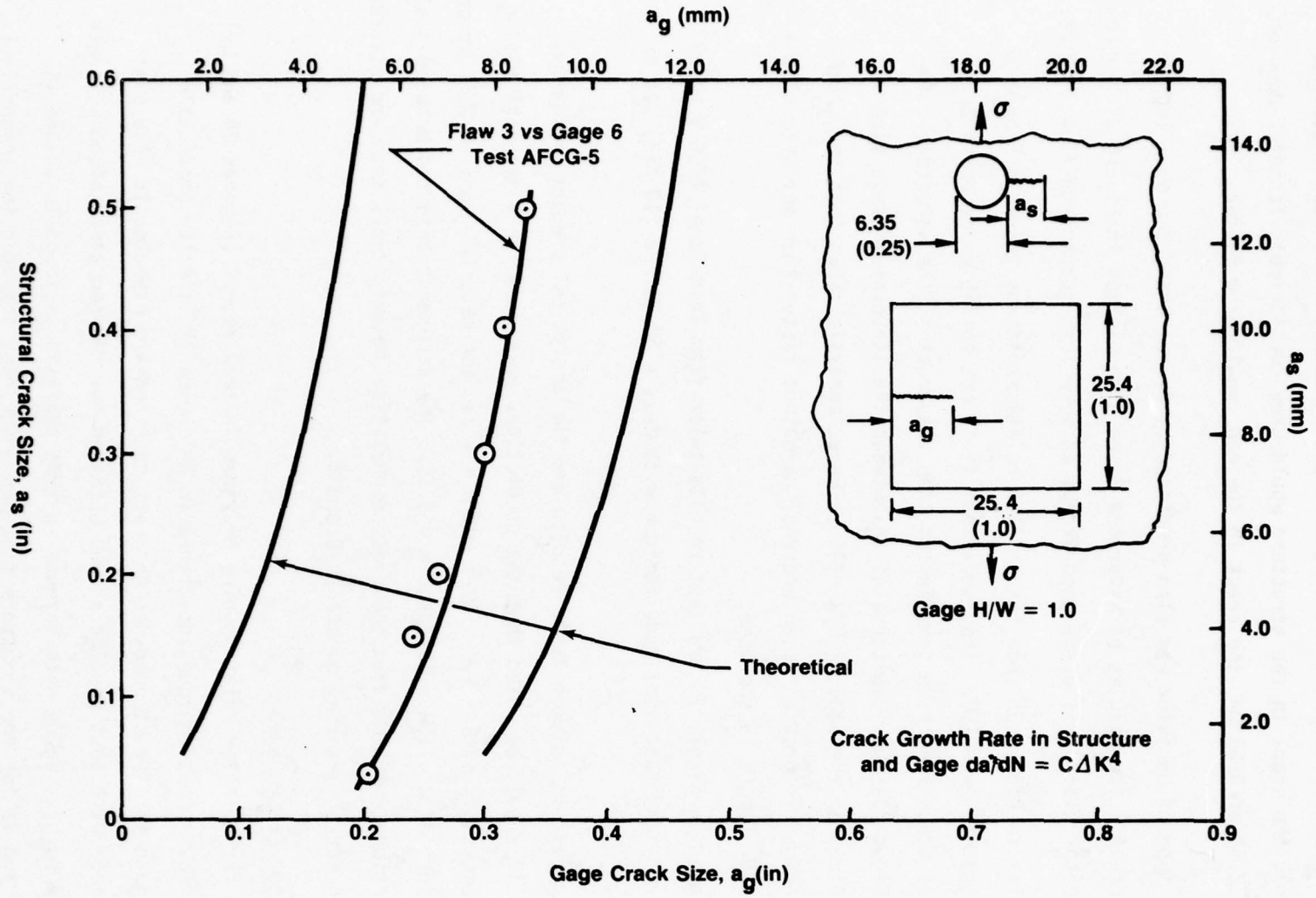

Figure 33. Relationship Between Crack Growth in Structure and Gage of H/W = 1.0

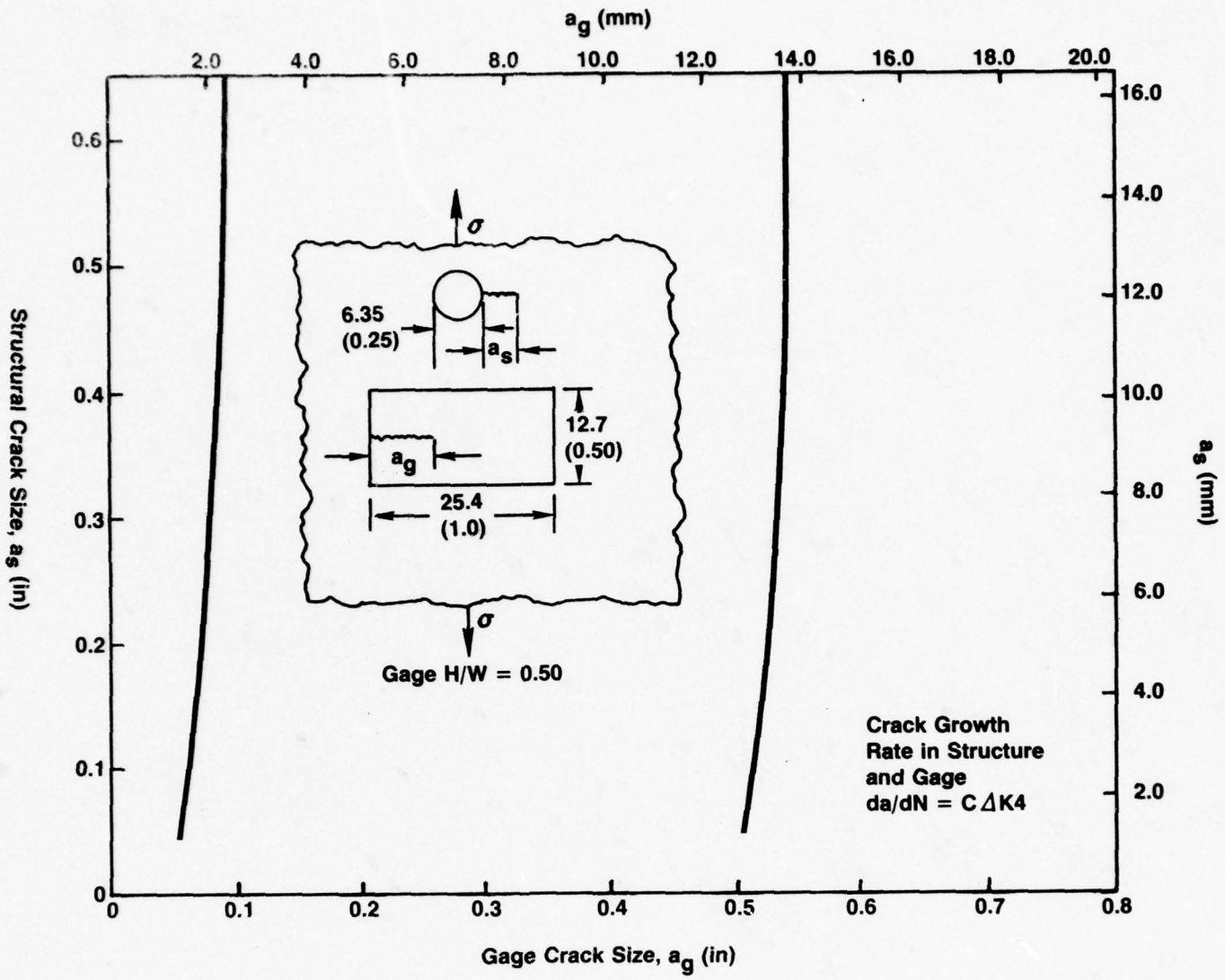

Figure 34. Relationship Between Crack Growth in Structure and Gage of H/W = 0.5

SECTION IV

SUMMARIZED PRESENTATION OF EXPERIMENTAL RESULTS

1. CRACK GROWTH PLOTS

Plots of crack growth results are presented in Figures 35 through 40 for Specimens AFCG-1 through AFCG-6, respectively. To obtain these plots, the structure flaw growth data (Flaws 1, 2, 3, 4 and 5) was averaged front-to-back (Side 1 to Side 2) and the data was hand corrected from an expanded plot of the raw data. The crack-gage data was plotted as recorded (uncorrected). Only the crack-gage data from Side 1 is presented in these plots. Plots of "both-side" data for each flaw is presented in Section IV of Volume II of this report.

2. COMPARISON PLOTS

2.1 Structure Flaw Growth Versus Structure Flaw Growth

Cross-correlation plots of structure hole edge flaw 3 & 4 and structure center notch flaw 5 were made. These plots are presented in Figure 41 with the data normalized to common initial flaw lengths of 1.27 mm (.05 In.) for the hole corner flaws and 6.35mm (.25 In.) for the structure center notch flaw. Also presented in Figure 41 is a tabulation of the diameter of each hole used in the plots. Figure 41A is the same plot as Figure 41 only with data from hole sizes deviating farthest from the average deleted. The purpose of these plots was to provide insight into "independence-from-load-history" which will be discussed later.

2.2 Crack Gage Flaw Growth Versus Structure Flaw Growth

Various cross correlation plots relating the flaw growth between crack gages and structure were made. Figure 42 presents such a plot for the center-notch-stepped crack gage (Type I) versus the structure hole edge flaws 3 & 4. Figure 42A presents the cross-correlation plot between center-notch-stepped

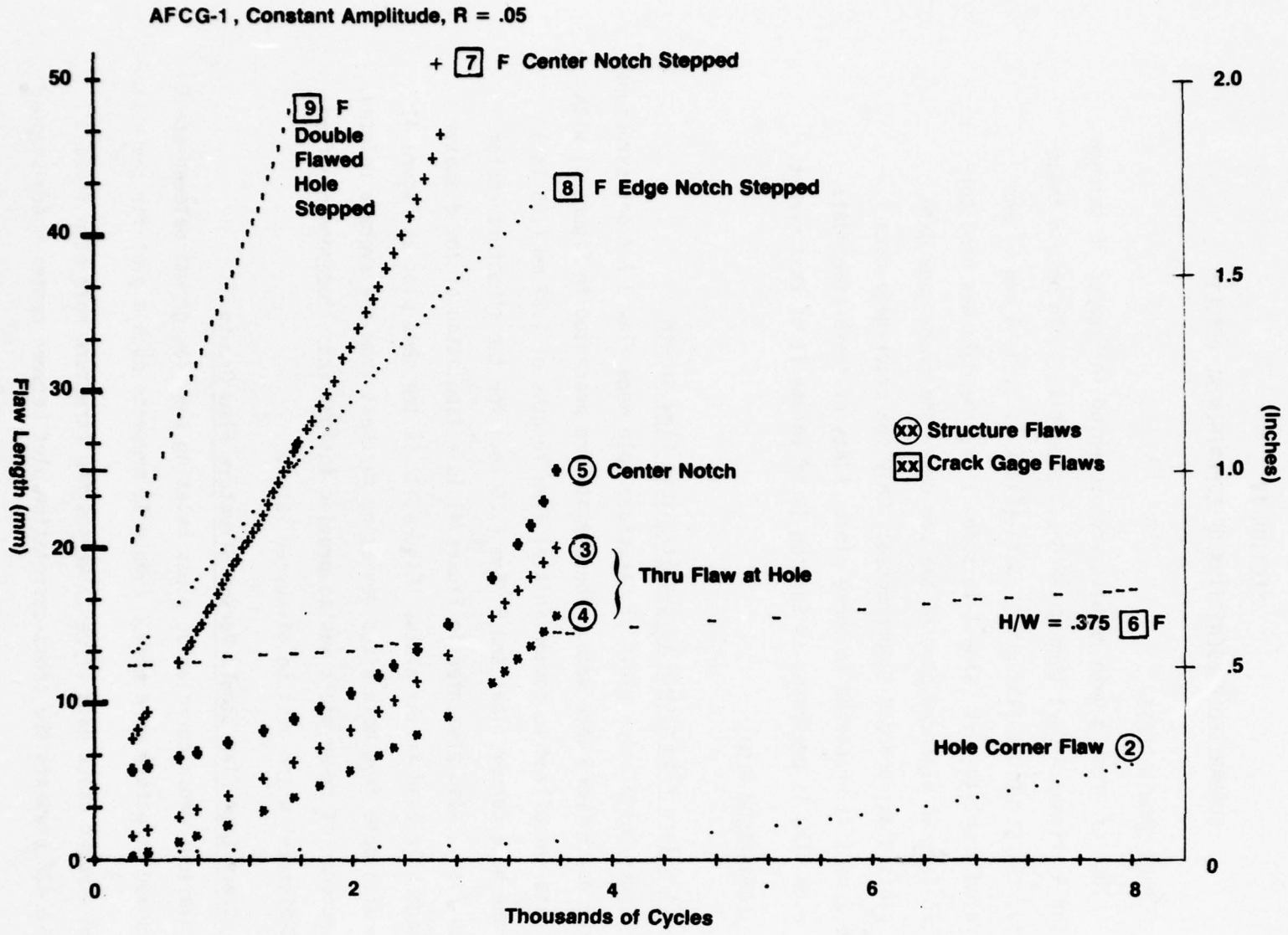

Figure 35. Crack Propagation Results Plot - Specimen AFCG-1

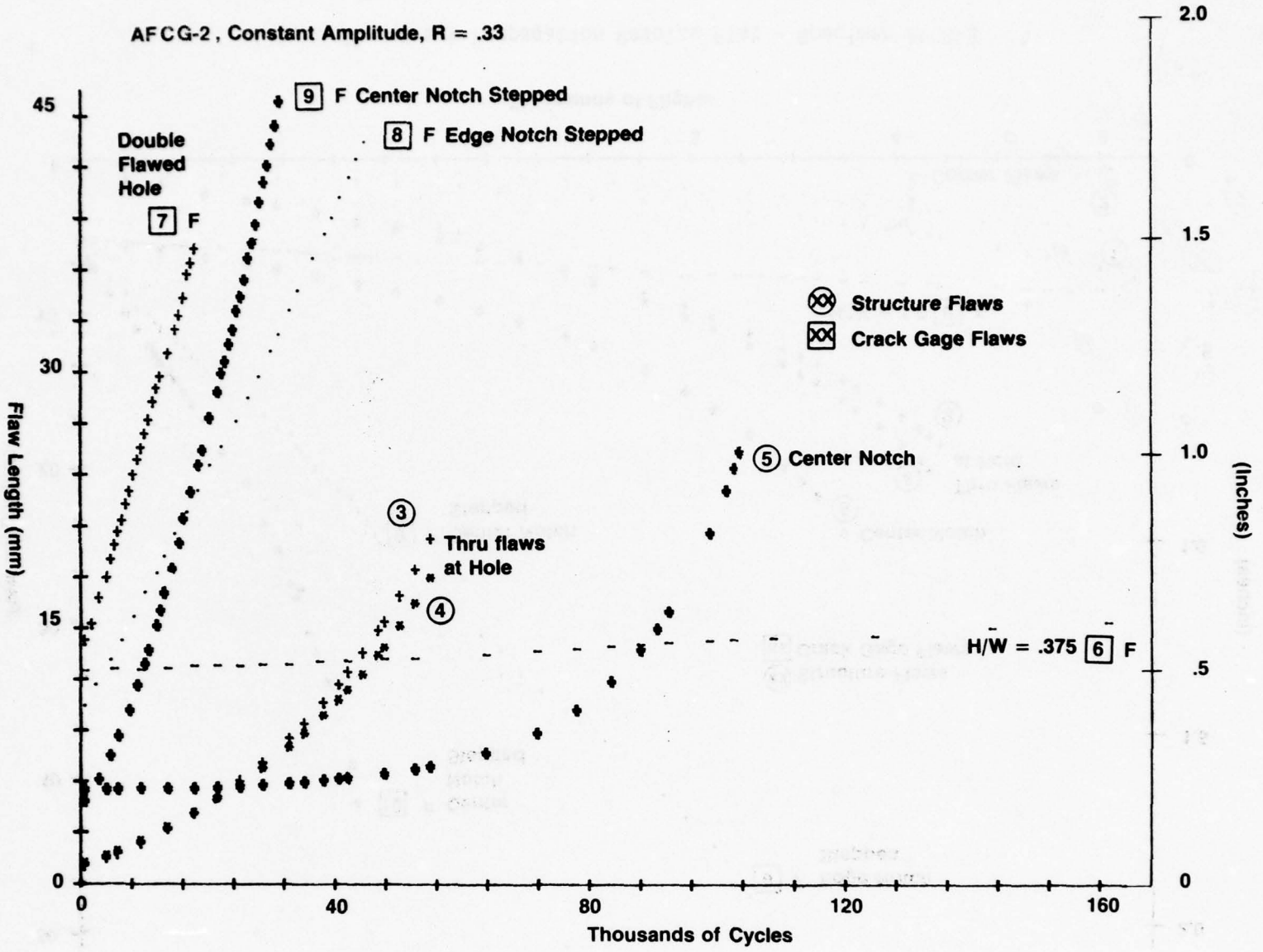

Figure 36. Crack Propagation Results Plot - Specimen AFCG-2

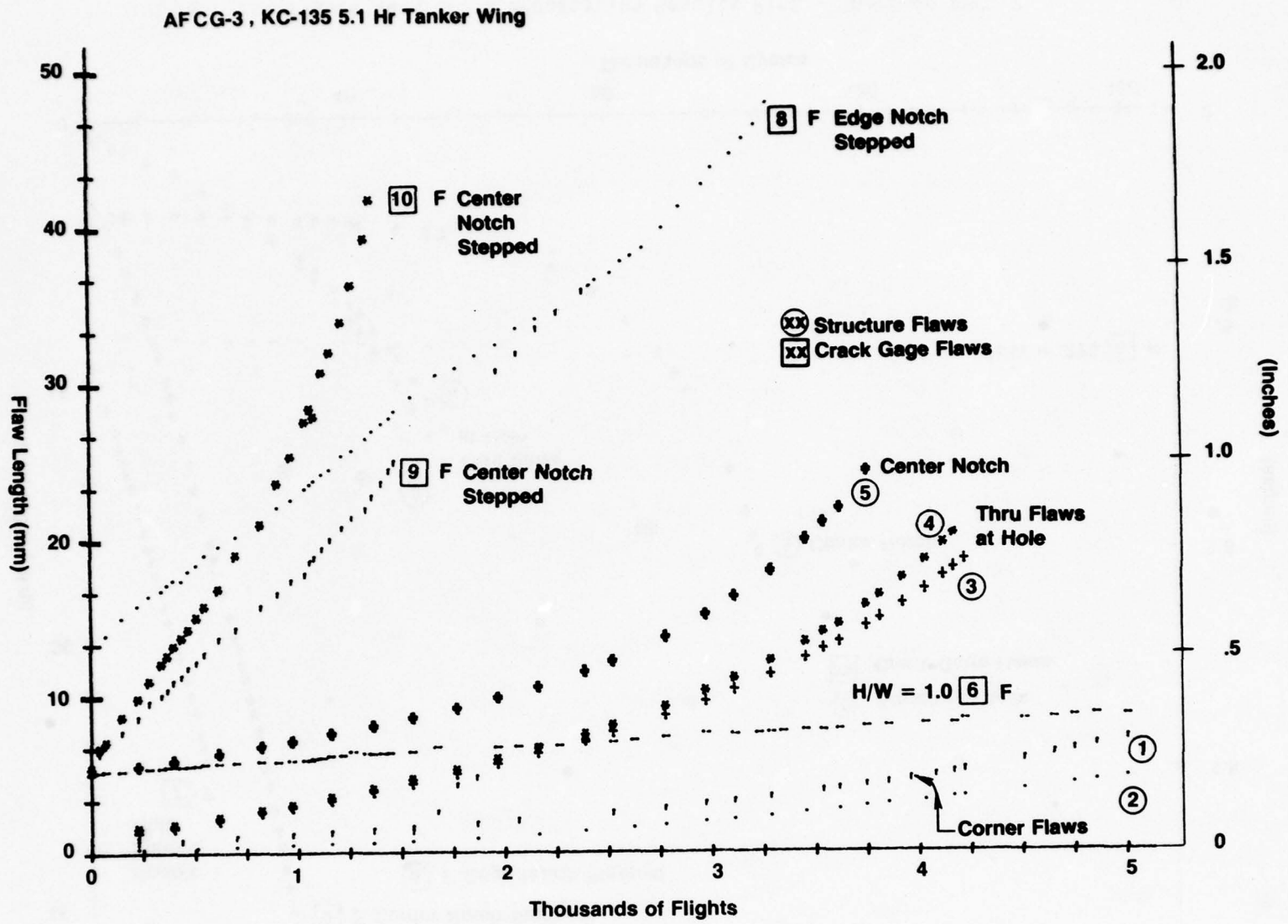

Figure 37. Crack Propagation Results Plot - Specimen AFCG-3

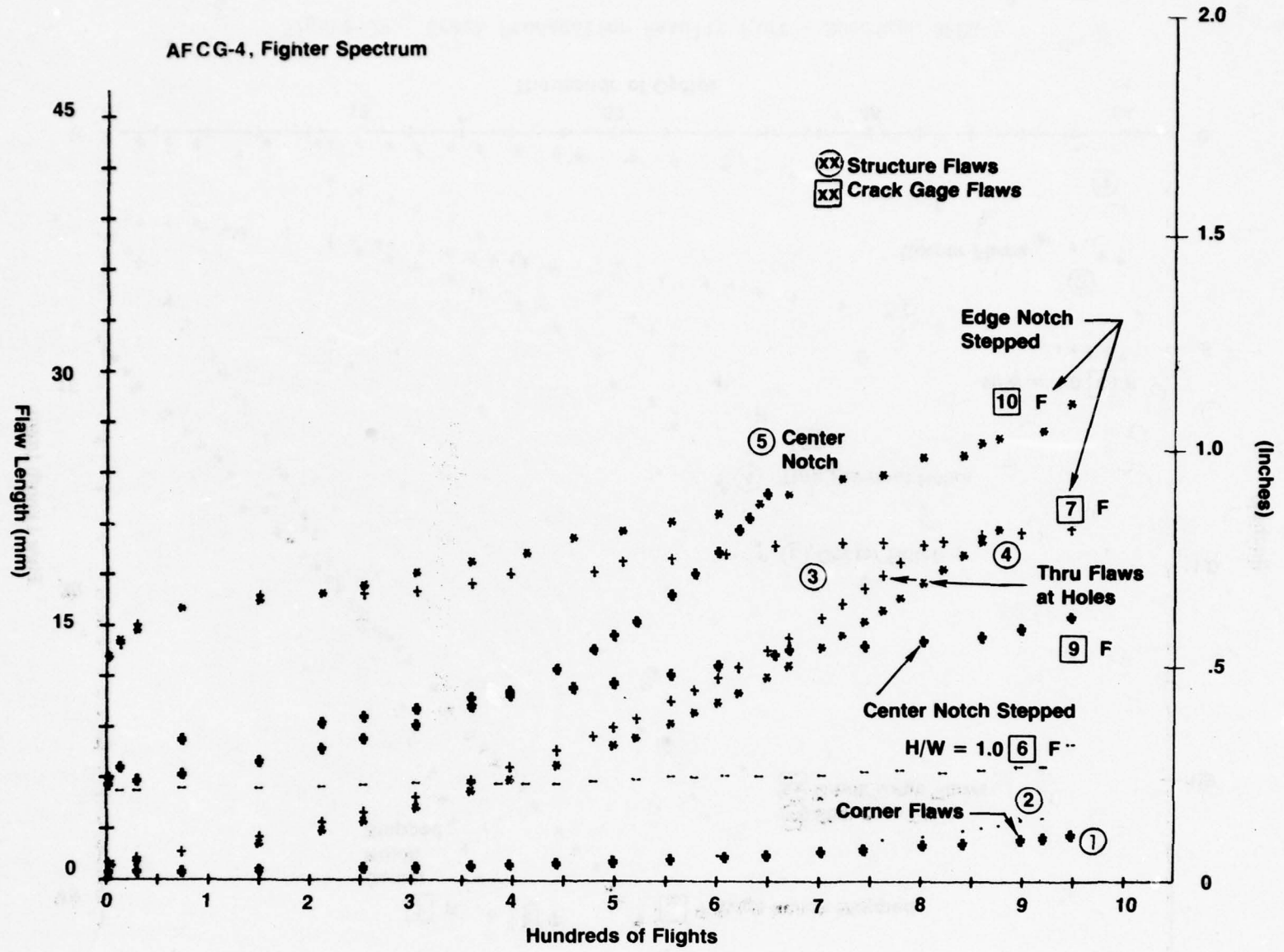

Figure 38. Crack Propagation Results Plot - Specimen AFCG-4

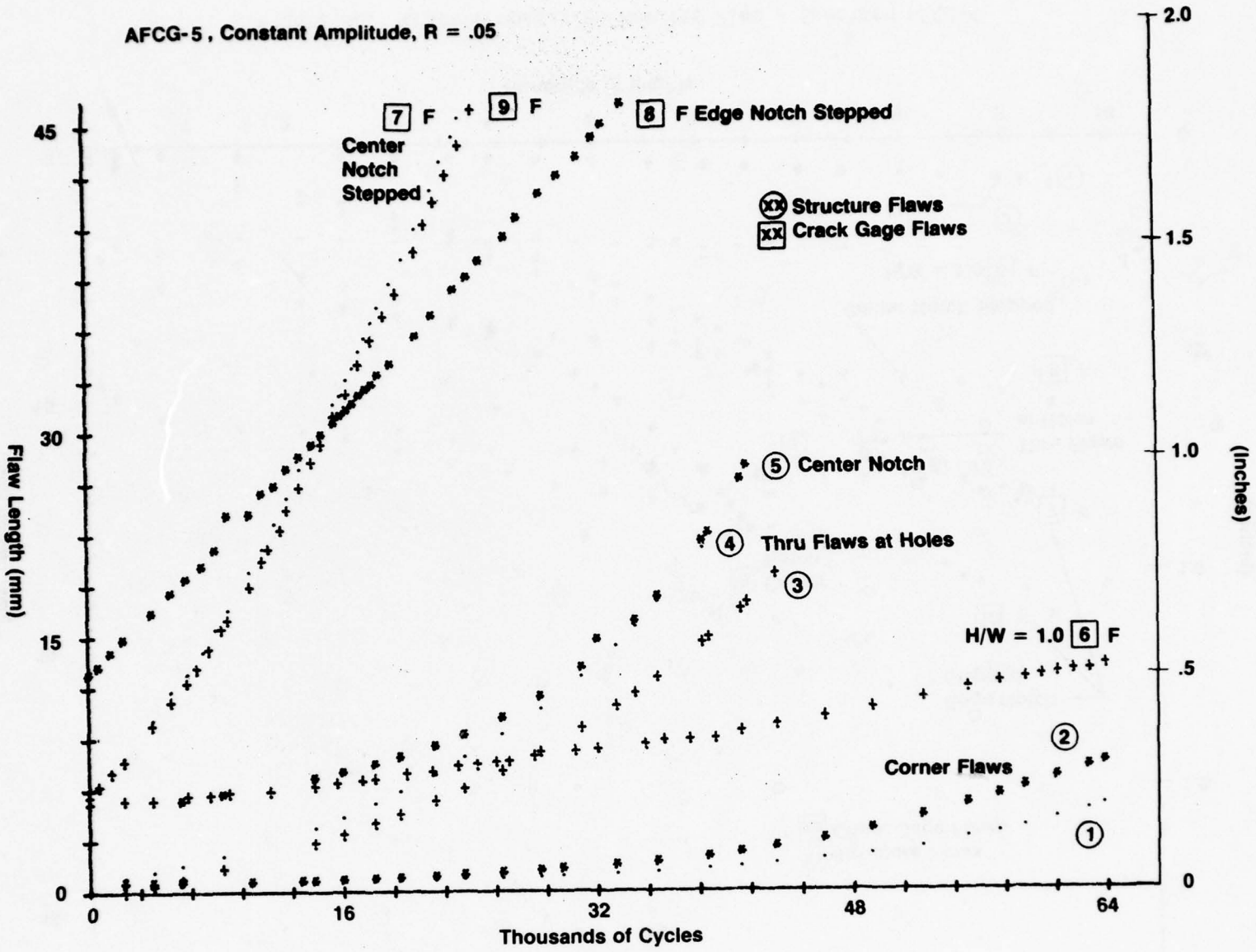

Figure 39. Crack Propagation Results Plot - Specimen AFCG-5

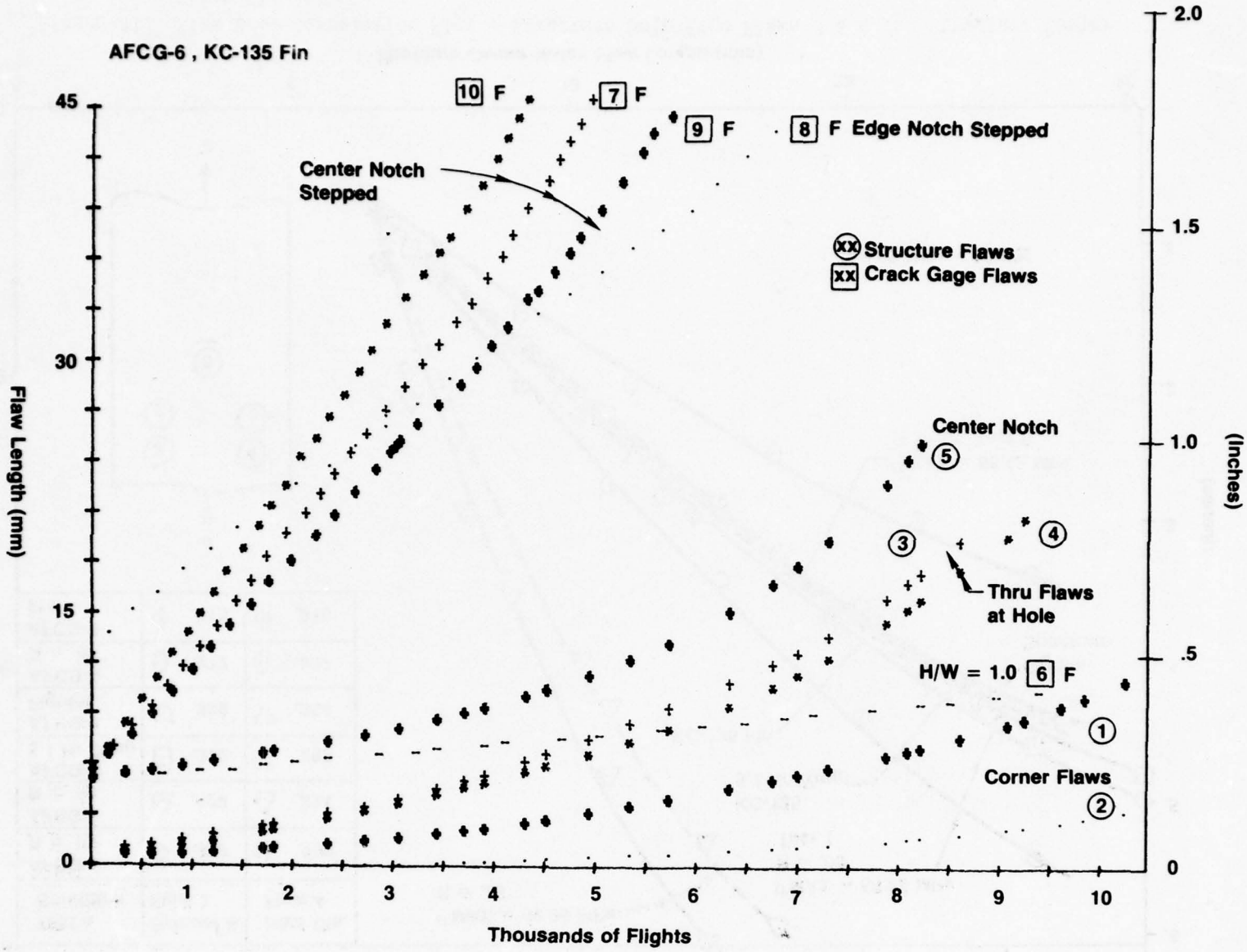

Figure 40. Crack Propagation Results Plot - Specimen AFCG-6

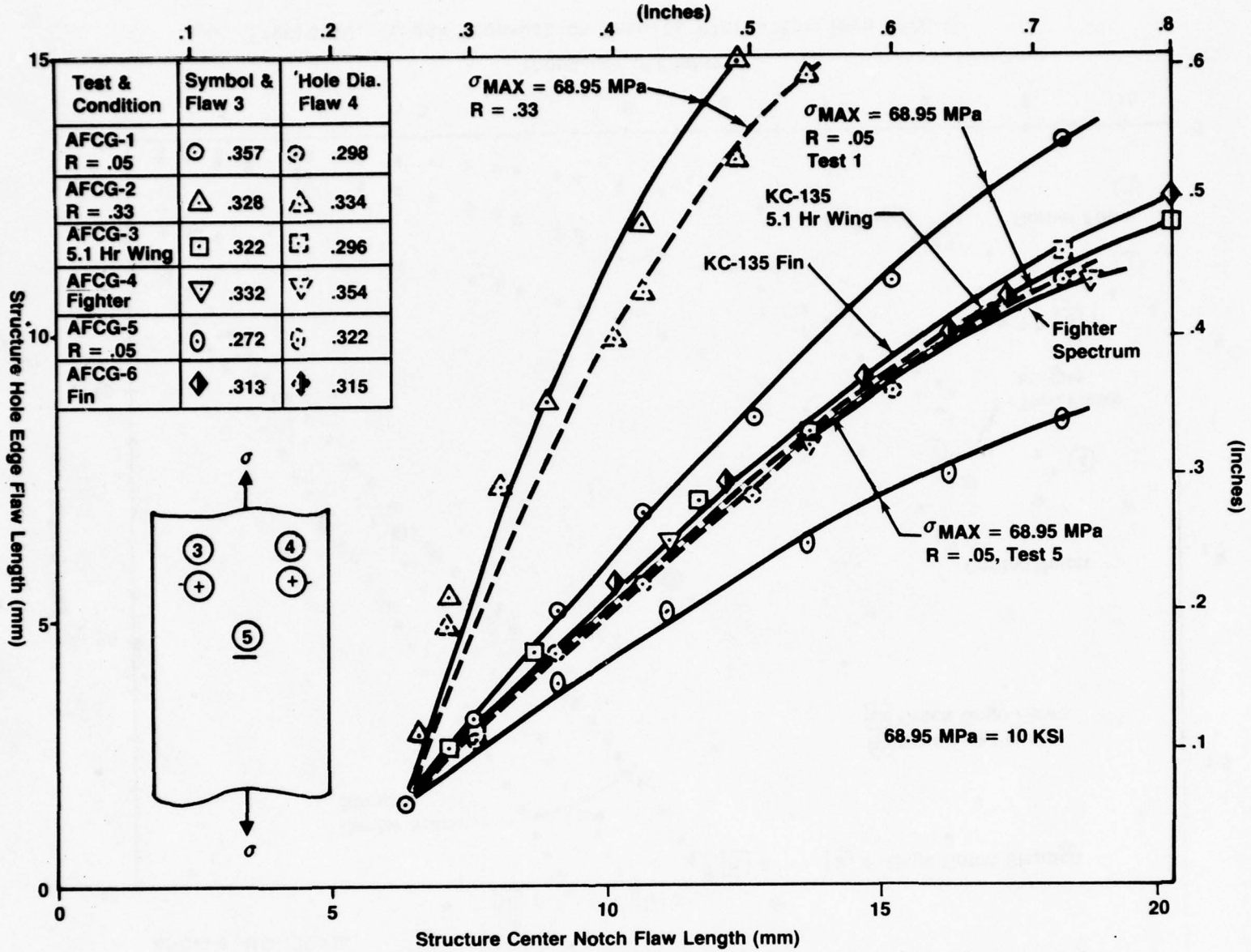

Figure 41. Flaw Grow Correlation Plot - Structure Hole Edge Flaws 3 & 4 Vs. Structure Center Notch Flaw 5

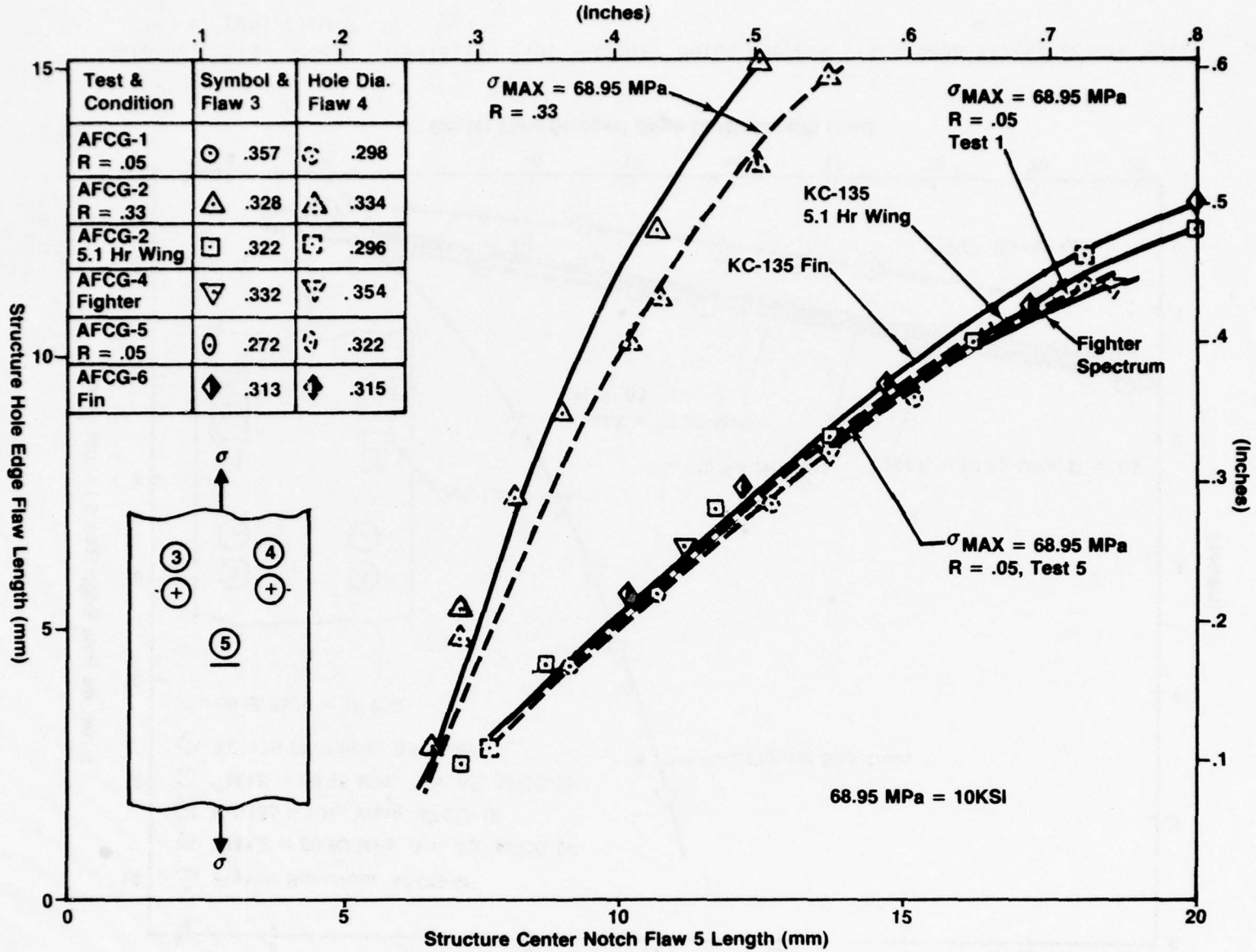

Figure 41A. Flaw Grow Correlation Plot with Scatter Removed - Structure Hole Edge Flaws 3 & 4 Vs. Structure Center Notch Flaw 5

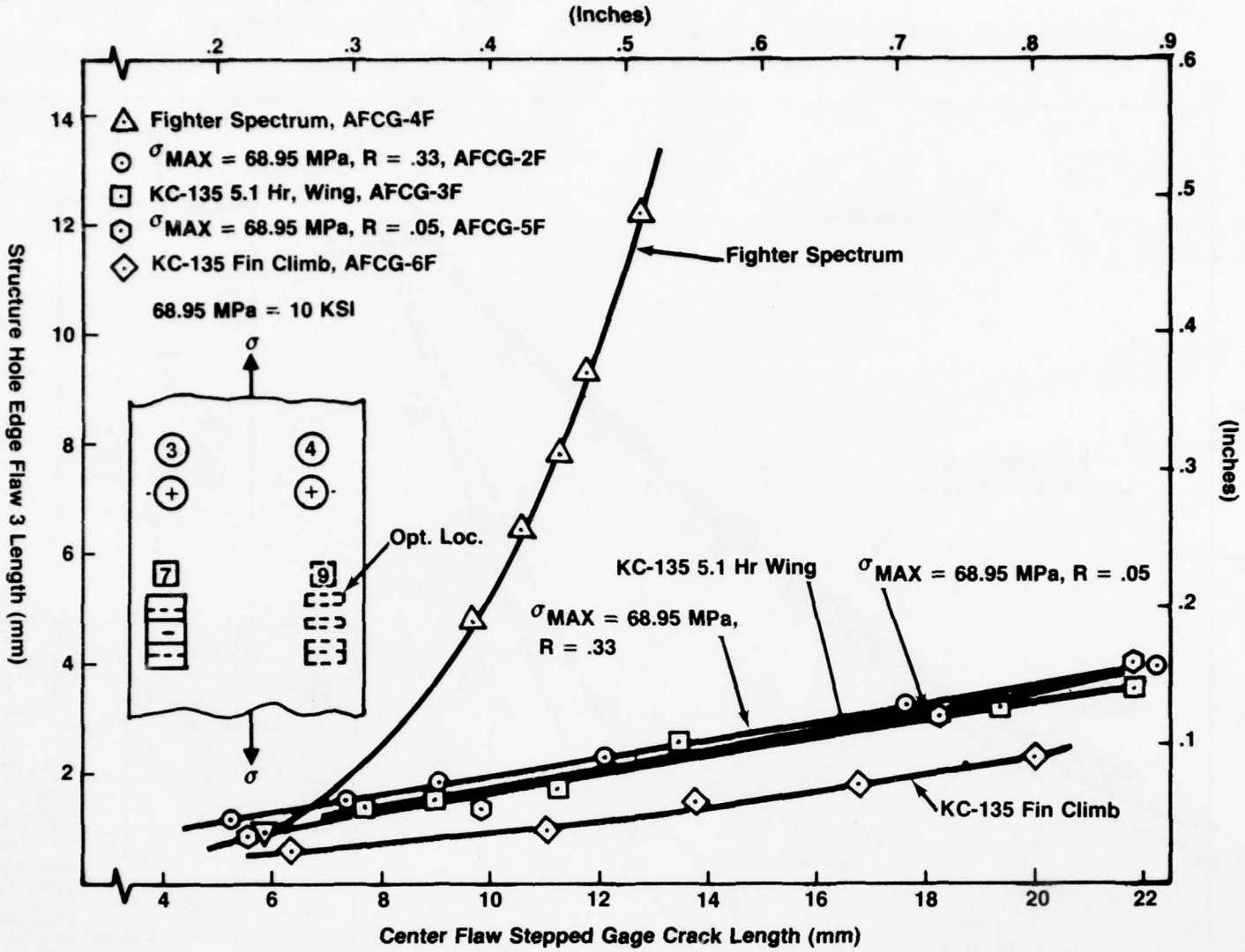

Figure 42. Flaw Growth Correlation Plot - Center Notch Stepped Crack Gage Vs. Structure Hole Edge Flaw 3

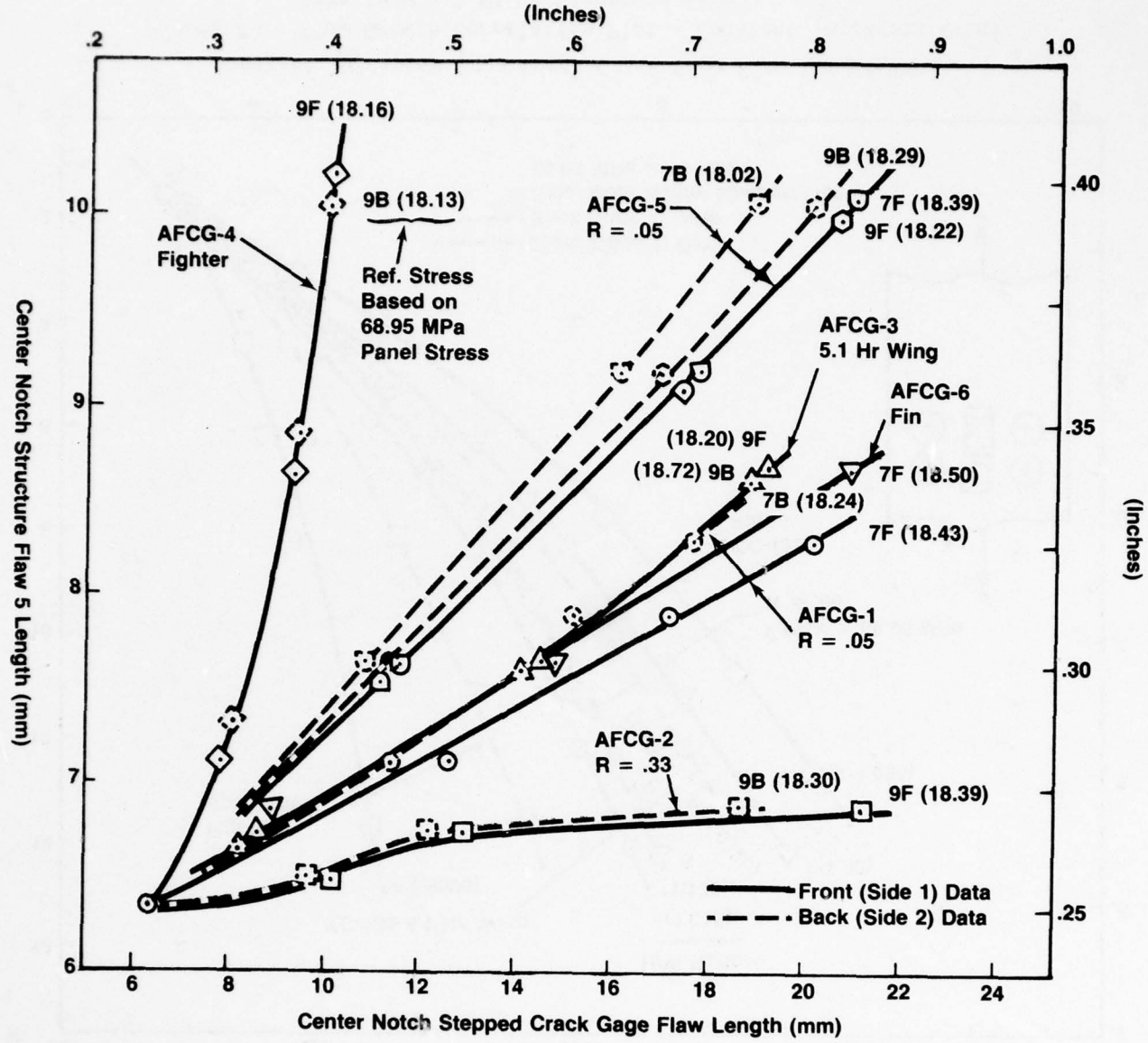

Figure 42A. Flaw Growth Correlation Plot - Center Notch Stepped Crack Gage Vs. Structure Center Notch Flaw 5

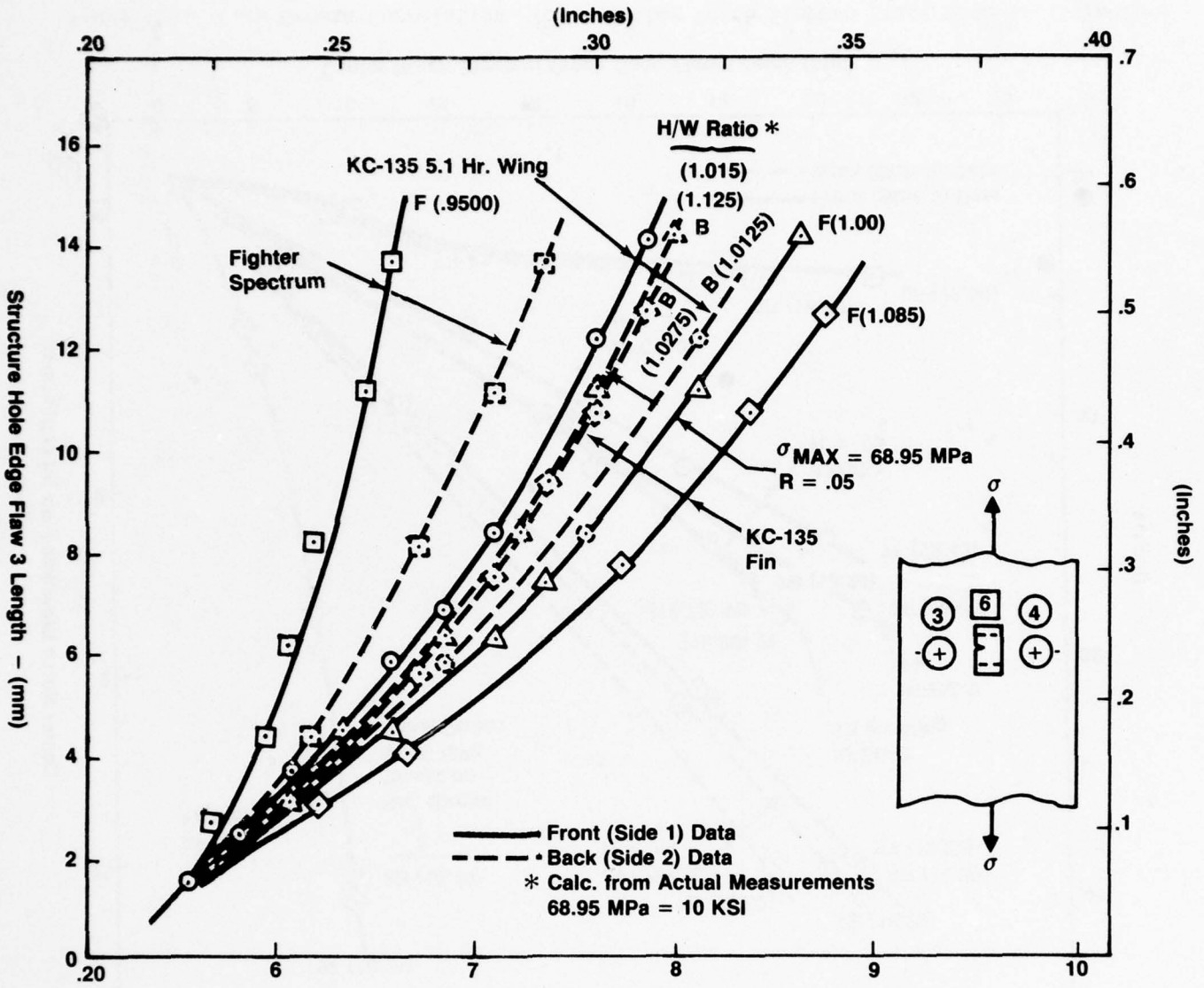

Figure 43. Flaw Growth Correlation Plot - Constant Thickness Crack Gage (H/W = 1.0) Vs Structure Flaw 3

crack gage and the structure center notch flaw 5. In Figure 42A, the results have been normalized to 6.35 mm (.25 In.) common starting length.

A similar cross plot of the constant-thickness crack gage of H/W = 1.0 versus structure hole edge flaw 3 is presented in Figure 43 with the data normalize to initial flaw sizes of 1.52 mm (.06 In.) for the structure hole edge flaws and 5.59 mm (.22 In.) for the crack gage flaws.

Significant observations from these plots will be discussed later in Section V of this report Volume I.

It is beyond the intent of this report to plot and cross-plot every possible correlation. It is left to future interpreters to compare results to suit their particular interest.

2.3 Crack Growth as a Function of Location

The stress survey test showed that the stress field near Crack-Gage Location 10 was slightly higher than at Crack-Gage Locations 7, 8, and 9. To evaluate the importance of this stress field difference, a plot was made of the center-notch-stepped crack gages located at Locations 9 and 10 of Specimen AFCG-3 and of Locations 7 and 10 of Specimen AFCG-4 for the single-edge-notch-stepped crack gages. These plots are presented in Figures 44 and 45.

These plots demonstrate conclusively that faster crack growth was obtained at Location 10 as opposed to Location 7 or 9. It follows that the stress intensity factor (SIF) is greater at Location 10 by the ratio of basic panel stress from Location 10 to the other locations of interest.

Comparisons of crack-gage response between Side 1 (Front) and Side 2 (Back) at identical geometric locations are presented in Figure 46 for both a single-edge-notch-stepped crack gage from Location 8 of AFCG-3 and the single-edge-notch-constant-thickness crack gage at Location 6 of Specimen AFCG-1. These plots are typical of the data obtained for all tests of this program.

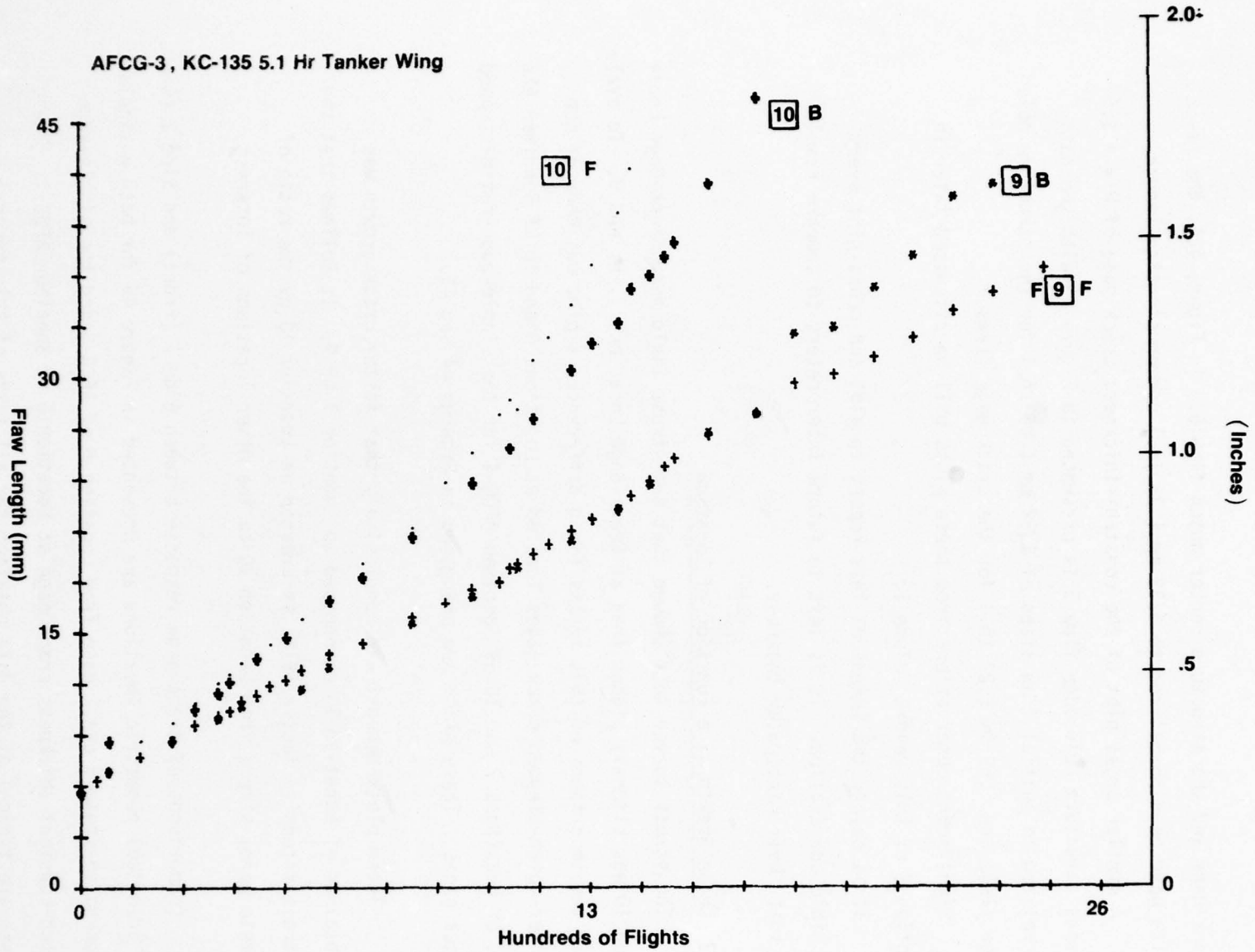

Figure 44. Crack Propagation Plots - Center Notch Stepped Crack Gage (Type I) at Locations 9 and 10, Specimen AFCG-3

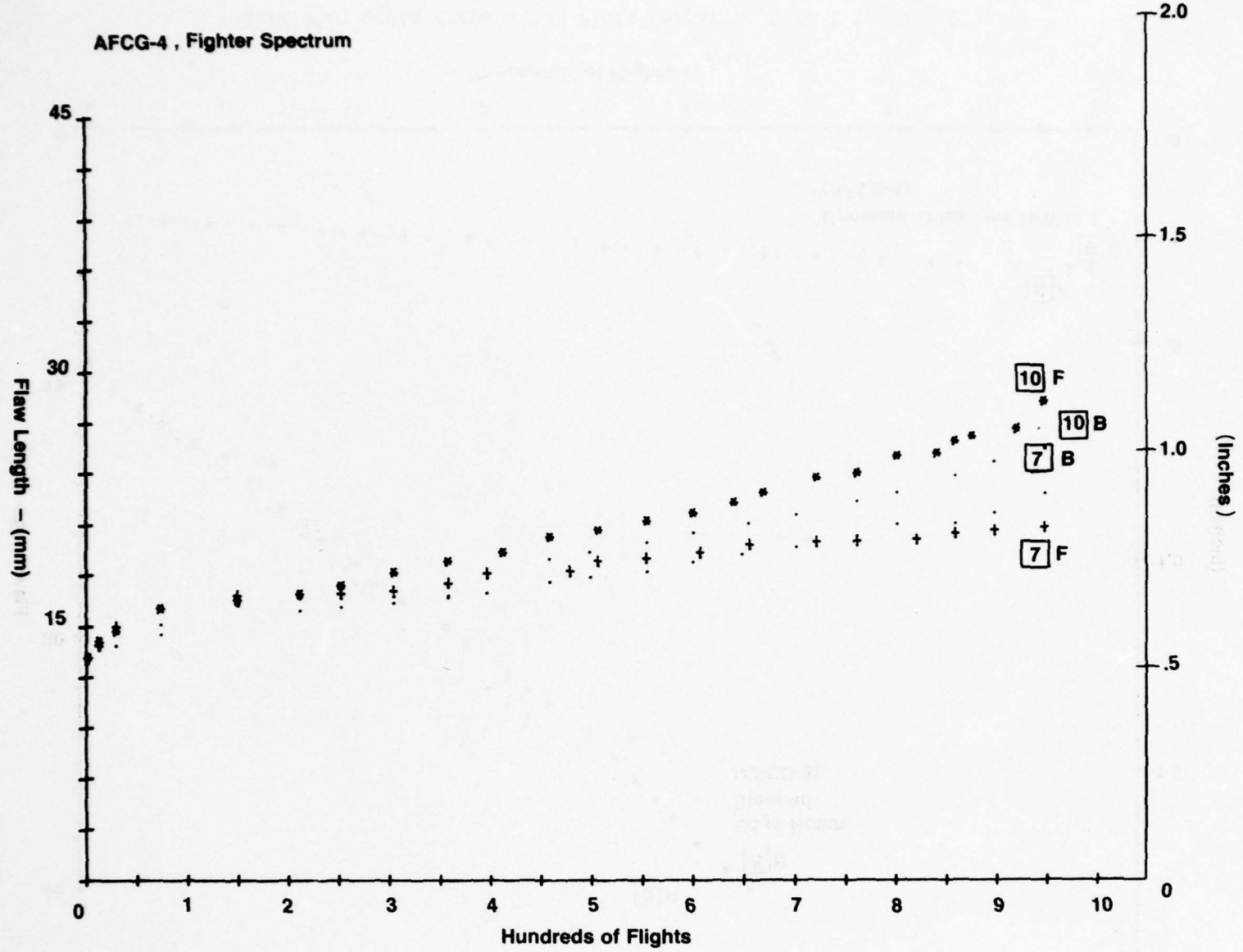

Figure 45. Crack Propagation Plots - Edge Notch Stepped Crack Gage (Type II) at Locations 7 and 10, Specimen AFCG-4

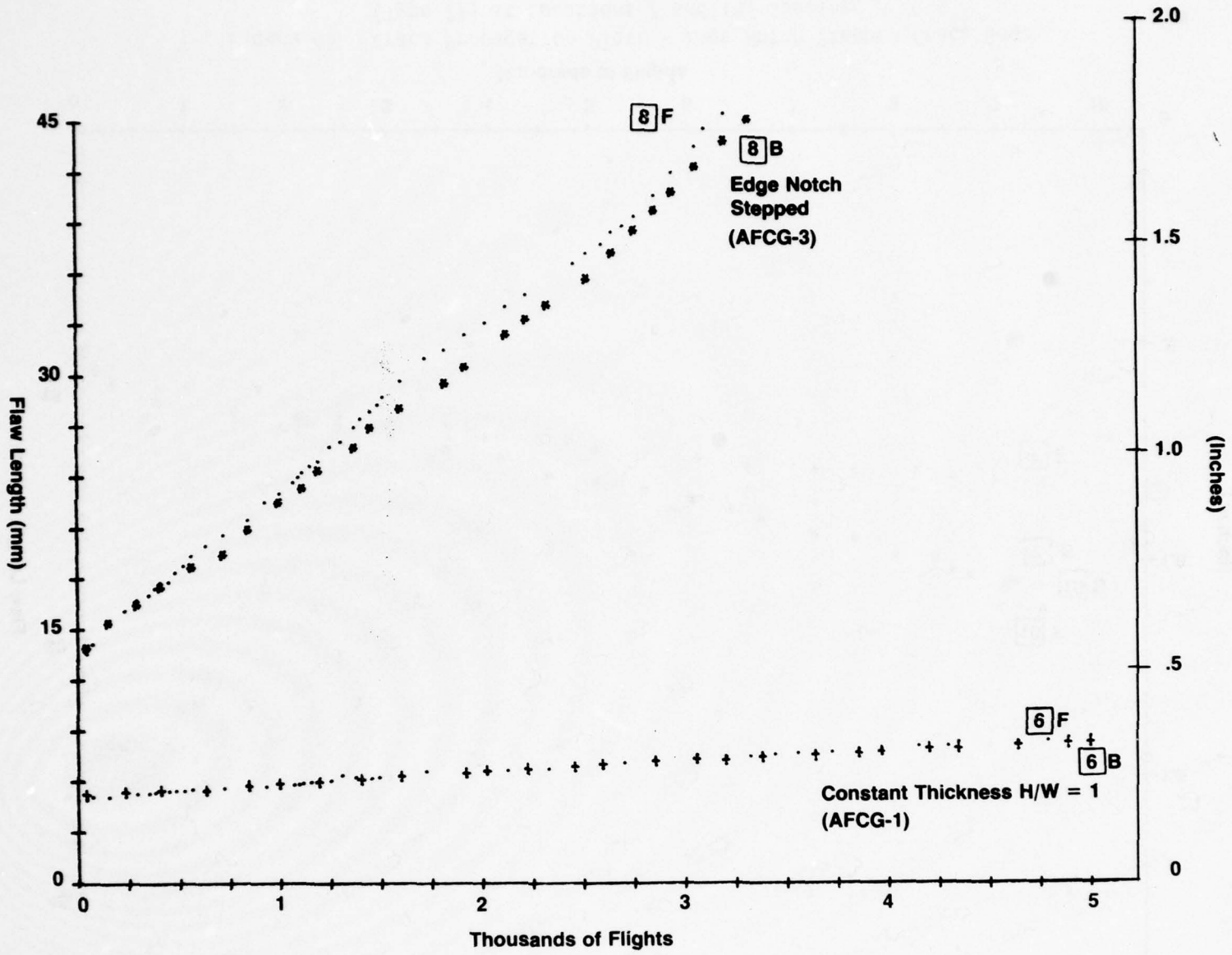

Figure 46. Crack Propagation Plots Comparing Side 1 to Side 2 Growth

3. CRACK GAGE LOAD MEASUREMENTS

The strain data from the unflawed-reference-stepped crack gage was used to calculate load transferred through the crack gage at Locations 7, 8 and 10. Plots of load versus basic panel stress are presented in Figures 47, 48 and 49.

Crack-gage load in the crack gages containing flaws can be obtained by graphical integration of the area under the stress-position curve. Figure 50 shows a plot describing the stress distribution of a center-notch-stepped crack gage for various load levels. This data was obtained from Gage Position 9 on Specimen AFCG-2 at a crack length of 23.6-mm (.9293-In.) after 17,800 cycles of testing. Figure 51 presents similiar stress distributions for crack lengths of 10.7, 23.6 and 37.6-mm at the applied panel load of 171.26 kN. From area under the curve calculations, load transferred into the crack gage was obtained for each crack length.

Figure 52 presents a plot of load transferred versus crack length. Also presented in Figure 52 is the linear approximation which assumes only the uncracked portion contributes to load transfer.

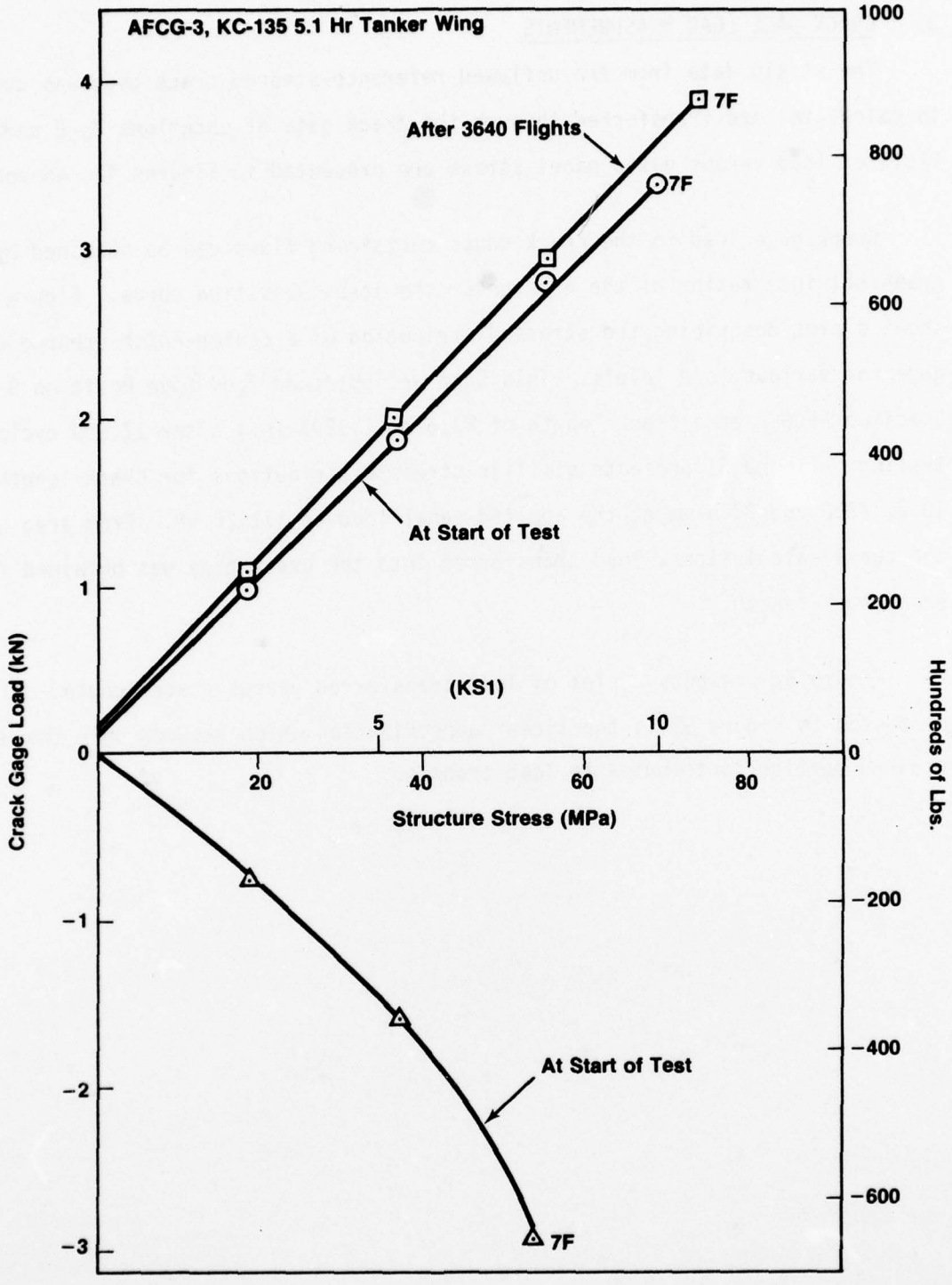

Figure 47. Gage Load Vs Structure Stress, Specimen AFCG-3, Location 7

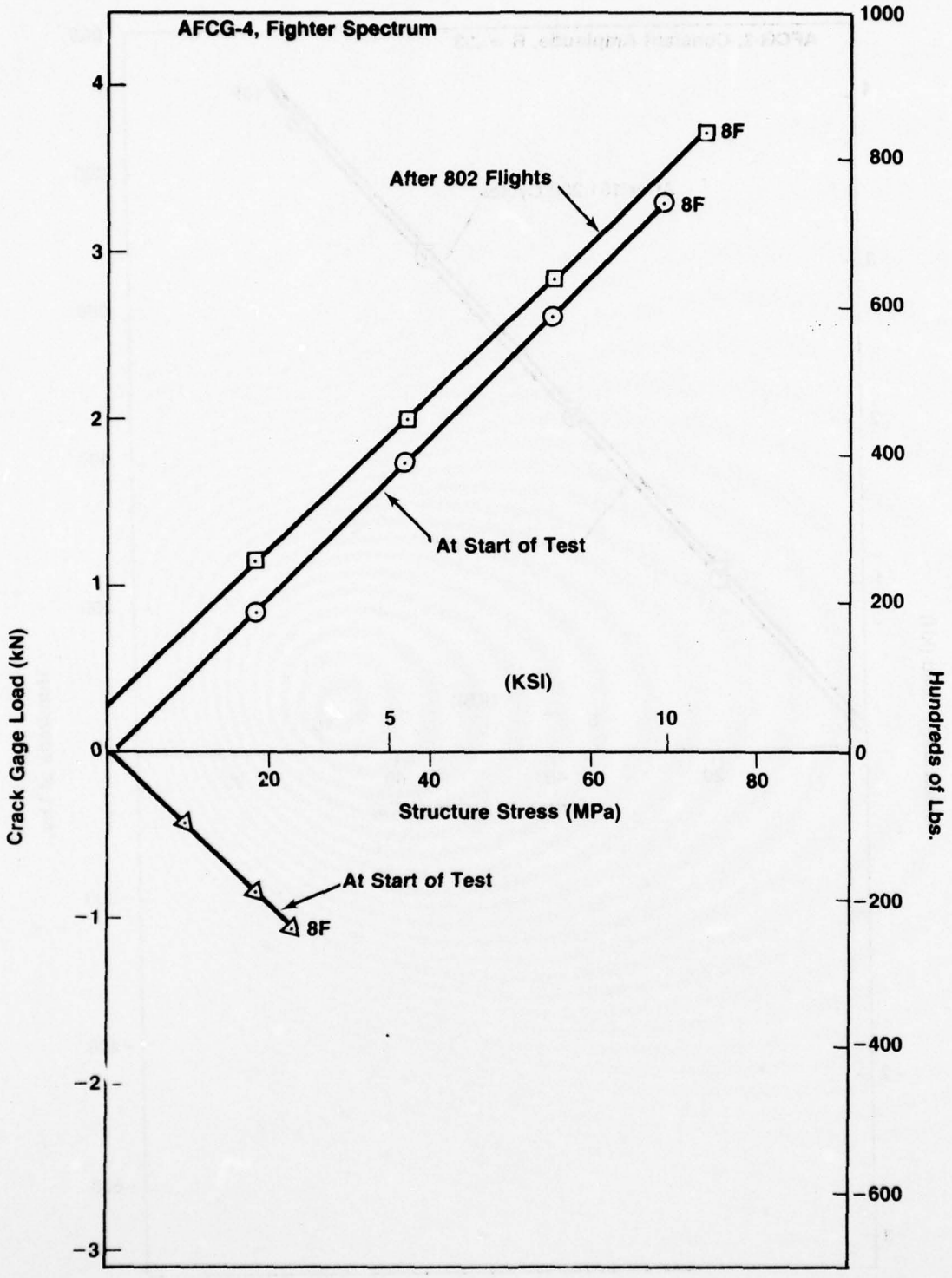

Figure 48. Gage Load Vs Structure Stress, Specimen AFCG-4, Location 8

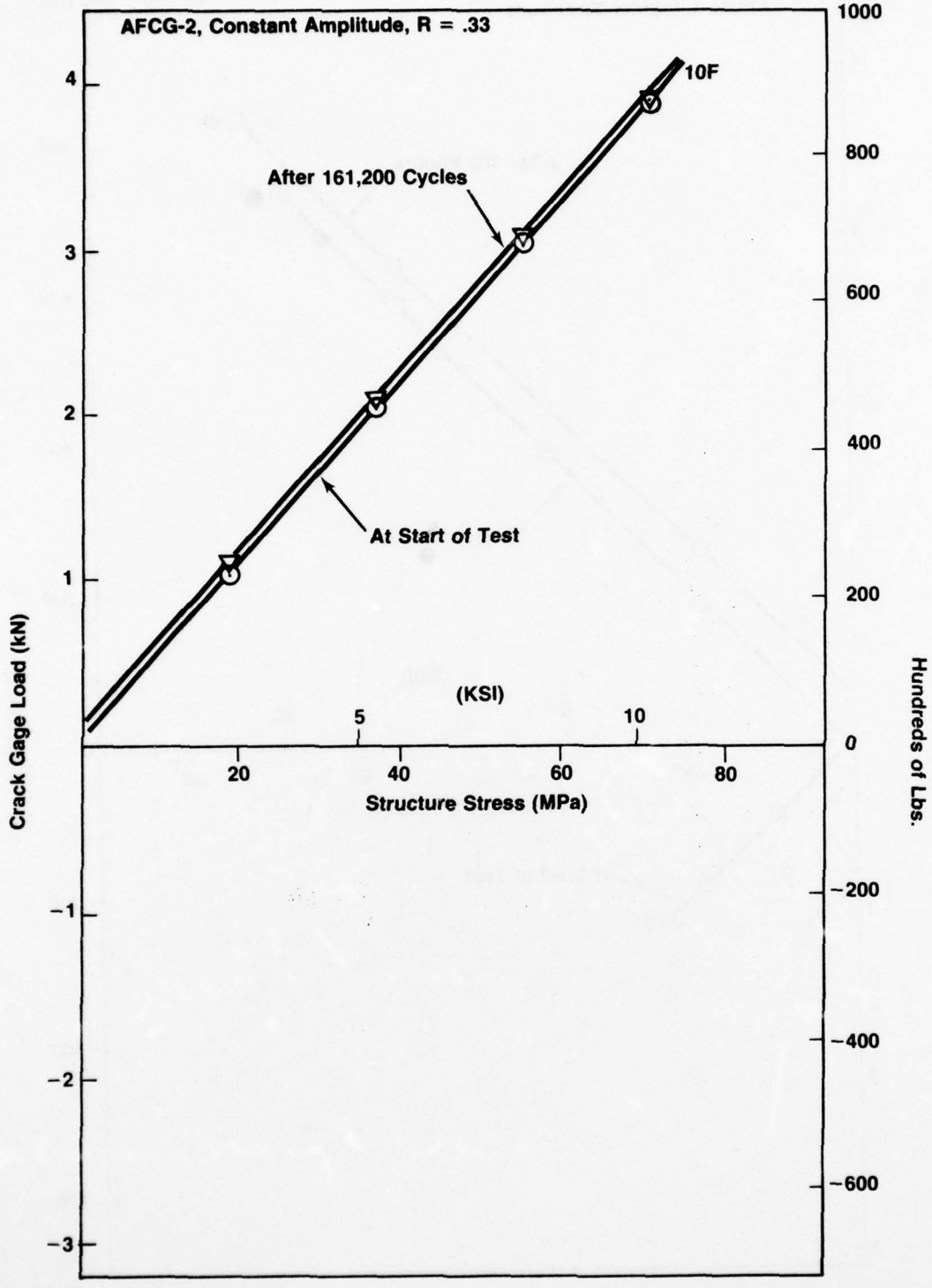

Figure 49. Gage Load Vs Structure Stress, Specimen AFCG-2, Location 10

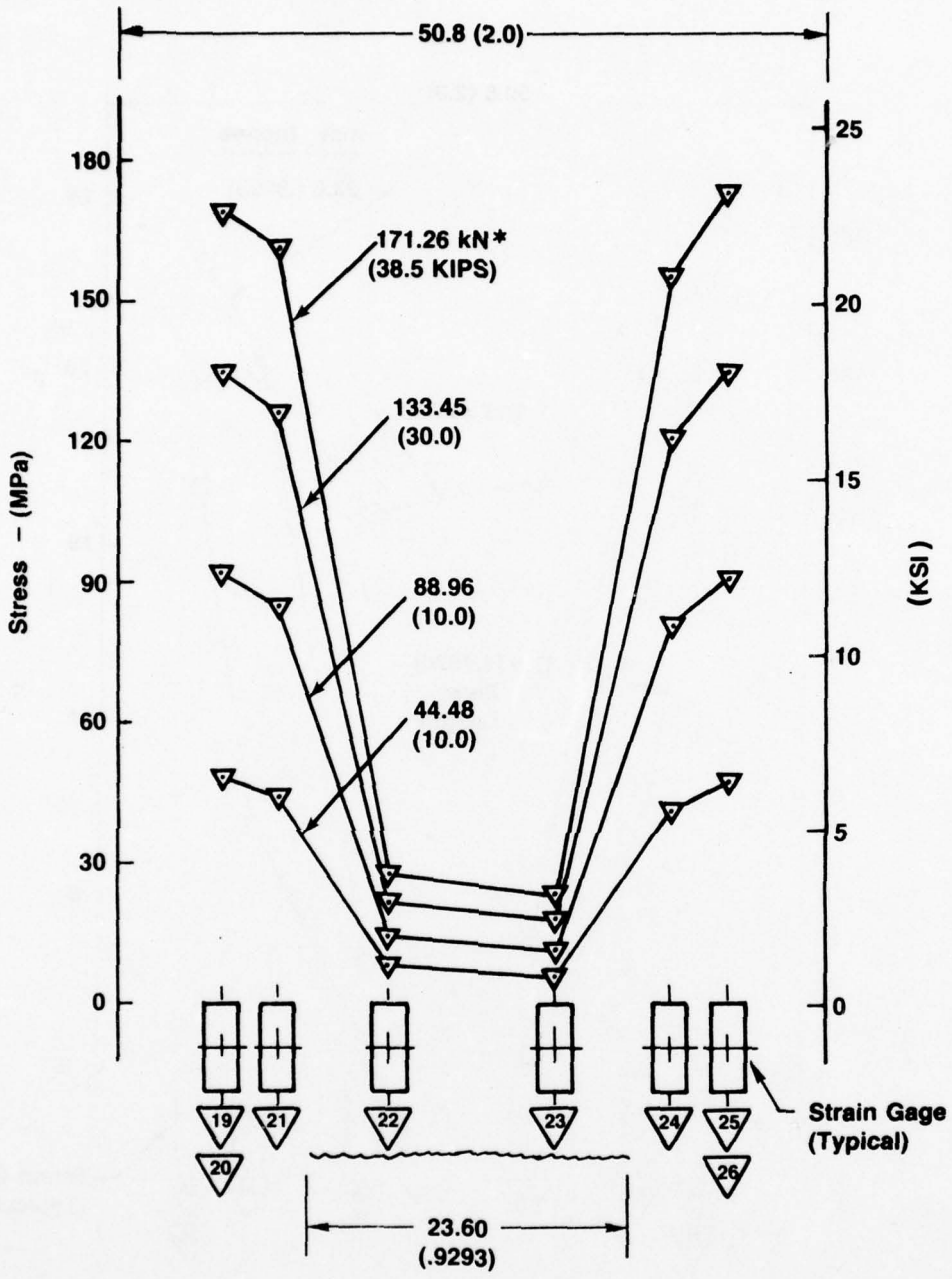

*Applied Load to Basic Panel

Figure 50. Crack Gage Stress Measurements, Gage 9, AFCG-2 at 17,800 Cycles (2a = 23.6 MM)

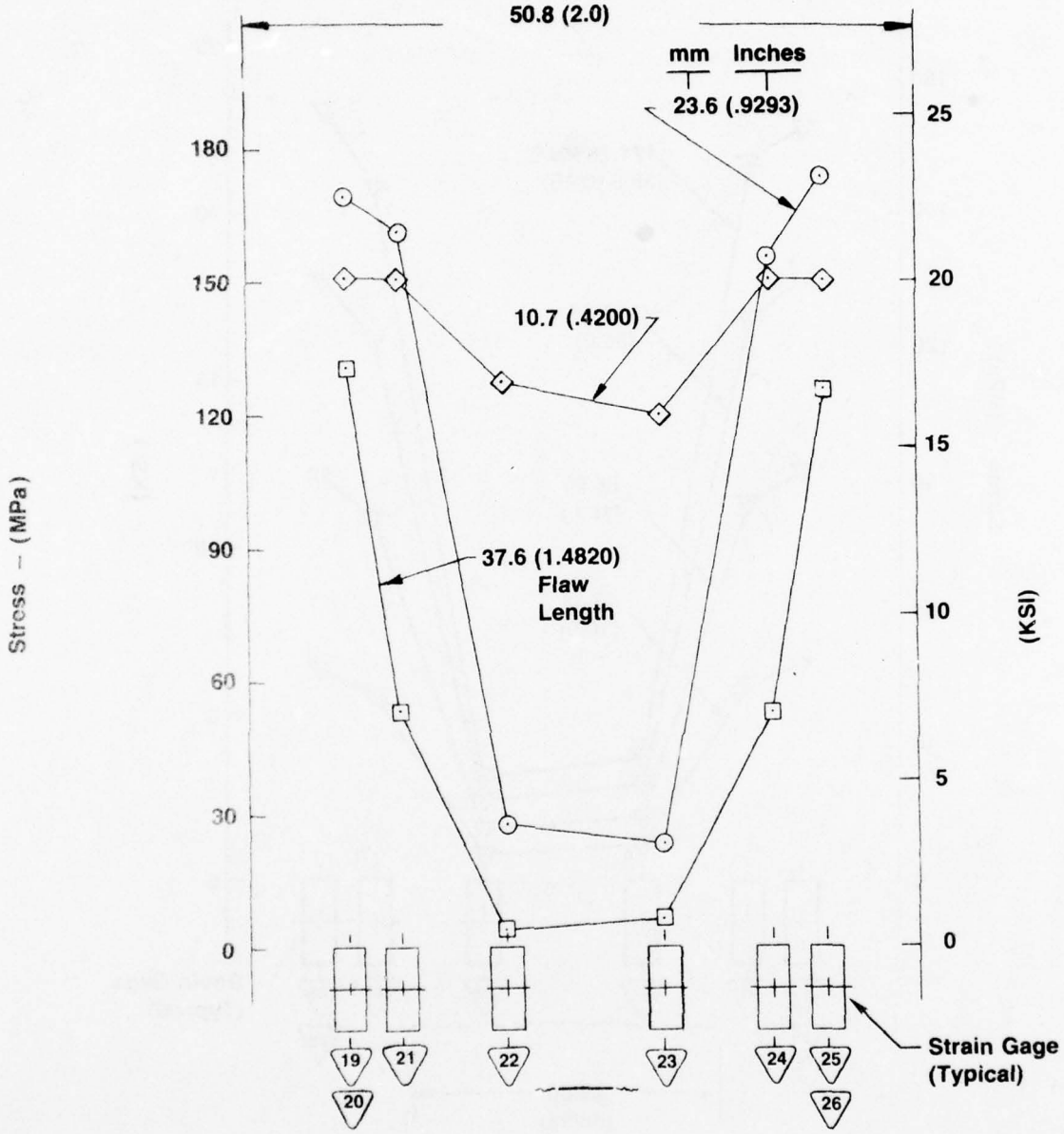

Figure 51. Crack Gage Stress Measurements, Gage 9, AFCG-2, Side 1, AFCG-2 at Three Flaw Lengths

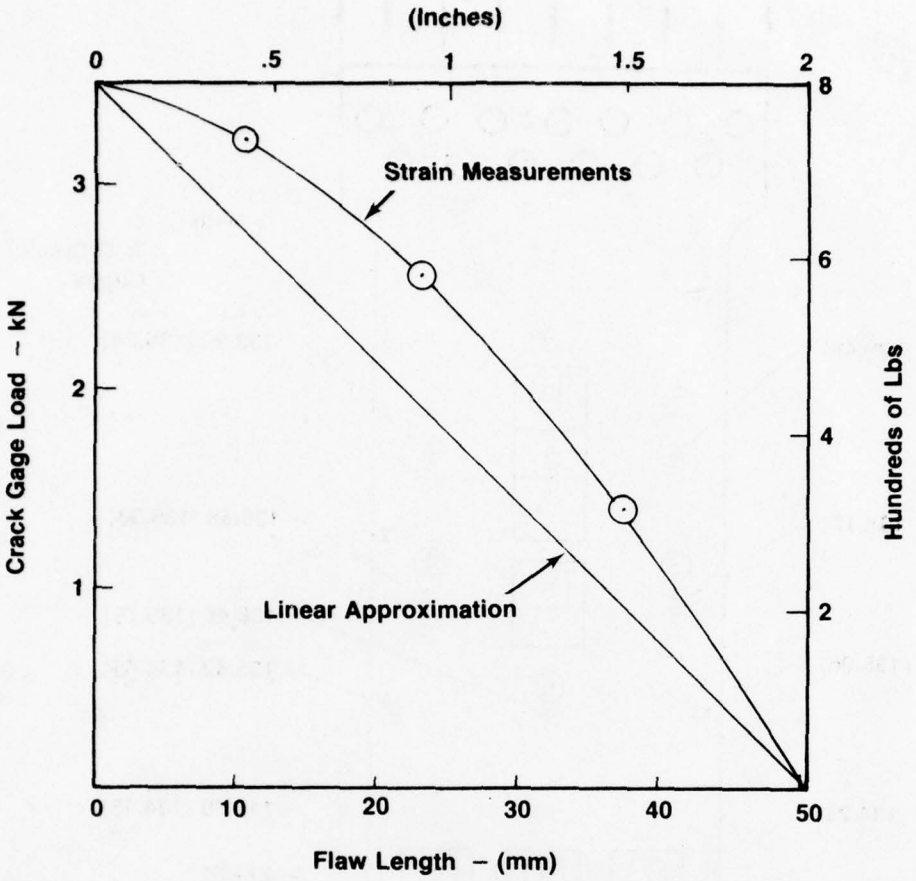

Figure 52. Measured Gage Load Vs Flaw Length for Center Notch Stepped Crack Gage

4. STRESS SURVEY SPECIMEN RESULTS

Results of the stress survey test conducted to evaluate stress field changes at structure flaw locations by the crack-gage installations are summarized in Figure 53. The maximum deviation in stress between the "with" and "without" condition was measured as 18.55 MPa between Locations 7 and 8 (Figure 53.) This corresponds to a percent deviation of 13.45%. The greatest difference measured at a structure flaw location was 3.86 MPa for a 2.8% deviation.

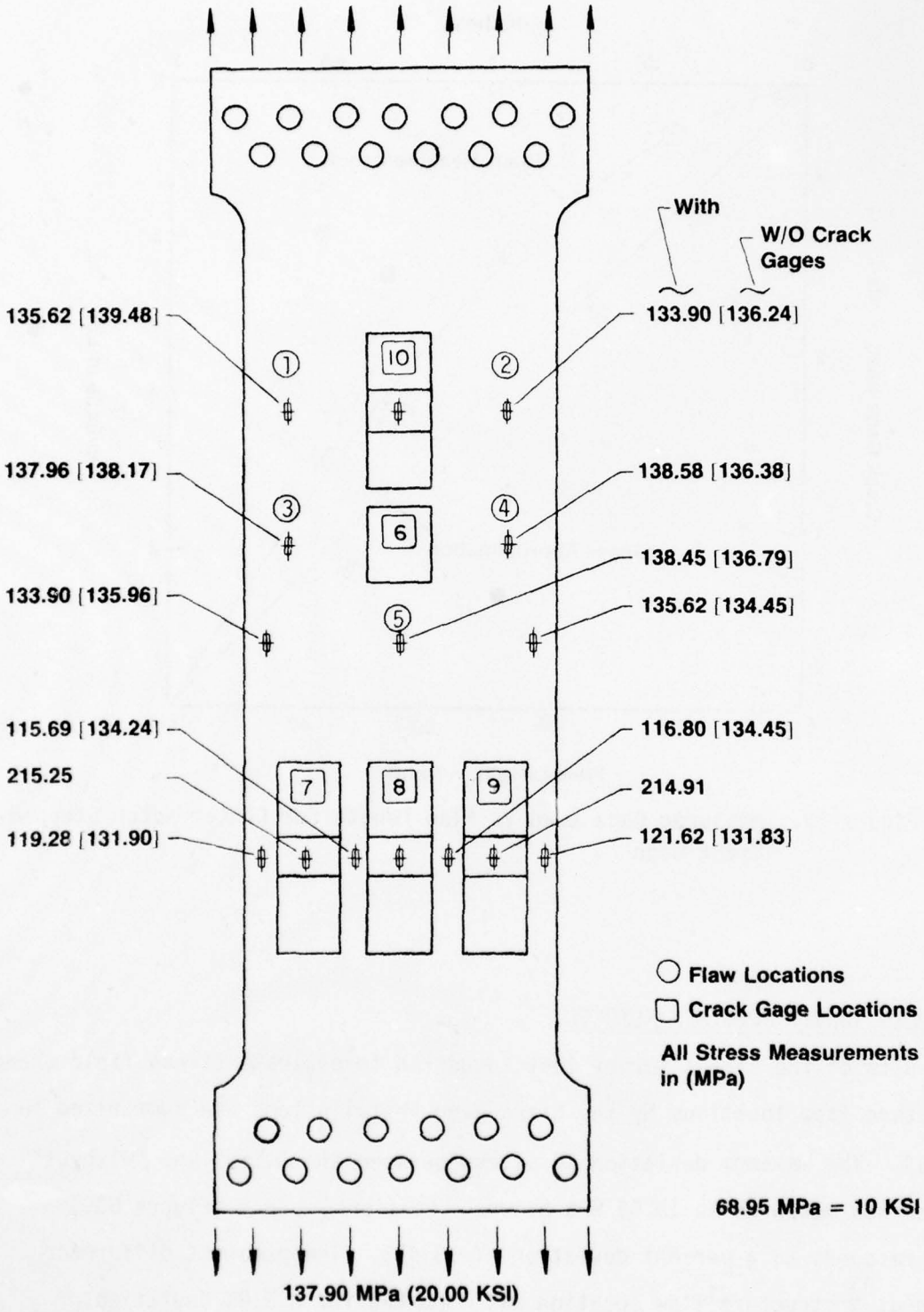

Figure 53. Stress Survey Test Results

AD-A076 421 BOEING WICHITA CO KS F/G 1/3
EVALUATION OF THE CRACK GAGE CONCEPT FOR MONITORING AIRCRAFT FL--ETC(U)
JUN 79 G G CASSATT F33615-77-C-5073
UNCLASSIFIED AFML-TR-79-4037-VOL-1 NL

2 OF 2
AD
A076421

END
DATE
FILMED
12-79
DDC

SECTION V

DISCUSSION OF RESULTS

1. STRESS FIELD INFLUENCE OF CRACK GAGE ON STRUCTURE

A crack gage bonded onto a structure reduces the structure stress locally adjacent to the crack gage. It is desirable for the reduction to be minimal. A crack gage bonded onto only one surface introduces local bending into the structure. This bending is described in Figure 54.

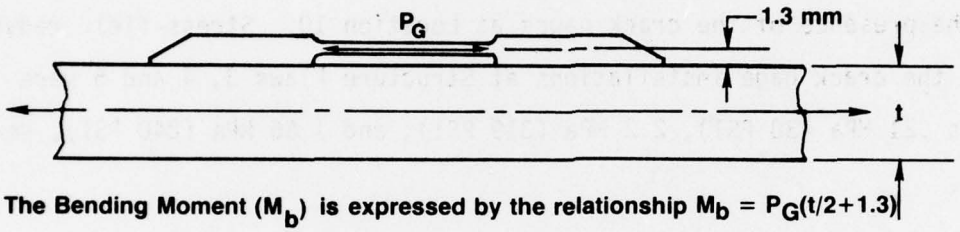

Figure 54. Crack Gage Load Shedding Schematic

For the parameters of this program, where t = 9.5-mm (0.375-In.) and P_G = 3.56 kN (800 Lbs.), the bending moment, M_b, becomes 21.5 N·m(190 In. Lbs). The average bending stress imposed on the basic panel calculates to be approximately 5.52 MPa (800 PSI). Such a stress value is significant as it is a proven fact that a 5- to 10%-stress difference can noticeably change crack-growth rates. Back-to-back crack-gage installations were used in this program to minimize bending. The load shedding would increase from approximately 3.56 kN (800 Lbs) for a single crack gage to 7.12 kN (1600 Lbs) for two crack gages for a basic panel stress of 68.95 MPa (10.0 KSI). Based on net area of the basic panel, a reduction in stress results on the order of 2.95 MPa (427 PSI) would be expected.

As six crack gages were located adjacent to each other at one end of the panel, a basic panel stress reduction of approximately 8.83 MPa (1280 PSI) would be theoretically expected in that area for a panel stress of 68.95 MPa (10.0 KSI) and 17.65 MPa (2560 PSI) for a panel stress of 137.9 MPa (20 KSI). Comparing local strain gages readings in that area with and without crack gages installed, a reduction of average stress of 14.75 MPa (2140 PSI) was measured. (See Figure 53).

For the end of the panel with two back-to-back crack gages, a basic panel stress field reduction of 3.1 MPa (450 PSI) was measured at Flaw Locations 1 and 2 by the presence of the crack gages at Location 10. Stress-field reductions from the crack gage installations at Structure Flaws 3, 4 and 5 were measured as .21 MPa (30 PSI), 2.2 MPa (319 PSI), and 1.66 MPa (240 PSI), respectively.

2. LOAD TRANSFERRED INTO CRACK GAGES

The load transferred into the crack gages was measured and found to agree closely with deflection analyses assuming zero bond flexibility. See Figure 19.

3. ADHESIVE DURABILITY

The measurements of stress in the unflawed reference crack gages at the start, during, and at the end of the tests verified that the load transferred into the crack gages did not change with test duration or number of repeated cycles over the range tested in this program. See Figures 47, 48, and 49. Post-test removal of the crack gages also verified the integrity of the adhesive joints.

Removal of the stepped crack gages from Specimen AFCG-6 revealed irregularities in the bond footprint and unbond length. The crack-growth results from the center notch stepped crack gages at Locations 7, 9, and 10, Figure 55, reveal irregular crack growth as well. The bond quality and an average unbond length

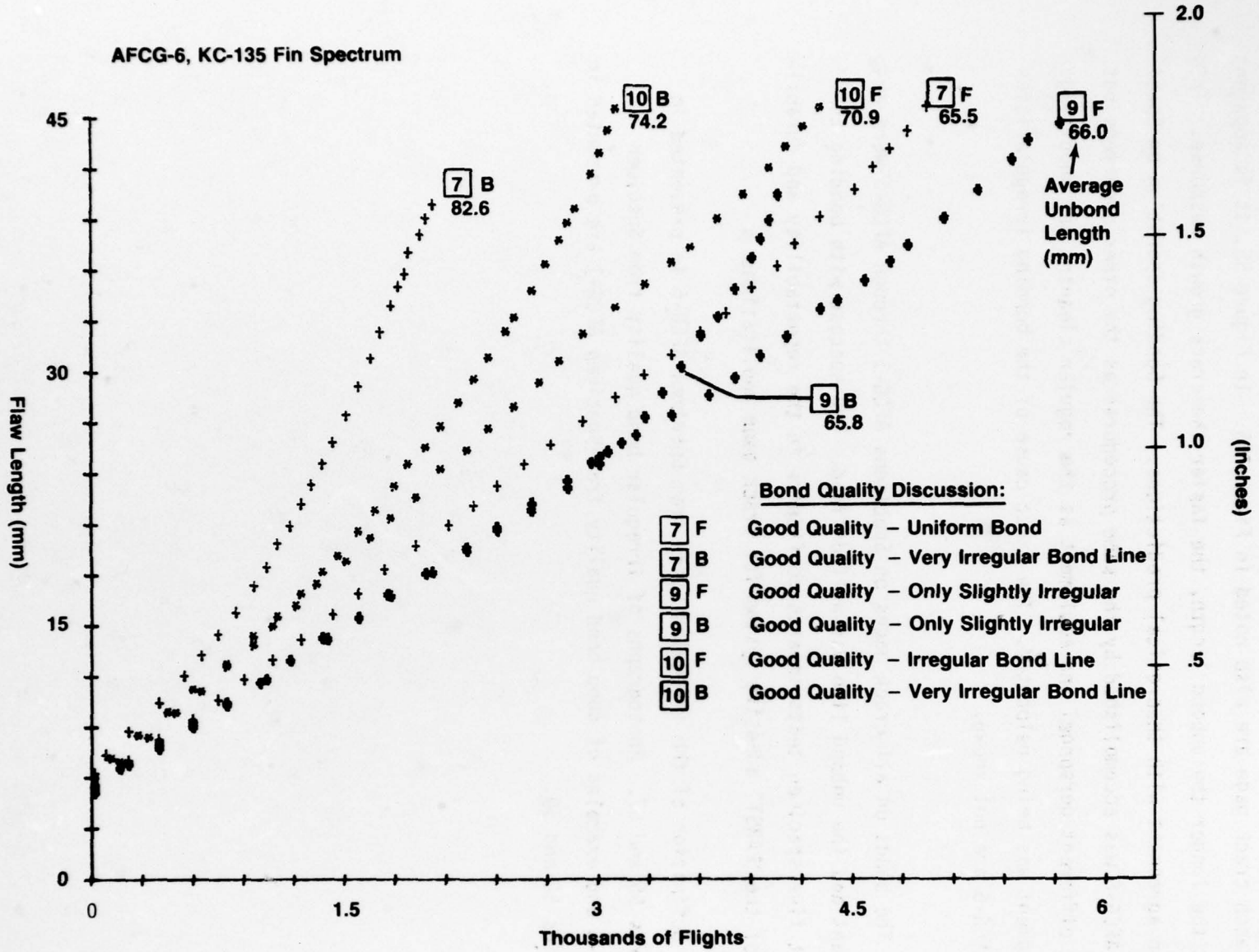

Figure 55. Crack Propagation Plots - Center - Notch - Stepped Crack Gages on Specimen AFCG-6

for each crack gage are also noted in Figure 55. In Figure 55, it is apparent that the longer the unbond length, the faster the crack growth response. This is in agreement with theoretical predictions. The bonding operation on Specimen AFCG-6 was accomplished by the same procedures as the other specimens but with different personnel and equipment as the regular cleaning and anodizing equipment was being relocated. The exact cause of the bonding irregularities on AFCG-6 are not known.

The bonds on all crack gages on Specimens AFCG-1 through AFCG-5 were excellent and the unbond line was well defined. The success with bonding the first five specimen tests imparts confidence in the repeatability and durability of the "PABST" adhesive system for crack gage applications.

Definition of the irregular bonds from Specimen AFCG-6 is presented in Figures 56 and 57. Photographs of irregular bond quality from Specimen AFCG-6 and examples of good bond quality from Specimen AFCG-1 are presented in Figures 58 and 59.

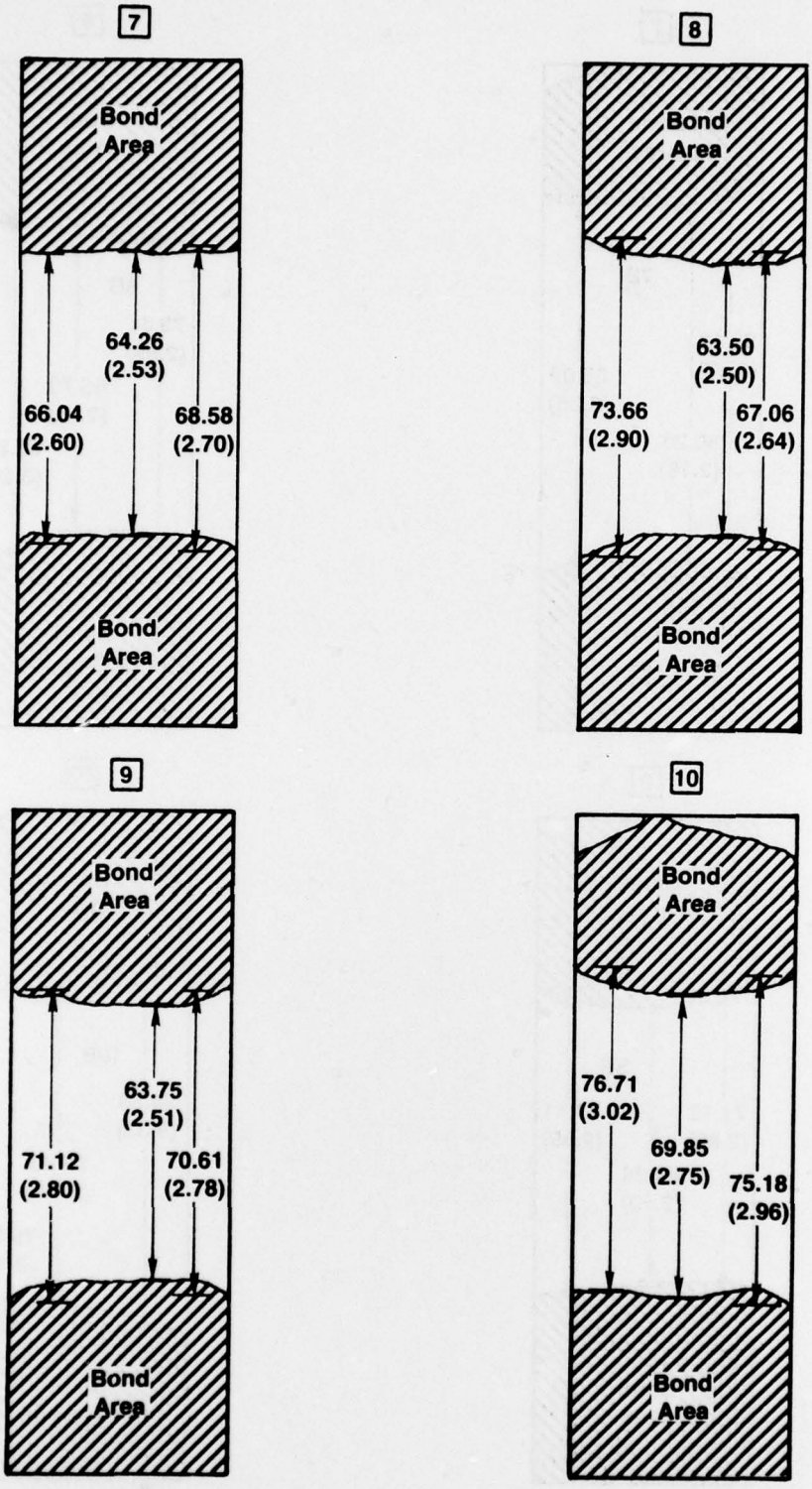

Figure 56. Bond Profiles, AFCG-6 Side 1

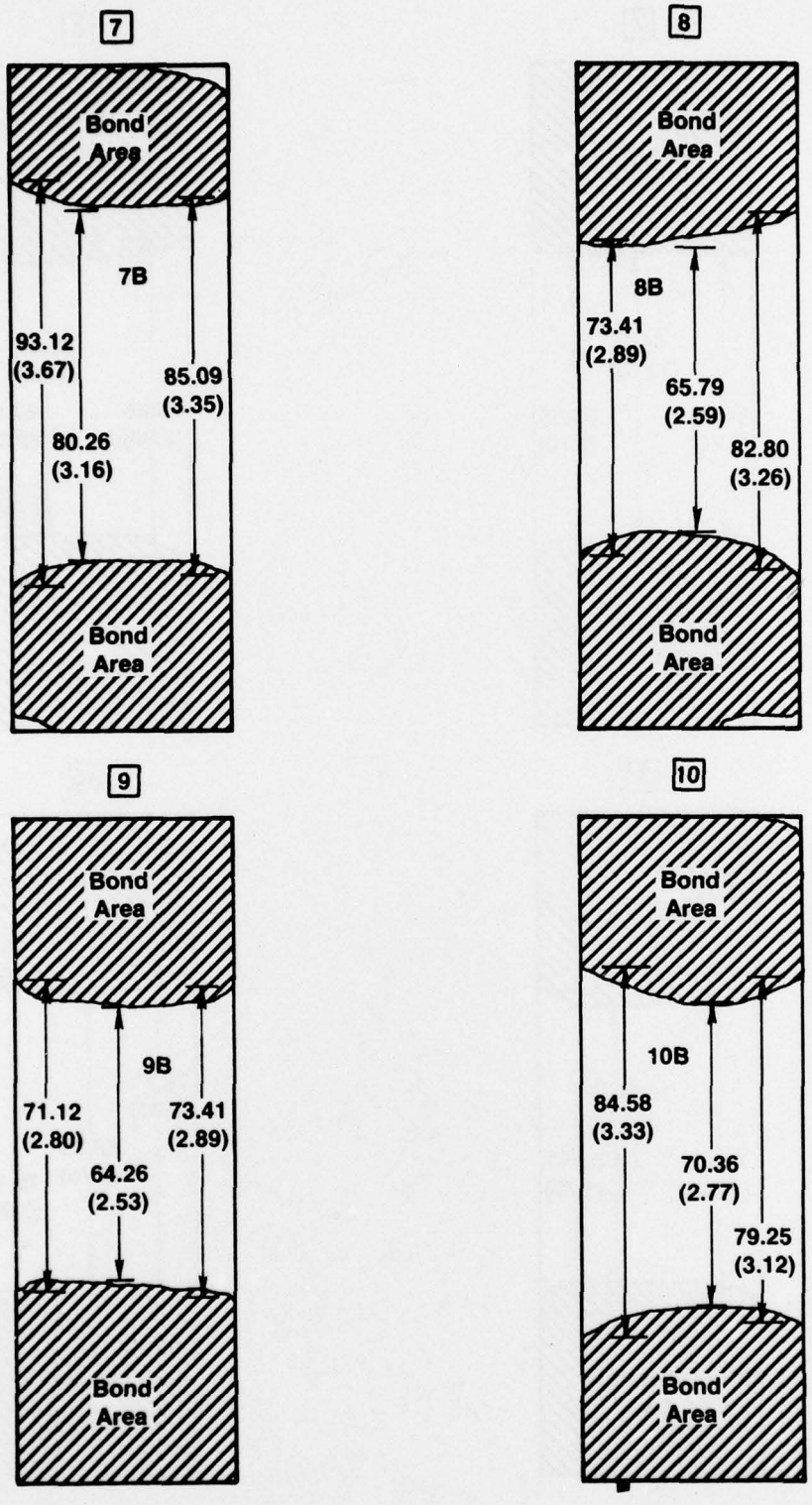

Figure 57. Bond Profiles, AFCG-6 Side 2

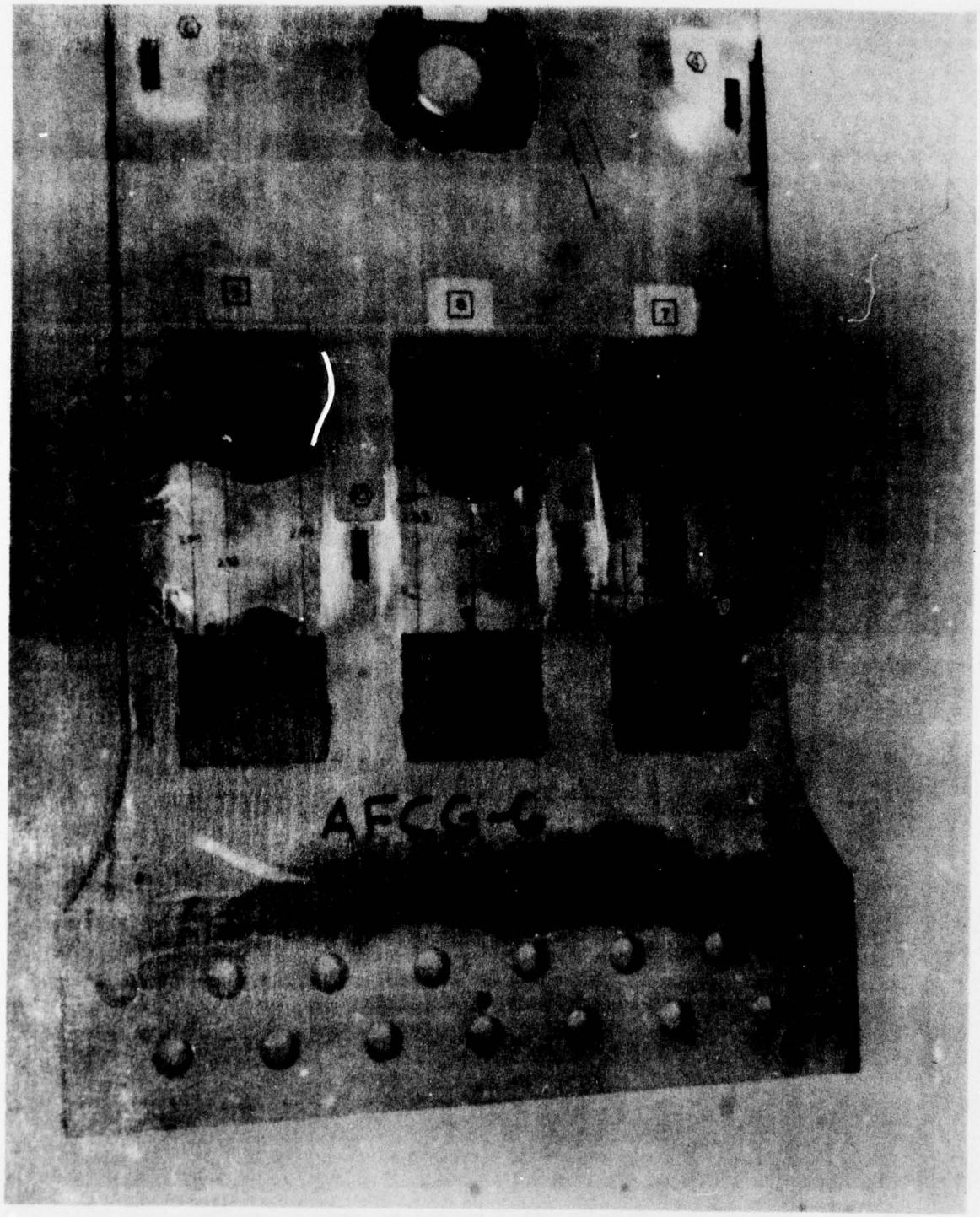

Figure 58. Irregular Bond Profiles, AFCG-6 Side 2

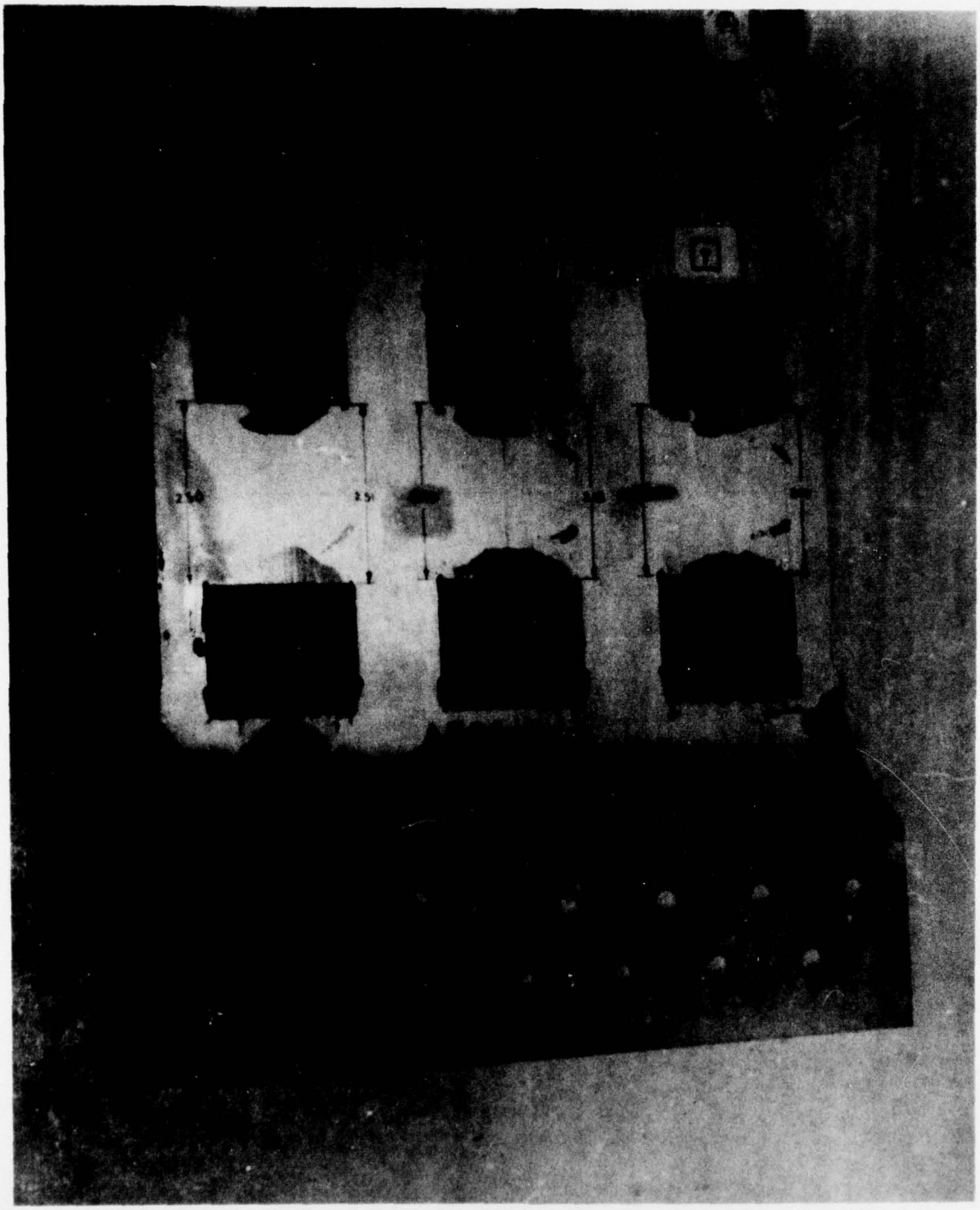

Figure 59. Uniform Bond Profiles, AFCG-1 Side 2

4. LOAD HISTORY INDEPENDENCE

Independence-from-load-history means that the relationship or "transfer function" between the crack growth of a given crack gage and structure flaw would remain the same regardless of the applied load profiles or magnitudes. This means that a given delta growth in the crack gage would always correspond to a given delta growth in the structure flaw.

The property of independence-from-load-history is a very desirable quality. It would essentially eliminate any analysis or interpretation of growth rates in either the crack gage or of the structure flaw it was tracking.

It is obvious that, if the crack gage and structure flaw were of identical material, experienced the same environment, load-time history, and exact SIF levels throughout their cyclic life, both flaws would be identical and the correlation would be independent-of-load-history and would be one-to-one.

It is desirable for the crack gage flaw to grow faster than the structure flaw it is tracking. Such accelerated growth was obtained with the stepped-design crack gages of this program. Bonded-on crack gages experience essentially a constant end deflection input from the structure to which they are attached. In contrast, most structures are loaded such that load, not deflection, is the repeatable input quantity. This stress amplification and deflection loading made the crack-gage situation different from the structure flaws of interest and independence-from-load-history does not automatically become a theoretical certainty.

Crane, Grandt and Gallagher (Reference 6) have demonstrated the load independence characteristic from flaw to flaw in a structure for constant amplitude tests. The plot in Figure 41 was made to see how well that load independence was demonstrated in this program between Structure Hole Edge Flaws 3 & 4 and Center Notch Flaw 5. As the range of SIF was similar for Flaw 3 and Flaw 5, the independence-from-load-history phenomenum was expected.

The test data (Figure 41) indicates a reasonable degree of independence-from-load-history except for specimen AFCG-2 tested at σ_{MAX} = 68.95 MPa (10 ksi), R = .33. When Figure 41 was replotted in Figure 41A only using data from the more nearly equal hole sizes, the independence-from-load-history is more pronounced. Again, however, the R = .33 test shows disagreement from the other tests.

The criteria for load independence is that the crack growth response of crack gage and Structure Flaws obey the linear Paris law for crack growth, $da/dn = C\Delta K^m$. The plot of da/dn vs Kmax for Flaw 5 of Specimen AFCG-2 (Figure 51, Volume II) shows substantial nonlinearity during the early portion of the test. In contrast, Flaws 3 and 4 show linear growth throughout the test. Therefore, independence-from-load-history could not be expected. Figure 42 which relates the growth of Structure Hole Edge Flaw 3 to a center-notch-stepped crack gage shows independence-from-load-history except for the fighter spectrum.

The plot of Figure 43 relating the slow-response, constant-thickness crack gage 6 to the Structure Flaw 3 shows agreement between the constant-amplitude test AFCG-5, the KC-135 wing test AFCG-3, and the fin spectrum of test AFCG-6. Disagreement is expressed for the fighter spectrum. The fighter spectrum also shows the greater retardation (Figure 26).

From the results of this program, it is concluded that there are exceptions to the "independence-from-load-history" property of correlation between flaw growth in crack gage and structure (Figures 42 and 43) and even between structure flaws of two types (Figure 41). These results also indicate that the deviation is related to the amount of retardation in a given flight load spectrum. This is in agreement with past experience which shows that retardation is related to stress intensity at the crack tip. Retardation is also greater for plain stress (thin crack gage) than for plane strain(thick structure) conditions.

5. FLEET TRACKING

A most needed range of flaw tracking for damage tolerance in existing fleets of large transport/bomber aircraft is from an initial hole corner flaw size of approximately 0.5-mm (0.02-In.) out to a mandatory repair length of 5.0-mm (o.20-In.) past the fastener hole.

To track such a structure flaw, it seems reasonable to desire a flaw extension in a crack gage of approximately 20.0-mm (0.80-In.). The unbond lengths of the stepped-design crack gages used in this program produced sensitivities significantly greater than this. Reduction in the unbond length would produce the desired sensitivity. The constant-thickness designs used did not produce enough sensitivity.

The corner flaws used in this program resulted in an initial aspect ratio of approximately 3.7 to 1 for distance down the hole to distance along the surface. See Figure 60 for a photograph of a typical initial flaw profile. Actual natural corner flaws normally have an aspect ratio of approximately 1.7-2.5 to 1. The initial flaw shape is very important in determining the crack-growth rates for short flaws.

Additional testing is in order which would carefully control initial flaw shape. The testing should include both filled and loaded fastener holes in realistic environments. One major concern is how to handle the difference between the environmental effects which a crack gage experiences and which a flaw hidden between structural elements such as skin and stiffeners would see.

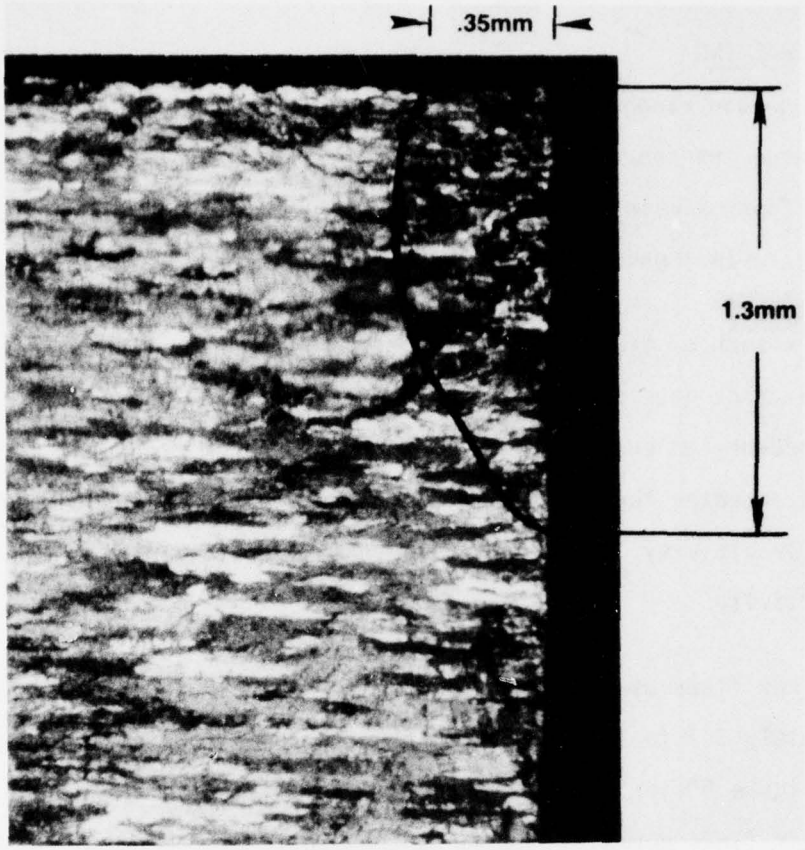

50X N 1787

Figure 60. Typical Initial Flaw Shape - AFCG-3, Hole 2

6. ENVIRONMENTAL IMPACT

The absolute success of the crack-gage concept for reliable flaw tracking of aircraft structures could conceivably result in several such crack gages being installed on every flying aircraft, both civilian and military.

Such a usage, although enormous, would not have any significant effect on the environmental quality. The processes which would be used are all existing ones which have established procedures and regulations. The usage of acids, chemicals, adhesives, etc. for crack-gage installations would be insignificant in comparison to that routinely used in the manufacture of new aircraft.

SECTION VI
CONCLUSIONS AND RECOMMENDATIONS

The results of this program have lead to the following conclusions:

- Adhesive systems do exist that can repeatibily introduce a known load into crack gages. The "PABST" Technology system used in this program is recommended. Adhesive join flexibility with the "PABST" system is negligible.

- The design technology exists to design a crack gages of a wide range of sensitivities to track very short or faster growing structure flaws. The constant thickness design is quite satisfactory when a lower sensitivity is needed. The stepped design offers a reliable means to readily adjust sensitivity by changing unbond length.

- Independence-from-load-history in the correlation between crack gage flaw growth and structure flaw growth does not unilaterally exist. "Independence" is significantly influenced by differences in environment, SIF levels, R ratios and retardation between crack gage and structure flaws.

- Finite element techniques utilizing constant end deflection inputs and strain energy release rate calculations (Ref. 12) provide satisfactory estimates of SIF relationships and predictions of crack gage flaw growth response.

- Valid comparisons of severity-of-usage between individual airplanes of a fleet can be obtained by comparisons of flaw growth in crack gages identically located on each aircraft. The only exception to this was exhibited by specimen AFCG-4 tested to the fighter spectrum.

- Within a region where independence-from-load-history exists, estimates of structure flaw growth can be adequately predicted by monitoring flaw growth in attached crack gages.

- A better understanding of the effects of retardation and environment on a thin (plane stress) crack gage flaw compared to a thicker (plane strain) structure flaw is mandatory.

- The logical evolution in crack gage design may be to use thicker crack gages and to more nearly match the SIF range between crack gage flaw and structure flaw being tracked. This would minimize the effects described above.

- The techniques developed in the performance of this program are practical for use in mass producing pre-cracked crack gages of accurate dimensions. These techniques consisted of conventional machine shop practices and laboratory test procedures.

The crack-gage-concept as stated earlier in this report is a very attractive concept. It has the ability to accumulate and integrate crack propagation damage actually measured on flight hardware in service. Also that service damage can be related to potential flaw growth in the structure. The results of this program have left the author with optimism in achieving that end. This program has also pointed out that caution must be exercized in the fabrication and installations of crack gages. Probably no crack gage can be a "cure all" with true independence-from-load-history for all loadings. However, crack gages can be used to correlate flaw growth potential for specific problems and as our understanding of crack gages increases, their range of application will inevitably expand.

REFERENCES

1. United States Air Force Contract Number F33615-77-C-5073 "Evaluation of Crack Gage Concept for Monitoring Aircraft Flaw Growth Potential".

2. "Airplane Damage Tolerance Requirements," Military Specification MIL-A-83444 (USAF), 2 July 1974.

3. "Aircraft Structural Integrity Programs, Airplane Requirements," Military Standard MIL STD-1530A (USAF), 11 December 1975.

4. H. W. Smith, Fatigue Damage Indicator, US Patent No. 3,979,949, assigned to The Boeing Company, Seattle, Washington, 14 September 1976.

5. G. E. Lambert and D. F. Bryan, "The Influence of Fleet Variability on Crack Growth Tracking Procedures for Transport/Bomber Aircraft," AFFDL-TR-78-158, November 1978.

6. R. L. Crane, A. F. Grandt, and J. P. Gallagher, "A Crack Growth Gage for Assessing Flaw Growth Potential in Structural Components," AFML-TR-76-174-R, October 1976.

7. M. Isida, "Effect of Width and Length on Stress Intensity Factors of Internally Cracked Plated under Various Boundary Conditions," International Journal of Fracture Mechanics, Vol. 7, No. 3, September 1971, pp 301-316.

8. PABST - Industry Review, "Primary Adhesively Bonded Structure Technology," 5 October 1976, McDonnel Douglas Corporation, Long Beach, California.

9. Hall, R. Shah, and W. Engstrom, "Fracture and Fatigue Crack Growth Behavior of Surface Flaws and Flaws Originating at Fastener Holes," AFFDL-TR-74-47, Volume 1, 1973.

10. Boeing Wichita Company Technical Proposal D3-11189-1, "Evaluation of the Crack-Gage Concept for Monitoring Aircraft Flaw Growth Potential," March 1977.

11. J. C. Newman, Jr., "Predicting Failure of Specimens with Either Surface Cracks or Corner Cracks at Holes," NASA TN D-8244, June 1976.

12. R. Shah, "Evaluation of Various Crack Gage Concepts for Monitoring Crack Growth in Structures," Boeing Company Document D180-22967-1, February 28, 1978.

13. O. L. Bowie, "Analysis of an Infinite Plate Containing Radial Cracks Originating at the Boundary of an Internal Circular Hole," Journal of Mathematics and Physics, Vol. 35, 1956, pp. 60-71.

14. R. C. Shah and D. D. Suen, "Stress Intensity Factors for Different Crack Gage Configurations," Boeing Company Document D180-25065-1, February 1979.

15. P. J. Torvik, "Applications of the External Principles of Elasticity to the Determination of Stress Intensity Factors," AFIT-TR-77-3, July 1977.

☆U.S.Government Printing Office: 1979 — 657-002/141